Feature Enhanced Speckle Reduction in Ultrasound Images

Algorithms for Scan Modelling, Speckle Filtering, Texture Analysis and Feature Improvement

A thesis submitted in partial fulfilment of the requirements for the degree of

Doctor of Philosophy in Computer Science

at the

University of Canterbury

by

Prerna Singh

21 August 2019

This thesis is dedicated to my beloved parents,

Mrs. Bala Singh and Mr. B P Singh.

ABSTRACT

This thesis aims to contribute to the advancement of research in the field of ultrasound image analysis by developing several novel algorithms in three key areas: (i) modelling, analysis and validation of synthetic ultrasound images, (ii) characterization and reduction of speckle artifacts, and (iii) enhancement of image features. These three areas have been identified based on existing gaps in research and their importance in advanced ultrasound image analysis frameworks for segmentation and classification.

Synthetic models of ultrasound image formation that can generate noise-free ground truth data with intensity and texture characteristics of real ultrasound images, are valuable for machine learning applications and performance evaluation of speckle reduction techniques. This thesis develops a complete framework for synthetic ultrasound image generation incorporating algorithms for image acquisition, sampling and speckle simulation. The framework allows us to simulate image acquisition in both sector and linear scans with varying axial and lateral resolutions.

Speckle artifacts appear in the form of granular noise in ultrasound images, degrading their diagnostic quality. This thesis presents novel algorithms for speckle reduction while preserving edges, fine details, and contrast of the image. The first despeckling framework presented in the thesis uses a novel application of clustering algorithms based on a transformation to wavelet sub-bands, and is inspired by the success of such methods for synthetic aperture radar imagery. The second despeckling framework uses a modified adaptive Wiener filter along with the Canny edge detection and an enhanced steerable pyramid transformation algorithm. Additionally, a coherence component extraction method is used to enhance the overall texture and edge features even in the darker portions of the image.

The filtering operations used in a majority of speckle reduction methods induce blurring that affects edges and other fine structures necessary for accurate clinical interpretation. Ultrasound images require contrast enhancement as they contain low intensity regions of very low contrast and resolvable details. This thesis proposes a modified version of the contrast limited adaptive histogram equalization specifically designed for ultrasound images, where the optimal clip-limit used by the algorithm is automatically determined based on the quality metrics evaluated from output frames, and the size of the image tiles (contextual regions) is also determined automatically using a global entropy function. The thesis also gives an in-depth analysis of the

proposed system using three different target distribution functions, and three interpolation techniques.

An integral part of the experimental analysis phase of every algorithm presented in this thesis is an extensive performance evaluation of the developed framework using both quantitative and subjective assessments of image quality. The synthetic images generated by our algorithm are analysed using second order statistical features, and texture features to compare their image quality against real ultrasound images, and to obtain the optimal sampling resolution and interpolation scheme. Similarly, the outputs of the despeckling frameworks are also analysed using several quantitative metrics of image quality such as structural similarity index and edge preservation index. Since image quality does not often directly correspond to usefulness, subjective evaluation by clinical experts is also given equal importance as quantitative evaluation.

The thesis demonstrates that the proposed framework for synthetic ultrasound image modelling can generate images with texture features closely matching real ultrasound images. The thesis proves the effectiveness of the novel clustering algorithm in wavelet transformed sub-bands for edge preserving speckle suppression. The thesis also establishes the capability of the proposed despeckling algorithm based on steerable pyramid transformation in achieving high speckle reduction levels while enhancing texture and image features. An extensive quantitative analysis of the modified contrast limited adaptive histogram equalization method shows that the proposed algorithm could generate outputs with improved visual quality, contrast, and structural content preservation in ultrasound images, compared to several well-known methods for feature enhancement. Finally, the thesis proposes an integrated framework based on the above methods for feature enhanced speckle reduction in medical ultrasound images.

The thesis also outlines future research directions based on the work presented in the thesis and on-going research work on the development of convolutional neural networks, using ultrasound video frames as input.

Index Terms: *Medical ultrasound scans, Synthetic ultrasound image modelling, Speckle simulation, Interpolation, Feature extraction and selection, Gray level co-occurrence matrix, Local binary patterns, Image quality measures, Speckle filtering, Clustering algorithm, Steerable pyramid transform, Contrast limited adaptive histogram equalization.*

GRAPHICAL ABSTRACT

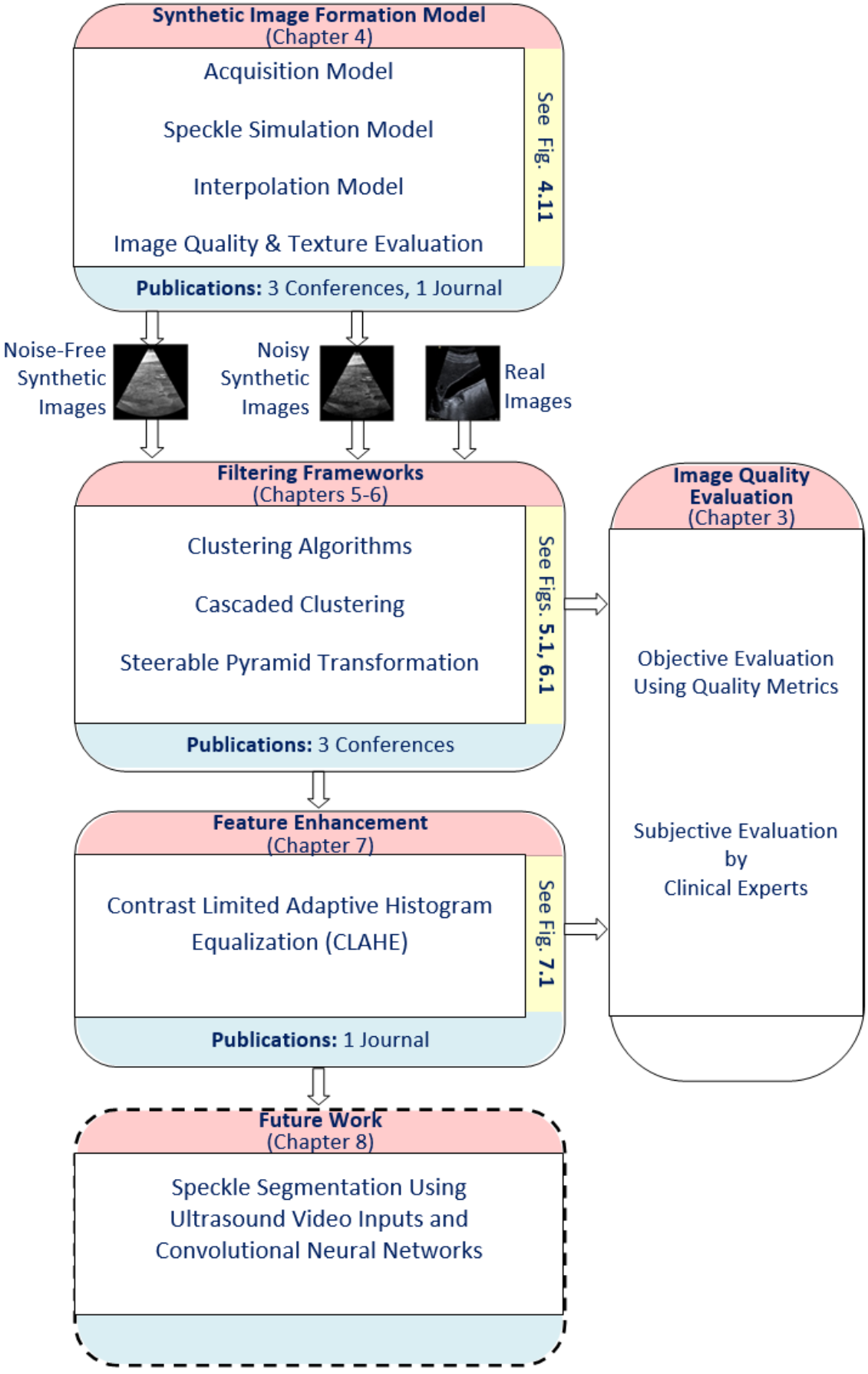

ACKNOWLEDGEMENTS

My wholehearted gratitude goes first to Dr. Ramakrishnan Mukundan, who expertly guided me through my PhD degree with his unparalleled knowledge and research experience in the field of medical image analysis. His unwavering enthusiasm and motivation kept me constantly engaged with the research. I appreciate his encouragement and advice throughout my research that made my PhD experience both productive and stimulating. I would also like to extend my thanks to my associate supervisor Dr. Rex De Ryke, for his guidance, encouragement, and feedback throughout this dissertation. His inputs were extremely valuable for my research work.

I acknowledge the help extended Dr. Khadijah Hajee Abdoula, Victoria Hospital, Quatre Bornes, Mauritius, Dr. Vivek Aggarwal, Thyroid Clinic, New Delhi, India, and Dr. Joe Antony, MD, India in providing their expert advice, valuable inputs and subjective evaluation of clinical post processed ultrasound images produced in this research. Dr. Joe Antony, MD, also provided several anatomical ultrasound scans used in this research work.

I gratefully acknowledge the College of Engineering Scholarship and the University of Canterbury Doctoral Scholarship, without which I would not have been able to pursue and accomplish my doctoral dissertation.

I am grateful to the Department of Computer Science and Software Engineering for providing a pleasant and friendly work environment. I would also like to thank the administrative and technical staff of the department for their constant help and support throughout my research.

My appreciation also extends to my lab companions (Tieta, Alan, Ori, Dibash, Hai Peng, Antony, David, and Sarmad) and departmental colleagues for all those light and cheerful moments that I shared with them.

I am fully indebted to my parents for their endless love, support and encouragement - they always believed in me and wanted the best for me. I would like to acknowledge my friend Yogesh Kumar for his understanding, and encouragement and for pushing me farther than I thought I could go.

I am most grateful to God for his incredible protection and support throughout my life.

CONTENTS

LIST OF TABLES

LIST OF FIGURES

LIST OF ABBREVIATIONS AND ACRONYMS

AFLF	Adaptive Fuzzy Logic Filters
BM3D	Block Matching 3D Filtering
BPF	Band Pass Filter
CCA	Common Carotid Artery
CCE	Coherence Component Extraction
CD-MAP	Curvelet Domain Using Diffusion Filter and MAP Estimation
CLAHE	Contrast Limited Adaptive Histogram Equalization
CNN	Convolutional Neural Network
CT	Computed Tomography
DFT	Discrete Fourier Transform
DHWF	Data-Driven Hyperbolic Wavelet-Fisz
DPAD	Detail Preserving Anisotropic Diffusion
DTCWT	Dual Tree Complex Wavelet Transform
DWT	Discrete Wavelet Transform
EPI	Edge Preservation Index
FCM	Fuzzy C-Means
FESR	Feature Enhanced Speckle Reduction
FPCM	Fuzzy Possibilistic C-Means
FSIM	Feature Similarity Index Metrics
GLCM	Gray Level Co-Occurrence Metrics
HMBS	Homogeneity Modified Bayes Shrink
HPF	High Pass Filter
HVS	Human Visual System
HWF	Hyperbolic Wavelet-Fisz
IQM	Image Quality Metrics
LBP	Local Binary Pattern
LMMWT	Laplacian Mixture Model and Wavelet Transform
LOG	Logarithmic
MAP	Maximum A Posteriori
MAWF	Modified Adaptive Wiener Filter
MR	Magnetic Resonance
MSE	Mean Square Error

NLM	Non-Local Mean
NLMLS	Non-Local Mean Local Statistics
NMCWDA	Non-Linear Multi-Scale Complex Wavelet Diffusion Based Algorithm
NMWD	Nonlinear Multiscale Wavelet Diffusion
NS	Neutrosophic
NSD	Neutrosophic Domain
PCM	Possibilistic C-Means
PFCM	Possibilistic Fuzzy C-Means
PMAD	Perona Malik Anisotropic Diffusion
PSNR	Peak Signal to Noise Ratio
SAM	Spectral Activity Measure
SAR	Synthetic Aperture Radar
SFM	Spatial Frequency Measure
SPT	Steerable Pyramid Transformation
SRAD	Speckle Reducing Anisotropic Diffusion
SSIM	Structural Similarity Index Metrics
TIBT	Translational Invariant Second-Generation Bandelet Transform
TV	Total Variation
TVMB	Modified Bayes Shrink with TV Regularization
UQI	Universal Quality Index
WGF	Wavelet Guided Filter

LIST OF RESEARCH PUBLICATIONS

1. **Singh, P.**, Mukundan, R., & Ryke, R. D. (2017). Synthetic models of ultrasound image formation for speckle noise simulation and analysis. International Conference on Signals and Systems (ICSigSys), Bali, Indonesia, 16-18 May 2017, pp. 278-284. doi:10.1109/icsigsys.2017.7967056.

2. **Singh, P.**, Mukundan, R., & Ryke, R. D. (2017). Modelling, Speckle Simulation and Quality Evaluation of Synthetic Ultrasound Images. 21th Medical Image Understanding and Analysis (MIUA), Univ. of Edinburgh, 11-13 July 2017, Springer CCIS 723, pp. 74-85. doi:10.1007/978-3-319-60964-5_7. (*This paper was selected for publication of an extended version in the Journal of Imaging*)

3. **Singh, P.**, Mukundan, R., & Ryke, R. D. (2017). Quality analysis of synthetic ultrasound images using co-occurrence texture statistics. 20th International Conference on Image and Vision Computing New Zealand (IVCNZ), Christchurch, New Zealand, 4-6 Dec 2017. doi:10.1109/ivcnz.2017.8402511.

4. **Singh, P.**, Mukundan, R., & Ryke, R. D. (2018). Texture Based Quality Analysis of Simulated Synthetic Ultrasound Images Using Local Binary Patterns. Journal of Imaging, 4(1), 3. doi:10.3390/jimaging4010003.

5. **Singh, P.**, Mukundan, R., & Ryke, R. D. (2018). A Comparative Analysis of Clustering Algorithms for Ultrasound Image Despeckling Applications. 2nd International Conference on Graphics and Signal Processing - ICGSP18. Sydney, Australia, 6-8 October 2018, ACM Proceedings. pp. 51-56. doi:10.1145/3282286.3282290

6. **Singh, P.**, Mukundan, R., & Ryke, R. D. (2018). A Novel Ultrasound Image Enhancement Algorithm Using Cascaded Clustering on Wavelet Sub-bands. 29th Irish Signals and Systems Conference (ISSC). Queen's University of Belfast, 21-22 June 2018. doi:10.1109/issc.2018.8585350.

7. **Singh, P.**, Mukundan, R., & Ryke, R. D. (2018). Enhanced Steerable Pyramid Transformation for Medical Ultrasound Image Despeckling. IEEE 20th International Workshop on Multimedia Signal Processing (MMSP). Simon Fraser University, Vancouver, Canada, 29-31 Aug 2018. doi:10.1109/mmsp.2018.8547091. (*This paper received the top 5% award by the IEEE Signal Processing Society, Vancouver*)

8. **Singh, P.**, Mukundan, R., & Ryke, R. D. (2019). Feature Enhancement in Medical Ultrasound Video using Contrast Limit Adaptive Histogram Equalization. Journal of Digital Imaging, Springer, doi: 10.1007/s10278-019-00211-5.

1 INTRODUCTION

One of the fundamental aims of ultrasound image analysis algorithms is to increase the diagnostic value of the images for improving workflow in diagnosis and treatment. Ultrasound images are inherently corrupted by speckle artifacts that degrade quality. Considerable amount of research work is still being done on the analysis and removal of speckle noise in medical ultrasound images. These algorithms primarily focus on the characteristics of speckle noise and try to minimize its effects on image interpretation. This thesis addresses the need for generating accurate synthetic models of ultrasound images for applications in speckle noise analysis, and proposes an innovative framework for simulated ultrasound image formation model that supports a wide range of image and noise characteristics useful for filtering methods and noise analysis. The thesis also contributes to the advancement of feature enhanced speckle reduction techniques by (i) developing novel frameworks for transformation based despeckling, and adaptive contrast enhancement, and (ii) performing extensive evaluation of the proposed methods using both synthetic and medical ultrasound images with a wide range of image quality metrics and qualitative assessments by clinical experts.

This chapter provides a general introduction to the research problems addressed in the thesis, outlines the research motivation and objectives, and discusses the main contributions.

1.1 Ultrasound Imaging

Ultrasound imaging modality is well suited for organ and tissue imaging, and is commonly used for medical diagnosis owing to several desirable characteristics that

minimize health risks such as non-invasiveness and absence of any form of ionizing radiation. It is also less expensive than other imaging methods like Computed Tomography, Magnetic Resonance Imaging, and Positron Emission Tomography. Medical ultrasound images are produced using ultrasonic waves in 3 to 20 MHz range that travel through body tissues when transmitted from a transducer. When a wave reaches an object or surface with a different texture or acoustic nature, it is echoed and received by the transducer array and transformed into electric current. The returning echoes are amplified in proportion to their return time called time gain compensation. A signal processing unit transforms these echoes into 2-dimensional images. Thus, ultrasound imaging involves signals which are produced through the coherent summation of echo signals from scatterers in the tissues. The commonly used modality of ultrasound image is B-mode (brightness mode) imaging in which the echoes are displayed as 2D gray scale image pixels. There are two major categories of scattering namely diffuse scattering that yields speckle in the image, and coherent scattering which forms dark and lighter features. This is an inherent property of medical ultrasound imaging and it decreases the image resolution and contrast and hence affects the diagnostic value of the imaging modality.

Different kinds of noise present in ultrasound images are amplifier noise, impulsive noise and speckle artifacts. Gaussian noise is a type of amplifier noise whereas speckle is a granular pattern with multiplicative nature, which is predominant in ultrasound imaging systems. The usefulness of the ultrasound imaging is degraded by the presence of the speckle content and it is multiplicative in nature. Speckle formation phenomena depends on a number of factors such as the presence of background tissue, other organs and anatomical structures like body fat, and breathing motion. The granular pattern of speckle artifacts reduces the image contrast and conceals image details. Speckle artifacts also make tasks such as feature extraction, classification, and segmentation difficult in image analysis applications.

Several filtering techniques have been used to reduce speckle in ultrasound images. Choosing the best technique for removing the speckle noise is a challenging task. The noise smoothening techniques can cause loss of texture details in an image that are important in clinical interpretations. Speckle reduction is a precondition for effective performance of several downstream processes like image restoration, classification and segmentation. These processes give a high importance to features such as gray scale, edge, texture, boundary, shape, and structure. Therefore, a detailed

analysis of image features and methods for their enhancement have also gained importance in the field of ultrasound image analysis.

1.2 Thesis Overview

This thesis focusses on novel algorithms and image analysis frameworks necessary for improving the quality of medical image analysis algorithms by reducing the speckle content present in the images and enhancing the features that are important for diagnostic interpretation. The research reported in the thesis can be grouped into three main areas: (i) modelling, simulation and quality evaluation of synthetic ultrasound images, (ii) edge preserving despeckling, and (ii) contrast enhancement. The methods developed as part of the above three research areas are integrated into a single framework for feature enhanced speckle reduction, after extensive quality evaluation of the outputs of each stage using several image quality metrics and subjective assessments by clinical experts. The following sections describe the need aspects including research motivation for carrying out this research, the goals of the thesis, the research questions addressed by the thesis, the main contributions and finally the overall structure of the thesis.

1.3 Research Motivation

In the field of ultrasound image analysis, feature enhanced speckle reduction algorithms are gaining importance due to their usefulness in segmentation and classification methods. Numerous methods have been recently reported in the literature for speckle artifact reduction in ultrasound images. For quantitative performance analysis of despeckling algorithms, we require ideal noiseless images, and also a model to generate realistic images where the amount of noise can be adjusted in a controlled manner. In existing methods, the images produced lack realism because either the image acquisition model was not considered or standard test images (eg. Lena) that bear no resemblance to ultrasound images were used. In addition, the texture features of the generated images were not evaluated and compared with that of real ultrasound images. The above has been the primary motivation for developing and evaluating a complete framework for the generation of synthetic ultrasound images.

Clustering algorithms have been successfully used for speckle noise suppression in synthetic aperture radar (SAR) images. Both SAR and ultrasound are coherent

imaging systems, and therefore the clustering techniques used for speckle suppression for SAR images could be adopted for ultrasound despeckling. However, no prior work on clustering based speckle suppression for ultrasound images has been reported. This has been the main motivation to test the feasibility of a despeckling framework using clustering algorithms, and to develop a useful technique by analysing the performance of several types of clustering methods. The second filtering method uses a powerful technique called steerable pyramid transformation to achieve both speckle reduction and sufficient improvement of visual features. Not much work has been reported in literature on steerable pyramid transformation methods for ultrasound image despeckling. Similarly, the contrast limited adaptive histogram equalization (CLAHE) method has been effectively used for feature enhancement in video compression, feature improvement of magnetic resonance and micro-angiography images, and image watermarking algorithms, but not for improving features in ultrasound images. This thesis addresses this gap and develops a novel and modified version of the CLAHE algorithm specifically suited for ultrasound images.

1.4 Research Questions and Objectives

As mentioned in the previous section, a framework for modelling synthetic ultrasound images whose image and texture features closely match those of real ultrasound images is the first step towards the development of a more comprehensive system for speckle reduction and feature enhancement. The main research questions in this area are listed below:

- What are the sampling schemes and interpolation methods required to generate accurate acquisition models of both sector and linear scans?
- How should the speckle artifact distribution be modelled?
- Which interpolation method generates images with minimal visual artifacts?
- What descriptors should be used to compare the texture characteristics of the generated images with real images?
- When the parameters controlling the resolution in a sampling method are adjusted from coarse to fine, do the values of the corresponding feature vector consistently tend towards the reference feature vector?
- What sampling scheme and the values of modelling and noise parameters generate synthetic ultrasound images which features that closely match real images ?

The main aim of this part of the research study is to develop a framework for modelling synthetic ultrasound images that allows variations in modelling and noise parameters, and to perform an extensive evaluation of texture features to determine the optimal set of parameters that generate synthetic images closely matching that of real ultrasound images.

The second part of this research study considers transformation based methods for speckle artifact suppression while preserving edge information. Several clustering methods (K-means, Fuzzy C-means , Possibilistic C-means etc.) are considered in the wavelet transformed sub-bands. A speckle reduction method based on enhanced steerable pyramid transform is also considered. The research questions in this area are listed below:

- Could transform based approaches be used for effective despeckling in ultrasound images?
- Can steerable pyramid transformation based speckle artifact suppression approach help to improve the visual image features e.g. contrast, edges, structural content, homogeneity etc.?
- What objective evaluation metrics should be used to validate the developed methods using synthetic ultrasound images, and to select the best model (clustering method, parameters etc.)?
- How should the usefulness of the developed system for real medical ultrasound images be verified?

The main aim of this part of the research study is to develop a framework for edge preserving speckle filtering using transform based approaches, and to carry out an extensive performance evaluation by comparing the speckle filtered synthetic images with the corresponding noise-free synthetic images. The thesis also aims to validate the proposed methods by performing a subjective evaluation of the outputs for real ultrasound images. In addition, the thesis also aims to establish the usefulness of the synthetically formulated images for the performance evaluation of the despeckling system.

The third part of this research study considers the need for effective contrast enhancement while maintaining the visual quality of the images, and proposes a modified version of the contrast enhanced adaptive histogram equalization algorithm. The main research questions in this area are listed below:

- Could the clip limit and tile size of the CLAHE algorithm be automatically evaluated based on image characteristics?
- How does the quality of the outputs vary with the choice of histogram distribution functions and tile interpolation schemes?
- What objective metrics should be used to evaluate the performance of the proposed CLAHE algorithm?

The aims of the thesis in this part of the research study are to develop and validate the proposed modified version of the CLAHE algorithm where the clip limit and tile size are automatically determined, and the performance evaluated using three different histogram distribution functions and three interpolation methods.

The final part of this research study integrates the previous two stages to form a feature enhanced speckle reduction framework. The main research questions for this part are listed below.

- Which of the two proposed filtering methods, when combined with the CLAHE algorithm, gives the best performance in terms of time complexity and the quality of the generated feature enhanced speckle filtered images?
- How could the usefulness of the combined feature enhanced speckle filtering framework be established?

The thesis aims to combine the proposed filtering methods with the CLAHE algorithm and compare the performance of both methods using real medical ultrasound images. This leads to the next and final aim of the thesis, which is to propose a fully evaluated feature enhanced speckle filtering pipeline that enhances the overall image quality and diagnostic value of medical ultrasound images.

1.5 Research Methodology

Based on the research goals discussed in the previous section, the research methodology adopted for achieving those aims can also be categorized into four main stages as detailed below.

Stage 1: In this stage, the framework for modelling synthetic ultrasound images is developed. Three different sampling schemes, namely, radial polar, radial uniform, and uniform grid are considered, along with three different interpolation techniques. The quality of the synthetically generated output images analysed by image quality metrics that are entropy, spectral activity measure (SAM) and spatial frequency measure (SFM). In the validation phase, two texture descriptors, namely, Gray Level Co-occurrence

Matrix (GLCM) and rotation invariant uniform Local Binary Patterns (LBP) are used to measure the texture similarity between synthetic and real ultrasound images.

Stage 2: In this stage, the outputs of the validation phase of the previous stage consisting of synthetic images that closely resemble real medical ultrasound images in terms of their image and texture characteristics are used to test the performance of filtering methods. Both the clustering algorithm and the steerable pyramid transformation algorithm are extensively tested to analyse their performance and to determine the optimal set of models (combinations of clustering methods) and their parameters. Objective quality metrics used in this process are Peak Signal to Noise Ratio (PSNR), Structural Similarity Index Metric (SSIM), Universal Quality Index (UQI), and Feature Similarity Index Matrix (FSIM). The optimal set of parameters obtained from the above testing phase is used when analysing the despeckling framework with real ultrasound images as inputs. In this analysis phase, the quality of filtered ultrasound images obtained as outputs is evaluated using subjective assessments by clinical experts.

Stage 3: In this stage, a novel contrast limited histogram equalization method is designed, and tested using real despeckled ultrasound images obtained at stage 2. Objective quality metrics used in this process are EPI, UQI, and SSIM.

Stage 4: The final development and analysis stage involves the integration of the filtering stage with the contrast enhancement stage to form a feature enhanced speckle reduction pipeline. The validation phase of this stage also involves the use of image quality metrics to determine the best combination (among clustering+CLAHE and SPT+CLAHE) and the optimal set of system parameters that provide the required result. The quality of outputs are further verified by subject matter experts and recorded as subjective assessment scores.

The four primary stages of the research methodology detailed above are also shown diagrammatically in Figure. 1.1 below.

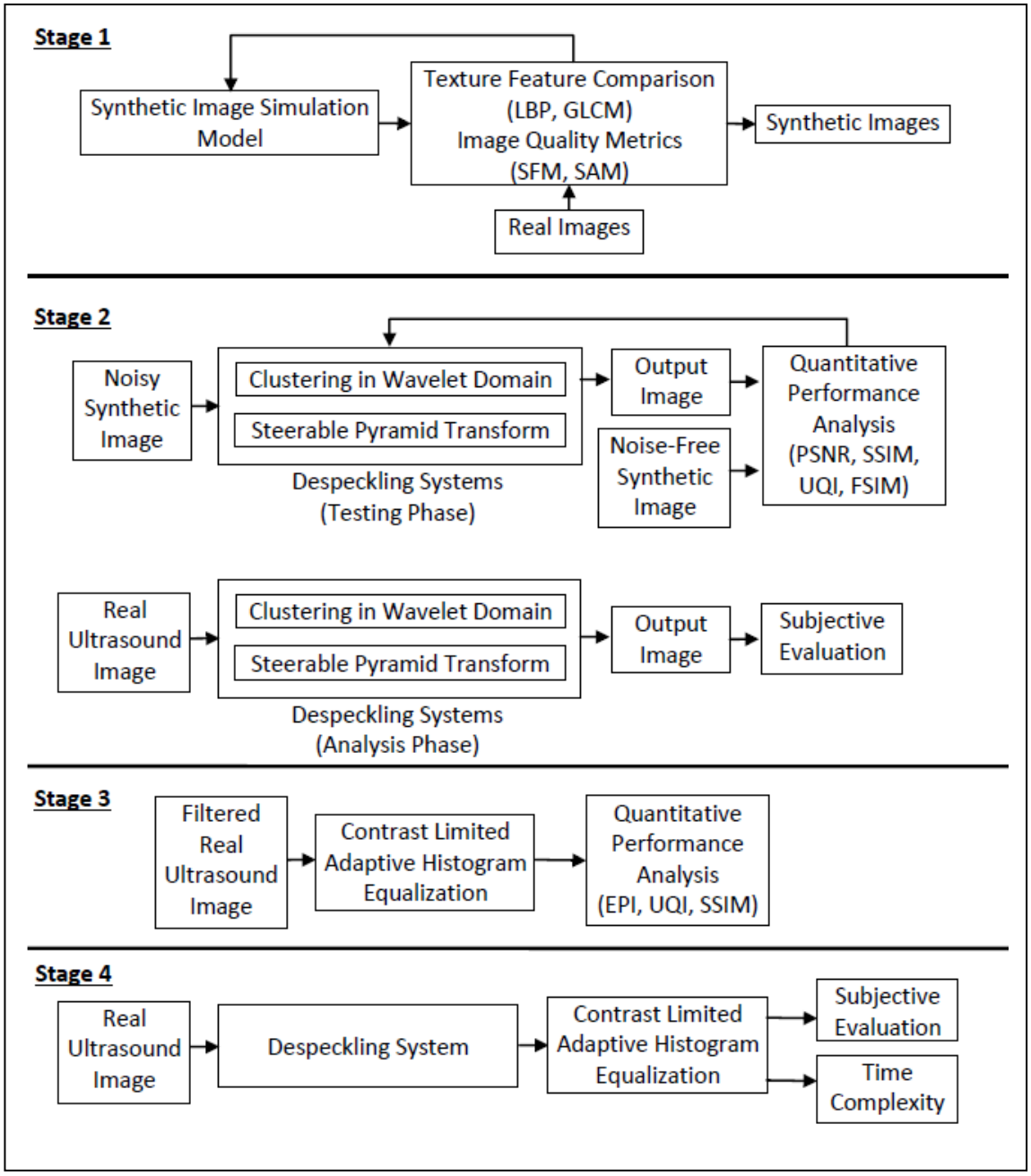

Figure 1.1: The four primary stages used in the research workflow.

1.6 Thesis Organisation

An overview of the contents of each chapter is given below.

Chapter 2 provides a background to this work. It gives a review of academic literature on synthetic ultrasound images, filtering methods for speckle reduction, despeckling using frequency domain transforms. It also gives an introduction to the features that are important in ultrasound image analysis and reviews methods on feature enhancement.

Chapter 3 describes the materials and important methods used to carry out the research presented in the thesis. Specifically, it describes the datasets used in the research, and gives an outline of the main algorithms used in each of the remaining chapters. It also gives a description of the image quality metrics used in the experimental evaluation of the algorithms.

Chapter 4 describes the first main contribution of the thesis, which is a complete framework for modelling and evaluating synthetic ultrasound images. It discusses in detail the sampling model, speckle simulation model, interpolation model and the evaluation model used in the framework. Experimental results obtained using various image quality metrics and texture descriptors are given in detail.

Chapter 5 describes the second main contribution of the thesis which is a novel algorithm for ultrasound despeckling using clustering algorithms in the wavelet domain. This chapter introduces various clustering algorithms and gives a detailed experimental evaluation of the proposed method using both synthetic and real ultrasound images.

Chapter 6 develops another novel transform based algorithm for ultrasound despeckling using steerable pyramid transformation. This chapter also introduces concepts related to the modified adaptive Weiner filter and coherence component extraction. Similar to the previous chapter, experimental analysis using synthetic and real ultrasound images are presented.

Chapter 7 develops a modified contrast limited adaptive histogram equalization algorithm for enhancing features in ultrasound images. It gives an outline of the processing pipeline along with a description of the methods to automatically evaluate the clip limit and tile size. Experimental results showing the variations in the output with the selection interpolation methods and histogram distribution functions are given.

2 BACKGROUND RESEARCH

Medical ultrasound image or video analysis continues to be an active area of research with the development of several new techniques for filtering, segmentation and classification that have found applications in computer aided detection and diagnosis systems. This chapter gives a discussion of relevant academic literature including an overview of current research trends and developments in important areas of this vast research field. The primary goals of this chapter are to

- provide the context of existing literature for the research work presented in the thesis.
- identify and describe the relationship between important aspects of the research work presented in the thesis and similar research work already reported in literature.
- determine any gaps in previous research and consider major issues in each topical area.

In this chapter, the review of literature has been divided into five distinct areas, one for each major areas of contribution of the thesis, as listed below.

1. Synthetic ultrasound image formation models: Novel modelling algorithms for generating synthetic ultrasound images with image and texture characteristics resembling real-ultrasound images, are presented in Chapter 4.
2. Speckle reduction using filtering techniques: Methods for reducing speckle artifact in medical ultrasound images by using different types despeckling systems are given in Chapter 5-7.

3. Speckle reduction using clustering based algorithms: In Chapter 5, 6, and 7, the thesis introduces methods for speckle reduction using clustering algorithms.
4. Speckle reduction using frequency domain techniques: The thesis proposes (Chapter 7) a method using steerable pyramid transformation and the analysis of signal and noise coefficients in the wavelet domain.
5. Feature descriptors, extraction and enhancement: Several techniques for computing shape, intensity and texture features in ultrasound images and methods for their characterization and enhancement are presented in Chapter 4 and 8.

To provide a clear distinction between research presented in the thesis and work reported in literature, *the description of work pertaining to the thesis is given in italics* in the following sections.

2.1 Modelling of Synthetic Ultrasound Images

This thesis has identified the need for generating noise-free synthetic ultrasound images with texture and intensity characteristics closely matching real ultrasound images, to which noise can be added in a controlled manner. Even though such images are particularly useful for the analysis of noise filtering algorithms and for generating ground truth data for evaluating the performance of filtering methods, only very limited research work has been reported in this area.

(Perreault & Auclair-Fortier, 2007) introduced a novel technique to simulate B-mode medical ultrasound speckle in synthetic images. Their work incorporated models for both ultrasound image acquisition and speckle formation. Their model used a sampling grid in a radial-polar arrangement to simulate the acquisition and quantization steps of image formation. However, the authors used standard test images that do not bear any resemblance to real ultrasound images. *This thesis extends their work by introducing three modelling grids, viz., radial-polar, radial-uniform, and uniform-grid, with which image formations of both sectoral scans and linear scans can be simulated. The thesis also has presented extensive image quality analysis to compare intensity, texture and noise characteristics of the generated images with real ultrasound images (Chapter 3).*

(Shams, Hartley, & Navab, 2008) presented a novel technique for simulation of ultrasound images from 3D CT images. The pre-processing phase yielded the fixed-view 3D scattering images and the run-time phase generated the view-dependent

ultrasonic artifacts for the aperture geometry and location within a volume of interest. A simple acoustic model was developed for simulation of ultrasound images by considering large scale reflections, effect of finite beam widths, view-dependent shadows, and attenuation due to reflections. *In comparison, our model uses three types of pre-specified patterns of sampling points to which speckle noise is added and interpolated to get the synthetic image. This model is computationally simpler, yet capable of generating images with variations in both axial and lateral resolutions and a range of noise parameters.*

(Song, Zhou, Wang, Zhao, & Elson, 2016) proposed a method that was able to generate both single and a sequence of fully developed speckle patterns with predefined correlation distribution using the principle of coherent imaging. The speckle pattern was generated with either uniform or arbitrary correlation distribution in the spatial and temporal domains. The few to one mapping was performed between input correlation matrix and the correlation distribution between simulated speckle patterns. *Our speckle model uses a two-dimensional circular Gaussian function for generating a complex distribution of incoherent phasors, and a combination of sampling and interpolation schemes that allow several parametric variations in the output image.*

2.2 Feature Analysis and Enhancement Methods

This section focusses on the review of academic literature in the field of feature representation and analysis used in medical image analysis. Specifically, two main texture descriptors, namely, local binary patterns, and gray-level co-occurrence matrices are considered.

This thesis explores several ultrasound texture feature analysis and enhancement methods to assess the quality of synthetic ultrasound images and to compare and match texture features of synthetically modelled images with real ultrasound scan images (Chapter 4). Feature improvement method are also considered to improve and preserve edge and fine details present in the ultrasound images (Chapter 5, 6 and 7).

(Zheng, Zhou, Zhou, & Gong, 2015) proposed a novel framework for edge mapping in ultrasound image segmentation application by using new multiplicative gradient operator of non-Newtonian type with Canny detection operator. Various edge detection methods were considered for the comparative analysis.

Canny Edge detection has been used in this thesis in chapters 5 and 6 to preserve the high frequency content (edges) before speckle filtering.

(Liao, Law, & Chung, 2009) proposed a novel method using dominant local binary patterns and circularly symmetric Gabor filter responses as image features for texture classification. It was experimentally established that the proposed method attained the highest classification accuracy in various texture databases and image conditions.

(Sorensen, Shaker, & Bruijne, 2010) presented a texture based algorithm for emphysema classification in CT images. Their method used local binary patterns as texture features. The LBP features jointly with intensity histogram were used for characterising the texture associated with emphysema within regions of interest.

(Alelaiwi, Abdul, Dewan, Migdadi, & Muhammad, 2016) proposed a facial recognition system for e- Health secure login using steerable pyramid transformation and local binary patterns. In this approach, steerable pyramid transformation was used to decompose facial images into several sub-bands of various scales and orientations, and local binary pattern used to convert sub-bands into binary texture patterns.

(X. Yang et al., 2012) used multi resolution ranklet transform to extract gray-scale invariant features from breast ultrasound images. They also used gray level co-occurrence matrix (GLCM) as texture features in a support vector machine to differentiate between malignant and benign masses.

(Gomez, Pereira, & Infantosi, 2012) analysed the variations of 22 co-occurrence statistics derived from GLCM to categorize breast lesions in ultrasound images. The co-occurrence statistics were computed based on six quantization levels, four orientations and ten distances. The Fisher linear discriminate analysis was used to assess the discrimination power of the extracted texture features.

This thesis explores texture feature analysis methods using GLCM and LBP in Chapter 4 for comparing the statistical and local texture features of the synthetically modeled images with real ultrasound images.

(Peng & Yang, 2010) developed an edge enhancement technique using an image block correlation method. Using the local correlation image they designed an adaptive edge improvement technique for both strong and weak edges present in the ultrasound images.

(Alkhatib, Hafiane, Tahri, Vieyres, & Delbos, 2018) introduced a texture feature based on adaptive median binary pattern for tracking algorithms such as particle filter,

mean-shift, and Kanade-Lucas-Tomasi. They used the algorithm for the development of a fully automatic nerve tracking system in ultrasound images with the accuracy of 95%.

(Sonali, Sahu, Singh, Ghrera, & Elhoseny, 2019) work presents a noise removal and contrast enhancement algorithm for fundus image. Integration of filters and contrast limited adaptive histogram equalization (CLAHE) technique is applied for solving the issues of de-noising and enhancement of color fundus image.

(G. Yadav, Maheshwari, & Agarwal, 2014)utilized the contrast limited adaptive histogram equalization (CLAHE) method to enhance videos containing dense fog. The authors used a Raleigh distribution function to define histogram shape.

(Yousefi, Qin, Zhi, & Wang, 2013) also used a similar method with Raleigh distribution to enhance the quality of optical micro-angiography images. The proposed method was compared with general histogram equalization method and other contrast enhancement methods both qualitatively and quantitatively.

2.3 Filtering Methods for Speckle Artifact Reduction

Filtering methods are commonly used in noise reduction in image and video processing applications. This section investigates various filtering based methods recently developed in the field of ultrasound images and video analysis for speckle reduction. *This thesis proposes novel filtering methods for speckle reduction in chapters 4-7.*

(Santos, Martins, & Mascarenhas, 2017) developed a new patch based method for ultrasound despeckling using modified block matching collaborative filtering (BM3D). In their work, they derived new stochastic distances for the Fisher Tippett distribution and used them as patch distance measures.

(Joseph, Balakrishnan, Balachandran Nair, & Rajan Varghese, 2013) developed a novel weighted linear filtering framework for despeckling ultrasound images with the help of local binary patterns. Their filtering method did not affect important content present in the images and outperformed other traditional filter based methods in terms of image quality and edge preservation.

(Zhang, Wang, & Cheng, 2015) focused on the comparison of despeckle filters particularly for breast ultrasound images. They categorized eleven despeckle filters into local adaptive, anisotropic, multi-scale, non-local means, and hybrid filter. They used data sets containing ultrasound breast images and simulated images for comparative analysis.

(Rafati, Arabfard, Zadeh, & Maghsoudloo, 2016) evaluated the filters used for speckle reduction in ultrasound images of the common carotid artery (CCA) as well as the brachial artery. They proposed an innovative merged speckle reducing anisotropic diffusion (SRAD) filter along with Canny edge detection. Their experimental results gave improved MSE and the PSNR values.

(Elyasi & Pourmina, 2016) introduced innovative approaches for speckle reduction based on TV regularization and modified Bayes shrink. They used discrete wavelet transform on the coefficients obtained from total variation. Then they applied soft thresholding and Bayes shrink on the detail sub bands coefficients without changing the coefficients of the approximation. The output image was obtained by inverse wavelet transform.

(Elyasi, Pourmina, & Moin, 2016) introduced a speckle reduction algorithm for breast cancer ultrasound images using a combination of homogeneity filtering and modified Bayes shrink methods. Their algorithm could effectively distinguish homogeneous regions from areas in the image containing speckle noise.

(Koundal, Gupta, & Singh, 2016) proposed a variational approach based on Gamma distribution in the neutrosophic (NS) area to improve ultrasound image quality. In this method, the image was transformed into the neutrosophic domain via three membership subsets (real, indeterminate and false), and filtering operation applied based on total variation regularization.

(J. Yang et al., 2016) proposed the modelling of intensity distribution using local statistics and a non-local mean (NLM) filter to reduce speckle using the redundancy information in noisy images. This approach estimated speckle statistics by local patches, and intensity of despeckled pixel is evaluated by the weighted average of all the pixels by using non-local mean filter.

(Sudeep et al., 2016) developed a speckle suppression frame work using non-local mean speckle filter based on Gamma distribution model. The scale and shape parameters of Gamma distribution estimated by maximum likelihood estimator. The unbiased non-local mean method was applied to determine the true underlying intensity value for each pixel present in the image. The analysis of proposed system was carried out on both synthetic and real B-mode ultrasound images to demonstrate the efficacy of the method.

(Hiremath, Prema T. Akkasaligar, & Badiger, 2010) presented various filters such as Lee, Kaun, Frost, and Wiener, and algorithms for speckle suppression in

medical ultrasound images. They also gave importance to transform domain methods e.g. wavelet, Laplacian pyramid, and Contourlet. Their study showed that a linear regression model for Gaussian representation of speckle artifacts was an efficient way to achieve speckle suppression and reduced computational cost.

(Coupe, Hellier, Kervrann, & Barillot, 2009) proposed a nonlocal (NL)-means filter using Bayesian framework designed for ultrasound noise model. They used synthetic phantom images corrupted with noise for quantitative evaluation.

(Panigrahi, Verma, & Singh, 2019) used speckle reducing anisotropic diffusion (SRAD) technique to filter speckle from ultrasound images prior to lesion segmentation. The segmentation algorithm used multi scale Gaussian kernel fuzzy clustering and multi scale vector field convolution methods.

(Perperidis et al., 2017) introduced dynamic histogram based intensity mapping for speckle suppression in cardiac B-mode scans. The method used temporal variations in the cumulative histograms of the images for contrast enhancement. The authors used both standard image quality measures and repeatability of clinical measurements to evaluate the effectiveness of the proposed techniques.

(Finn, Glavin, & Jones, 2011) provided a comprehensive description and evaluation of fifteen speckle reduction filters. They used both simulated images and clinical videos for performance comparison. They also performed quantitative analysis using image quality metrics to assess the capability of the filtering techniques in preserving edges, reducing image distortion and improving contrast. Their work concluded that the OSRAD diffusion filter was the optimal method capable of strong speckle suppression.

(Mishra, Chaudhury, Sarkar, Soin, & Sharma, 2018) presented a framework for speckle suppression based on the modified anisotropic diffusion filter. Their method was able to remove spurious edges by using image pixel relativity information along edge's probability density function to manage the diffusion flux flow. The authors used measures such as signal-to-noise ratio, mean square error and structural similarity index to compare the performance of the proposed filter against existing methods. They also used subjective evaluation by expert radiologists.

(Zhu et al., 2017) proposed a framework for the reduction of speckle using the concept of phase congruency. To efficiently distinguish speckle noise from features, they included a feature asymmetry metric in the objective function's regularization

term. The authors used simulated on the real ultrasound images to evaluate the proposed methods.

(Saadia & Rashdi, 2016) proposed a two stage methodology by utilizing the fuzzy weighted mean and fractional integration filter to achieve the denoising of ultrasound images. In the processing stage, fuzzy logic was used to assign weights to cells in a 3×3 window around each pixel. This stage achieved noise suppression while preserving features and edges. In the second stage, they used a fractional order integration filter to further enhance the image.

(Sivakumar, Gayathri, & Nedumaran, 2010) presented an extensive comparative study of wavelet filters, nine single scale spatial adaptive filters namely Frost, enhanced Frost, median, Lee, enhanced Lee, Kuan, Gamma map, Wiener, Homomorphic speckle filters, and two diffusion class filters that are speckle reduction anisotropic diffusion (SRAD), Perona Malik anisotropic diffusion (PMAD) filters. The authors used twenty-one image quality metrics for performance analysis. Their study showed that SRAD filter followed by wavelet despeckling filters gave optimum performance compared to other filters.

(Panayides A et al., 2013) examined three video despeckle filters namely linear filtering, hybrid median filtering and speckle reducing anisotropic diffusion filtering methods. Their experimental analysis used ten atherosclerotic plaque ultrasound videos, and considered both subjective and objective video quality assessments. Linear filtering gave best results followed by hybrid median filtering.

(Loizou & Pattichis, 2015a) (Loizou & Pattichis, 2015b) documented a total sixteen different despeckle filters based on linear filtering, non-linear filtering, diffusion filtering, and wavelet filtering. Experimental results obtained using ultrasound phantom, artificial, and real time ultrasound videos were visually evaluated by two medical experts, and quantitative evaluation performed using image quality metrics. Their study suggested that a first order statistic despeckle filter may be applied on ultrasound images to improve the visual perception and quality of images.

(Szczepański & Radlak, 2017) presented a fast spatial and spatiotemporal filters for ultrasound imaging and videos with the aim of suppressing multiplicative noise. Additionally, the new extended neighbourhood model was introduced, based on Neumann concept derived from cellular automata theory. The proposed system was driving satisfactory results in terms of visual inspection.

2.4 Despeckling using Frequency Domain Transform

Multiscale representation has the capability to decompose images into various levels or sub-bands and helps to analyse independent sub bands depending on the requirements of the application such as compression, noise removal, watermarking etc. In the case of speckle noise, a log transform converts multiplicative noise to additive noise. Wavelets and steerable pyramid transformations have been found to be important multiscale transformation methods used in ultrasound image analysis. *This thesis discusses multiscale decomposition methods and log transforms to reduce speckle artifacts from both synthetically modelled and real ultrasound mages (Chapters 5, 6) and to simultaneously preserve significant signal information (Chapter 7).*

(Andria, Attivissimo, Maria Lucia Lanzolla, & Savino, 2013) developed a despeckling method using adaptive data driven thresholding operator based on parametric exponential function applied on wavelet domain coefficients. The proposed method was found to be capable preserving features while reducing speckle in ultrasound images.

(Durand, M. Fadili, & Nikolova, 2009) proposed the variation method using curvelet transform of the log transformed image along with an optimal hard thresholding. The reconstruction was performed applying a hybrid varaitional method to the thresholded curvelet coefficients. Performance evaluation was done on gray scale of images Lena and Boat of size 256×256 pixels.

(Sahu, Bhateja, Krishn, & Patel, 2014) introduced the concept of image fusion using a pyramidal level decomposition using the Laplacian and steerable pyramid in the discrete cosine transform domain. From the human visual system (HVS) point of view, the implemented technique provided better edges and information content.

(Moussa & Khlifa, 2015) proposed a new image denoising technique which was based on the combination of bilateral filter and stationary wavelet transform. They developed a new multi-scale bilateral filter using a new neighbourhood parent-child relationship. The proposed method was found to be effective in contrast improvement, speckle noise reduction, and edge preservation.

(Elamvazuthi, Muhd Zain, & Begam, 2013) experimented with several despeckling filters such as Wiener, average, median, Anisotropic diffusion, and wavelet filtering methods. The experimental evaluation performed using peak to signal ratio image quality measure showed that a combination of Daubechies–Wiener and anisotropic diffusion yielded superior performance.

(Kang, Young Lee, & Yoo, 2015) proposed a novel feature enhanced speckle reduction (FESR) method based on multiscale analysis and characteristic enhancement filtering. In this technique, speckle noise is reduced using diffusion filtering while clinically important features are preserved by edge enhancement filtering. A modified homomorphic filtering was used to enhance low contrast signals. The authors showed that the FESR technique outperformed other techniques such as anisotropic diffusion (OSRAD) and nonlinear multiscale wavelet diffusion (NMWD) filters.

(Farouj, Freyermuth, Navarro, Clausel, & Delachartre, 2017) proposed a method that uses the hyperbolic wavelet transform followed by a Fisz transformation based variance stabilization technique for removing speckle artifacts in ultrasound images. The noise variance was estimated using the isotonic Nadaraya Watson estimator.

(Gai, Zhang, Yang, & Yu, 2017) developed an algorithm for ultrasound image despeckling by using monogenic wavelet transform (MWT) and the Bayesian framework. The effectiveness of the proposed method has been evaluated using real medical ultrasound images and also the synthetic images.

(Dai, Chen, Wang, & Fu, 2015) proposed a novel system for ultrasound image despeckling by combining quantum inspired bilateral filtering and wavelet based thresholding. Their method is designed based on the assumption that signal coefficients follow generalized Laplace distribution while the noise coefficients follow Gaussian distribution. Their method suppress speckle content while preserving high contrast features.

(Sa-ing, Vorasayan, C. Suwanwela, Auethavekiat, & Chinrungrueng, 2017) proposed a framework to deal with both speckle suppression and structural preservation using multiscale adaptive regularization method. Here, the Laplacian pyramid is used to segregate image noise, texture, and object layers and then adaptive regularization Savitzky-Golay filter used on noise and texture layers. The experimental study considered various quality metrics on synthetic and real ultrasound images to show the effectiveness of the proposed method.

(C, rajan, Thangaraj, & Padma, 2018) developed a system based discrete wavelet packet transform and directional filter banks with fuzzy clustering technique to reduce speckle from the ultrasound medical images. The presented framework was able to reduce speckle artifacts while preserving geometrical features.

(Uddin et al., 2016) presented a system for 2D and 3D medical ultrasound images to reduce the speckle content using multi-scale complex wavelet-diffusion based

algorithm (DTCWT). In this framework 2D ultrasound images, the normalized wavelet modulus was modeled as Rayleigh- mixture distribution and 3D imaging modeled as a Maxwell-mixture distribution. The genetic algorithm was used in combination with the expectation maximization method to estimate mixture parameter. The experimental analysis considered clinical data, synthetic data, and physical phantom to show the effectiveness of the method.

2.5 Speckle Reduction using Unsupervised and Supervised Learning Techniques

Speckle suppression in ultrasound imaging modality using unsupervised learning algorithms is relatively a new area of research. Not work have been reported for speckle suppression in ultrasound imaging modality using unsupervised learning algorithms. Sufficient amount of work have been addressed for synthetic aperture radar (SAR) speckle reduction using unsupervised methods. No prior work has been reported on ultrasound images scan speckle reduction using convolutional neural networks. *This thesis presents novel unsupervised techniques based algorithms for speckle characterization and speckle artifact separation in ultrasound scans (Chapter 5).*

(Shanthi & Valarmathi, 2013) proposed a speckle removal and edge preservation system for synthetic aperture radar (SAR) images using Possibilistic Fuzzy C-Means clustering (PFCM) in the translational invariant second-generation bandelet transform (TIBT). In this proposed work first edges are removed using Canny edge detector, TIBT computed in the log transformed images. At the second phase PFCM is applied to high sub-bands and determine the minimum and maximum cluster centers. Here, noise coefficients sets to zero and signal component preserved. The quality of output images are compared with other clustering algorithms e.g. K-Means and Fuzzy C-Means using image quality metrics.

This thesis extends their work by performing comparative analysis of five different clustering algorithms individually and in combination e.g K-Means, Fuzzy C-means, Possibilistic C-Means, Fuzzy Possibilistic C-Means, and Possibilistic Fuzzy C-Means in the area of ultrasound speckle separation (Chapter 5).

(Vimalraj, Esakkirajan, & Sreevidya, 2017) proposed a method to despeckle ultrasound images using dual tree complex wavelet transform (DTCWT) and Possibilistic Fuzzy C-Means clustering. The comparative study was performed with other state of art filters.

(K. Zhang, Zuo, Chen, Meng, & Zhang, 2016) investigated feed-forward denoising convolutional neural networks using residual learning and batch normalization in the training process. Their method was effective in handling Gaussian noise with unknown noise levels.

(Jifara, Jiang, Rho, Cheng, & Liu, 2017) designed the deep feed forward denoising convolutional neural networks model using residual learning method and batch normalization for medical image denoising. In this paper, only X-ray images and mammograms were considered. The quality of the denoised images was evaluated using standard image quality metrics such as peak signal to noise ratio and structural similarity.

(Foucher, Beaulieu, Dahmane, & Cavayas, 2017) presented a CNN algorithm for speckle reduction in single-channel multi-dimensional SAR images. The proposed CNN system was trained on artificial dataset and tested on real SAR images.

(Wang, Zhang, & M. Patel, 2017) proposed a deep-learning based method for multiplicative noise for SAR images. They used batch normalization and rectified linear unit (ReLU) activation functions in the CNN. A component wise division residual layer was used to estimate speckle noise.

(Islam, Mahbubur Rahman, Ahmad, & Swamy, 2018) proposed a convolutional neural network (CNN) model for reducing combinations of Gaussian and impulse noise from images. A computationally efficient transfer learning model was used to obtain the end-to-end map from noisy images to noise free images. The CNN based method provided better results compared to sparse representation and patch based methods.

(Sadda & Qarni, 2018) described the design, training and evaluation of a deep neutral network for eliminating the noise from medical fluoroscopy videos with applications in angiography. The network was trained with images corrupted with Gaussian, speckle, and salt & pepper noise.

2.6 Chapter Summary

The literature review presented in this chapter has identified the importance of filtering techniques and transform based methods for characterization and reduction of speckle artifacts in ultrasound scans. *The thesis uses several of these state-of-the art methods for comparative analysis of the proposed methods.* Most of the methods reviewed also used synthetic images for evaluating the effectiveness of the noise reduction algorithms. However, the synthetic images were constructed from either standard test images (Lena, Boat etc.) or phantom images. This revealed a significant research gap in the field of synthetic ultrasound image and noise modelling. *This thesis has addressed this gap and presented an extensive study of synthetic image generation techniques taking into account various noise and beam parameters related to image acquisition systems.* Nearly all papers on noise reduction methods used quantitative and qualitative evaluation of their algorithms for performance comparison. *The thesis uses a range of image quality metrics to measure the effectiveness of the proposed methods. It also uses subjective evaluation by radiologists and sonographers to assess the usefulness of the generated images and videos considering various visual and texture features commonly used in clinical evaluations.*

The literature review has also identified research gaps in the fields of ultrasound images speckle artifact filtering and feature enhancement. *Two filtering methods have been developed and comparative analysis performed with various well-established state-of-the-art work in the field. The thesis also proposes a modified contrast limited adaptive histogram equalization algorithm for feature enhancement.*

3 MATERIALS AND METHODS

This chapter gives an outline of the materials and methods used in the research work presented in the thesis. The aim of this chapter is to provide an overview of various databases used in the experimental analysis, and also the main algorithms used in the following parts of this research study (Chapters 4-7). This chapter also gives a discussion of various quantitative and qualitative measures used in the experimental evaluation phase of the development of each algorithm.

3.1 Materials

The experimental phase of this research work presented in chapters 5-7 considered two types of databases (i) synthetically modeled ultrasound images explained in detail in chapter 4, and (ii) various real medical ultrasound scans of human anatomical structures acquired from two sources: the Canterbury District Health Board (CDHB), Christchurch, and an online gallery www.ultrasound-images.com owned by Dr. Joe Antony, for which prior permission was obtained for the use of the images in this research work. Some examples of both types of images are shown in the Figures 3.1-3.3.

Figure 3.1: Synthetically modelled ultrasound images of varying beam parameters.

Figure 3.2: Real medical ultrasound scans of thyroid, gallbladder, and liver (from CDHB).

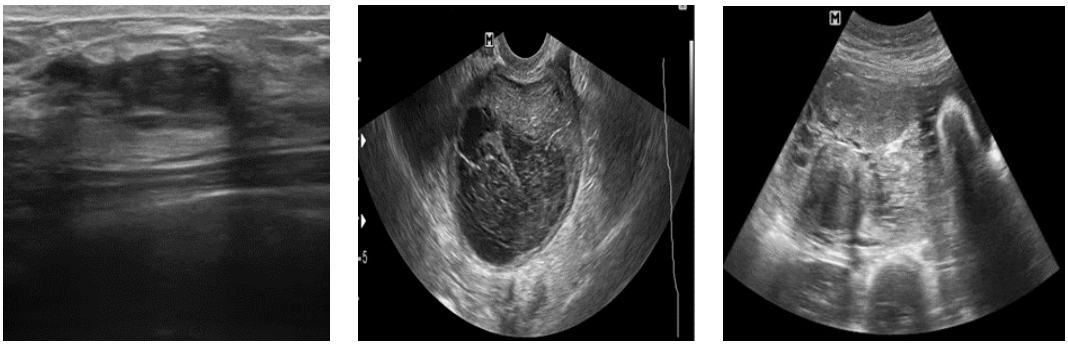

Figure 3.3: Real medical ultrasound scans of malignant breast mass, ovary cyst, and uterus fibroid (from online gallery).

3.2 Methods

This thesis has explored and developed various algorithms for ultrasound scan modelling, texture analysis, speckle filtering, and feature improvement, which are presented in detail in subsequent chapters. Table 3.1 below gives an overview of the important methods used in each algorithm, and also the processes used for evaluating the quality of the generated outputs.

Table 3.1: Overview of the methods and systems adopted in the research work.

Systems	Methods	Evaluation Processes
Modelling of Synthetic Ultrasound Images (Chapter 4)	**Acquisition Models:** 1. Radial Polar 2. Radial Uniform 3. Uniform Grid **Speckle Simulation Model** **Rectification Model** **Interpolation Techniques:** 1. B-linear 2. Cubic 3. Lanczos-3	Entropy Spectral Activity Measure Spatial Frequency Measure Gray Level Co-occurrence Matrices Local Binary Pattern Subjective Evaluation by Clinicians
Filtering Frameworks (Chapters 5,6)	**Clustering Algorithms:** 1. K-means 2. Fuzzy C-means 3. Possibilistic C-means 4. Fuzzy Possibilistic C-Means 5. Possibilistic Fuzzy C-Means **Steerable Pyramid Transformation Techniques:** 1. Canny Edge Detection 2. Modified Wiener Filter 3. Discrete Fourier Transform 4. Coherence Component Extraction	Peak Signal- to-Noise Ratio Structural Similarity Metric Universal Quality Metric Feature Similarity Index Subjective Evaluation by Clinicians
Feature Enhancement Framework (Chapter 7)	**Contrast Limit Adaptive Histogram Equalization**	Structural Similarity Metric Universal Quality Metrics Edge Preservation Index Subjective Evaluation by Clinicians

3.3 Image Quality Assessment

This thesis gives extensive importance to quality assessment of the generated outputs of the various proposed systems/algorithms presented in Chapters 5-7. The quality of the output images are evaluated to determine the improvements in signal-to-noise ratio, measure the similarity with the input images in terms of structure, feature etc., and to assess the overall usefulness from a clinician's perspective. The subjective analysis in this research study was done by experienced radiologists and sonographers. The subject matter experts considered diverse image quality aspects to determine the usefulness for diagnostic interpretation and reasoning, and assigned scores on a five point scale. The objective analysis is performed by using image quality metrics that are detailed below.

3.4 Image Quality Measure

To evaluate the performance of the proposed speckle filtering algorithms and feature enhancement methods (Chapters 5-7), the quality of the output images are compared with the reference images using various metrics such as peak signal to noise ratio, structural similarity metric, universal quality index, edge preservation index, and feature similarity index (Sivakumar, Gayathri, & Nedumaran, 2010). A brief outline of each of these metrics is given in the following sections.

3.4.1 Peak Signal to Noise Ratio (PSNR)

The peak signal-to-noise ratio measures how closely the filtered image resembles the original reference image. It is used to measure the quality (in decibels) of the reconstructed images.

$$\text{PSNR}=10\log_{10}\left(\frac{\text{v}^2}{\text{MSE}}\right) \tag{3.1}$$

$$MSE = \frac{1}{M*N}\sum_{x=1}^{M}\sum_{y=1}^{N}\left(n_o(x,y) - n_r(x,y)\right)^2 \tag{3.2}$$

where, $n_o(x,y)$ and $n_r(x,y)$ are the output and reference images, *MSE* is mean square error and *v* is the maximum possible value in the input image.

3.4.2 Structural Similarity Index Metric (SSIM)

The SSIM can be defined as quality metric, which is based on the HVS. Structural similarity between input and output image is given by,

$$SSIM = \frac{(2\mu_o\mu_r+2.55)(\sigma_{or}+7.65)}{(\mu_o{}^2+\mu_r{}^2+2.55)(\sigma_o{}^2+\sigma_r{}^2+7.65)} \ , \ -1 < SSIM < 1 \quad (3.3)$$

where μ_o, μ_r and σ_o, σ_r are the means and standard deviations of the two images (output and reference image), and σ_{or} is the covariance between the two images.

3.4.3 Universal Quality Index (UQI)

The UQI quality metric is used to provide information on the distortion between two images by combining three factors namely, contrast distortions, luminance distortions, and loss of correlation. UQI can be estimated using the equation given below.

$$UQI = \xi.\tau.c \quad -1 < UQI < 1 \quad (3.4)$$

$$\xi = \frac{\sigma_{or}}{\sigma_o\sigma_r}, \ \tau = \frac{2\mu_0\mu_r}{\mu_o{}^2+\mu_r{}^2} \ , \ c = \frac{2\sigma_o\sigma_r}{\sigma_o^2+\sigma_r^2} \quad (3.5)$$

where, ξ is the correlation coefficient that defines the correlation between original image and processed image, τ measures the similarity of mean luminance between the two images and c refers to contrast similarity of the images.

3.4.4 Feature Similarity Index Metric (FSIM)

The FSIM measures the similarity between two images. It is defined based on the luminance components of a color image or a gray scale image. Generally, human visual systems (HVS) interpret an image mainly through its low-level features or high frequency components. The FSIM metric is defined as

$$FSIM = \frac{\sum_{\in\Omega} z_{pc}(x) z_G(x) pc_m(x)}{\sum_{\in\Omega} pc_m(x)} \quad (3.6)$$

where, $z_{pc}(x)$ and $z_G(x)$ measure the similarities in phase congruency and in gradient magnitude respectively. Phase congruency decides the significance of the local structure present in the image and is a dimensionless quantity. Gradient magnitude can be expressed by gradient operator which is defined by a convolutional mask. For a given location of x, $pc_m(x)$ denotes the maximum phase congruency between two images.

3.4.5 Edge Preservation Index (EPI)

The EPI measure is generally used to ensure that a certain operation performed on an image preserves edges. If the edges are preserved well, then EPI will have a value close to unity. The Edge Preservation Index metric between two images is given as

$$\mathbf{EPI} = \frac{\sum_{x=1}^{M-1}\sum_{y=1}^{N-1}(\Delta \boldsymbol{n_r}(x,y)-\Delta \boldsymbol{n_r}')(\Delta \boldsymbol{n_o}(x,y)-\Delta \boldsymbol{n_o}')}{\sum_{x=1}^{M-1}\sum_{y=1}^{N-1}(\Delta \boldsymbol{n_r}(x,y)-\Delta \boldsymbol{n_r}')^2(\Delta \boldsymbol{n_o}(x,y)-\Delta \boldsymbol{n_o}')^2} \quad (3.7)$$

where $\Delta n_r(x,y)$ and $\Delta n_o(x,y)$ represents the edge images of reference image $n_r(x,y)$ and denoised output images $n_o(x,y)$. $\Delta n_r{}'$ and $\Delta n_o{}'$ are mean intensities of Δn_r and Δn_o repectively. $\Delta n_r(x,y)$ and $\Delta n_o(x,y)$ are the high pass filtered versions of images $n_r(x,y)$ and $n_o(x,y)$, obtained using a 3×3 pixel standard approximation of the Laplacian operator.

3.5 Chapter Summary

This chapter of the thesis gave an overview of the image datasets used and the various methods adopted for ultrasound modelling, texture analysis, speckle suppression, and feature enhancement algorithms presented in the following chapters. The quality evaluation processes used have been outlined, and the definitions of the objective quality metrics that formed a common basis for the evaluation of methods presented in subsequent chapters have been presented. The next chapter provides the details of the proposed framework for modelling and analysis of synthetic ultrasound images.

4 SYNTHETIC MODELS OF ULTRASOUND IMAGE FORMATION AND TEXTURE FEATURE ANALYSIS

Speckle noise reduction algorithms are extensively used in the field of ultrasound image analysis with the aim of improving image quality, interpretation and diagnostic accuracy. The absence of noise free ground truth data necessitates the generation of synthetic images with features closely resembling real ultrasound images. Synthetic ultrasound images find applications in speckle noise reduction and evaluation algorithms. The modelling of realistic and synthetic ultrasound images with accurate noise and texture characteristics is driven by the need for accurate ground truth data against which the outputs of speckle noise filtering algorithms can be compared. There are three main requirements which such synthetic image generation methods must satisfy: (i) the modelling algorithms should take into account the primary characteristics of the image acquisition system such as the geometrical properties of a sector scan, axial resolution and lateral resolution, (ii) the system should support parametric variations allowing the user to generate a wide range of images with corresponding variations in the intensity and speckle artifacts distribution, and (iii) the generated images should closely resemble real ultrasound images. It is therefore important to evaluate the quality of the images generated by the modelling and simulation algorithm to ensure that the

synthetic images have the required texture features. To our knowledge, no prior work has been reported on texture feature assessment of synthetic ultrasound images.

This chapter presents three novel sampling schemes that could be used for speckle simulation based on a speckle formation model and an ultrasonography image acquisition model. The proposed algorithm has four phases. Initially, the image geometry is altered to fit the sectoral scan of an ultrasound beam by sampling process that simulates the acquisition and quantization steps of image formation. Rectification is performed in second phase. In the third phase, speckle is added to the sampled pixels using the speckle model to get a per-pixel noisy image. The last phase involves interpolation, which is carried out to fill the empty space between the grid's pixels. In the evaluation model, objective assessment of the quality of the generated images is performed by using entropy, spatial frequency measure, spatial amplitude measure, gray level co-occurrence texture statistics, and local binary pattern. The quality of such synthetic images is further validated using subjective evaluations performed by clinical experts. The quality analysis is used to identify the sampling and interpolation model and the optimal set of modelling parameters that generate synthetic ultrasound images whose image and texture features closely match that of real medical ultrasound images.

4.1 Sampling Models

There are two techniques of ultrasound scanning namely sector scan and linear scan. The sector scan uses transmission delays on the array elements to focus the beam and steer it in a particular direction. The sector type of scanning of ultrasound beam is performed by sampling a grid of pixels. The dependence of axial resolution is on the wavelength and the number of repetitions forming the ultrasonic pulses. So, the size of a resolution cell is based on the fact that the spatial resolution of the ultrasound image is less than that of the image. The axial resolution loss due to pulse length is simulated by sampling the synthetic image. Here, discuss below the implementation aspects of three types of sampling methods.

4.1.1 Radial Polar Sampling

The radial polar sampling method uses a geometrical structure that is closely corresponds to sector scanning. With reference to Figure 4.1, the angle Φ subtended by the sector is uniformly divided into *n* beams (lateral resolution), and along each beam we create *m* sampling pixels (axial resolution) with uniform spacing. The size of the

input synthetic image with Gaussian noise is assumed to be $w \times h$ pixels. This method generates non-uniform spacing in the rectangular Cartesian space with the density of points increasing towards narrower regions of the sector. The limitations of this method are that sampling requires two parameters n and m, sampling artifacts due to non-uniform spacing between samples, and the requirement for complex interpolation. The pseudo code for computing the sampling points is given in Figure 4.1 below. The input synthetic image is denoted by $I_0(x, y)$, and the sampled image by $I_p(x, y)$.

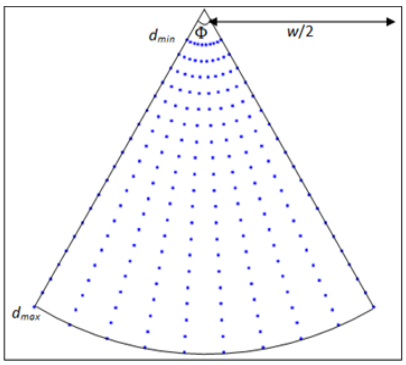


```
for i = 0 to n–1 do
    θ = (3π–Φ)/2 + i Φ / (n–1)
    for j = 0 to m–1 do
        d = d_min + j (d_max–d_min) / (m–1)
        x = d cosθ + w/2
        y = – d sinθ
        I_p(x, y) = I_0(x, y)
```

Figure 4.1: Radial-polar sampling points with Φ=60°, n = 10, m = 20 and pseudo code for computing sampling points.

4.1.2 Radial Uniform Sampling

The radial-uniform sampling method generates m equi-spaced sampling pixels along the radial direction as in the case of radial-polar sampling. However, the non-uniformity in the distribution of points in radial-polar sampling is corrected by maintaining a constant arc distance Δ between points along each arc. Then to get a sampling pattern that corresponds to the geometrical structure of the sector scan while preserving a uniform distribution of points within the scanned region as shown in Figure 4.2. The implementation of the radial-uniform sampling scheme is very similar to that of radial-polar with the addition of the arc length constraint. The pseudo code for the algorithm is given in Figure 4.2.

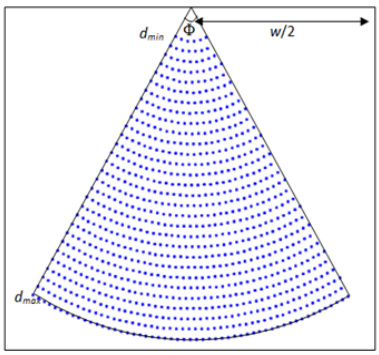


```
for j = 0 to m–1 do
    d = d_min + j (d_max–d_min) / (m–1)
    θ = (3π–Φ)/2
    θ_step = Δ / d
    while θ < (3π+Φ)/2 do
        x = d cosθ + w/2
        y = – d sinθ
        θ = θ + θ_step
        I_p(x, y) = I_0(x, y)
```

Figure 4.2: Radial-uniform sampling points with Φ=60°, m = 30, Δ = 10 and pseudo code for computing the sampling points.

4.1.3 Uniform Grid Sampling

Sampling using a uniform grid involves generating equally spaced points along x and y directions, where points that fall outside the sector are removed using the line equations of the sector boundary. This method produces a sampling that corresponds to the linear scan, while the shape of the region matches the sector scan's shape (Figure 4.3). The resolution of sampling pixels is controlled using a single spacing parameter δ which denotes the distance between consecutive points (step size) along x and y directions. The uniform grid sampling method provides a uniform density of points within the imaged region and allows a simple bi-linear interpolation scheme. The pseudo code for computing the sampling points is given in Figure 4.3 below.

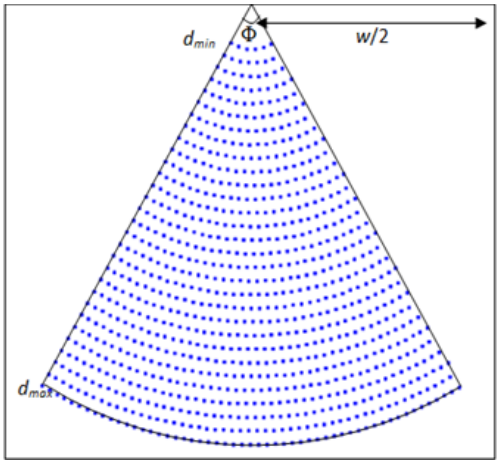

Line equation:

$f(x, y, \theta) = (x - w/2)\sin\theta + y\cos\theta$

Distance equation:

$d(x, y) = \sqrt{(x-(w/2))^2 + y^2}$

$\theta_1 = (3\pi - \Phi)/2$

$\theta_2 = (3\pi + \Phi)/2$

for $i = 0$ to $w-1$ **in steps of** δ **do**

  for $j = 0$ to $h-1$ in steps of δ do

    if $f(i, j, \theta_1) < 0$ **and** $f(i, j, \theta_2) > 0$

    and $d(i, j) > d_{min}$ **and** $d(i, j) < d_{max}$

      $I_p(i, j) = I_0(i, j)$

Figure 4.3: Uniform grid sampling points with Φ=60°, δ = 12 and pseudo code for generating sample points.

Real time ultrasound image acquisition systems also generate images using linear scan transducers. The model presented in Figure 4.3 can be easily modified to simulate linear scans or rectangular beam shape. The images in Figure 4.4 show examples of simulated linear scans with varying spacing (δ) between consecutive sampling points along x and y directions.

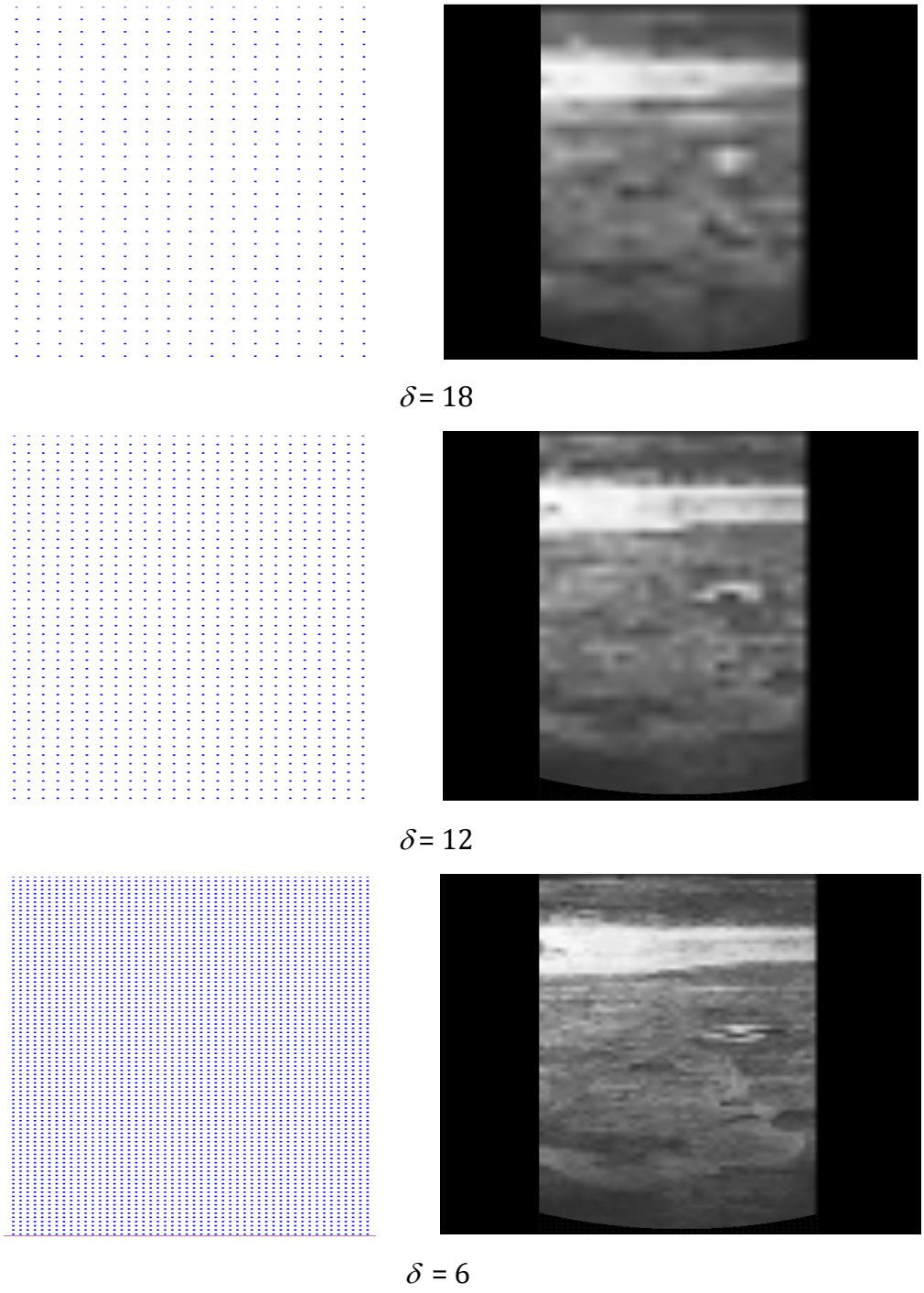

Figure 4.4: Uniform grid sampling points for varying step size δ = 18, 12, and 6 and the corresponding synthetic linear scan images.

4.2 Rectification Model

Image processing operations such as interpolation and convolution that use rectangular kernels will require pixels to be arranged in a rectangular grid. A kernel based interpolation of the points generated by the radial-polar sampling will therefore require a transformation of the points into an $n \times m$ grid. This transformation can be easily

incorporated into code for sampling given earlier in Figure 4.1. The updated pseudo code for this computation of the rectified image is given in Figure 4.3. In the code, the rectified image is denoted by $I_r(i, j)$. The transformation of sampling points using the above algorithm is shown in Figure 4.5. The sampling points obtained using the uniform grid method already have a rectangular structure and do not require further rectification. The radial-uniform sampling method produces a pattern with varying number of points along each arc. This pattern does not allow a straightforward rectification of the points.

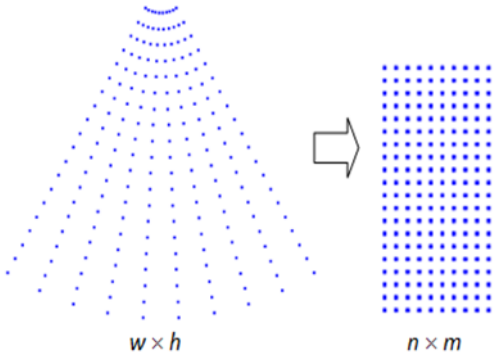


```
for i = 0 to n–1 do
    θ = (3π–Φ)/2 + i Φ / (n–1)
    for j = 0 to m–1 do
  d = d_min + j (d_max–d_min) / (m–1)
    x = d cosθ + w/2
    y = – d sinθ
    I_r(i, j) = I_0(x, y)
```

Figure 4.5: Transformation of points into a rectangular set using the rectification process (n = 10, m = 20) and pseudo code for computing the rectified image from the sampling points obtained using radial polar method.

4.3 Speckle Simulation Model

For speckle simulation, the method adopted was proposed by Perreault and Auclair-Fortier (Perreault & Auclair-Fortier, 2007) . Their model is based on a complex distribution of incoherent phasors (u, v) given by a two dimensional Gaussian function g_σ. The complex amplitude of each pixel is initialized with the square root of the sampled intensity value. The number of incoherent phasors $M(x, y)$ at each pixel (x, y) is set as the value of a random number under a uniform distribution within a pre-specified range [a, b]. The incoherent phasors are generated and added M times to both the real and imaginary components of the complex value at each pixel. The noisy intensity value is then given by the amplitude of the complex number. The pseudo code for the above computation is given in Figure 4.6 below.

```
for each sampled pixel in Ip(x, y) do
complex A = ( √Ip(x, y) ,  0)
    M = Uniformly distributed random number in [a,b]
    for i = 1 to M   do
        (u, v) = 2D Gaussian value using gσ
        A = A + (u, v)
    Is(x, y) = |A|^2
```

Figure 4.6: Pseudo code for computing speckle noise at each sampled pixel.

4.4 Interpolation Model

Interpolation is the final phase of ultrasound speckle simulation. It interpolates the noisy gray level intensities at the sampled points to fill the empty space left by the sampling step to obtain a full sector image. We could use any of the well-known image interpolation method for this phase. In general, the interpolated value at a specified coordinate (x, y) of an image I is computed by grouping the sample values at neighbouring pixels (l, m) using the following formula (Li, Wang, Zheng, Liu, & Xu, 2015):

$$I(x,y) = \sum_{l,m \in Z} \varphi(x-l, y-m) I(l,m) \tag{4.1}$$

where, $\varphi()$ denotes a two-dimensional interpolation/synthesis function that provides the weights of the linear combination of sampled intensity values. The interpolation given in equation (4.1) can be further generalized by replacing the sample values with coefficients c_{lm}:

$$\boldsymbol{I(x,y) = \sum_{l,m \in Z} \varphi(x-l, y-m)} \tag{4.2}$$

The interpolation in equation (4.2), introduces the additional step of determining the coefficients c_{lm} from samples $I(l, m)$. Based on this concept, basis functions with better performance than the standard form are obtained. B-splines, cubic Hermite and Lanczos-3 kernel interpolation are defined in this manner (Burger & Burge, 2008) (J Gonzales et al., 2013) (Perreault & Auclair-Fortier, 2007).

When sampling points do not have a regular structure, a distance weighted interpolation scheme could be used. If the four closest neighbours of (x, y) are given by (l_i, m_i), i = 1..4, then the interpolation equation is given by

$$I(x,y) = \frac{\sum_{i=1}^{4} \frac{1}{d_i} I(l_i, m_i)}{\sum_{i=1}^{4} \frac{1}{d_i}} \tag{4.3}$$

where, d_i denotes the distance between the points (x, y) and (l_i, m_i).

The sampling points obtained using the radial-polar method will have a rectangular grid structure after rectification. The uniform grid method produces all sampling points directly in a rectangular structure. In both these cases, we can store the sampled values with the addition of speckle noise, in a two dimensional array $S[i][j]$, $i = 0..n-1$, $j = 0..m-1$, so that the values can be accessed quickly without re-computing them. The pseudo-code for the general interpolation algorithm where sampled points are arranged in a grid structure is given in Figure 4.7.

```
for each pixel (x, y) within the sector do
    Compute the neighbourhood points (l, m)
    Obtain sampled intensity values I(l, m) = S[l][m]
    Compute I(x, y) using Eq. (1).
    Clamp I(x, y) to the range [0, 255].
```

Figure 4.7: Pseudo code for computing the interpolated pixel values.

4.5 Quality Evaluation Model

One of the key requirements in the analysis of image modelling and simulation algorithms that use synthetic data is image quality assessment. Image quality metrics are also extensively used in the evaluation of compression and noise filtering algorithms (Xia, Li, & Wang, 2012). In this chapter, the following quality measures are considered: entropy, spatial frequency measure (SFM), spectral activity measure (SAM) (Grgic, Grgic, & Mrak, 2004). Parametric variations at each stage of this phase are used to produce a large number of synthetic images with varying intensity and texture characteristics. Among all the synthetic images generated by simulation model a set of candidate images are considered that have features similar to real ultrasound images by using global image quality metrics such as entropy, SFM, and SAM. The texture characteristics of these candidate images are further analysed using gray level co-occurrence matrix, and local binary pattern to obtain the final set of synthetic images with the most realistic and desirable noise and texture features that are close to real ultrasound images. In other words, these quality metrics determine the optimal set of sampling and noise parameters that would produce simulated ultrasound images closely matching the texture features of real ultrasound images. The images generated in this manner could be used to evaluate the performance of the algorithms for speckle noise filtering.

Entropy: It measures the degree of randomness in an image, and is defined as

$$E = -\sum_j P_j \, log_2 \mathrm{P_j} \tag{4.4}$$

where, P_j is the probability associated with gray level j, and is usually computed as the ratio of the histogram value of the intensity j to the total number of pixels.

Spatial frequency measurement (SFM) is a way to measure the overall activity level in an image. SFM is expressed as,

$$SFM = \sqrt{g_R + g_C} \tag{4.5}$$

where, g_R and g_C denote the mean pixel-level intensity gradients along rows and columns evaluated on an image of size $M \times N$ pixels as given below (Mirza, Kumar, & Shakher, 2005):

$$g_R = \sqrt{\frac{1}{MN}\sum_{i=1}^{M-1}\sum_{j=1}^{N-1}(I(i,j) - I(i,j-1))^2} \tag{4.6}$$

$$g_C = \sqrt{\frac{1}{MN}\sum_{i=1}^{M-1}\sum_{j=1}^{N-1}(I(i,j) - I(i-1,j))^2} \tag{4.7}$$

The spectral activity measure (SAM) is a measure of image predictability (higher values indicating higher predictability). For an image of size $M \times N$ pixels, it is defined in terms of the Discrete Fourier Transform (DFT) coefficients of the image in the frequency domain as follows:

$$\frac{\frac{1}{M.N}\sum_{j=0}^{M-1}\sum_{k=0}^{N-1}|F(j,k)|^2}{\left[\prod_{j=0}^{M-1}\prod_{k=0}^{N-1}|F(j,k)|^2\right]^{\frac{1}{M.N}}} \tag{4.8}$$

where, $F(j, k)$ denotes the DFT coefficient at position (j, k) (Grgic, Grgic, & Mrak, 2004).

4.5.1 Gray Level Co-Occurrence Matrix

In statistical texture analysis, texture features are computed from the statistical distribution of observed combinations of intensities at specified positions relative to each other in the image. Depending on the number of intensity points (pixels) in each combination, the texture features are classified into first-order, second-order and higher-order statistical features. The gray level co-occurrence matrix method is a way of extracting second order statistical texture features that contains information about the positions of pixels having similar gray level values. The image texture can be characterised using several statistical parameters extracted from the GLCM matrix. Therefore, GLCM finds several applications in medical image analysis where texture based identification, quality analysis, classification and segmentation algorithms are used (X. Yang et al., 2012) (Mitrea, Nedevschi, Socaciu, & Badea, 2012). In our work, the elements $q(k, l)$ of GLCM are defined for an image I of size $M \times N$ pixels as follows:

$$q(k,l) = \#\{(m,n) \in S |\ I(m,n) = k,\ I(m,n+1) = l\} \tag{4.9}$$

Equation (4.6) defines the gray level co-occurrence matrix for 0° orientation (horizontal proximity) without considering the background region (exterior of the sector region *S*) of the synthetic ultrasound images. The gray levels have been quantized into 8 levels (*i.e.*, $L = 8$). Each GLCM was normalized by the sum of all its elements to calculate the co-occurrence relative frequency between level *k* and *l*. Therefore,

$m = 0 \ldots M-1, \quad n = 0 \ldots N-2.$ (4.10)

$$\sum_{k=1}^{L} \sum_{l=1}^{L} q(k,l) = 1. \quad (4.11)$$

Each entry in GLCM matrix is considered to be the probability that a pixel with value *k* will be found adjacent to a pixel of value *l*. In this proposed work we have extracted 22 features from the GLCM matrix as shown in Table 4.1 (Gomez, Pereira, & Infantosi, 2012) (M. Yang et al., 2013)), of real and synthetic ultrasound images. All images in our analysis had a fixed size of 256x256 pixels.

Among the primary GLCM features listed in Table 4.1, contrast measures local variations of gray level present in an image. Image with large neighbouring gray level differences are associated high contrast. Homogeneity measures image smoothness as it assumes larger values for smaller gray tone differences in pairs of elements. It has maximum value when all elements in the image are same. GLCM contrast and homogeneity are strongly, but inversely, correlated in terms of equivalent distribution in the pixel pairs population. It means that homogeneity decreases if contrast increases while energy is kept constant. Energy of the GLCM matrix measures the textural uniformity that is related to pixel pair repetitions in the image. High energy values occur when the gray level distribution has a constant or periodic form. Energy and contrast are the most useful GLCM parameters in terms of visual assessment. The entropy computed from the GLCM is large when the image is not texturally uniform.

Table 4.1: Texture features extracted from gray level co-occurrence matrices.

Features	Equations
Autocorrelation	$\sum_{k}\sum_{l}(k.l)\ q(k,l)$
Contrast	$\sum_{k}\sum_{l}\lvert k-l\rvert^2\ q(k,l)$
Correlation I	$\sum_{k}\sum_{l}\frac{(k-\mu_k)(l-\mu_l)\ q(k,l)}{\sigma_k\sigma_l}$
Correlation II	$\sum_{k}\sum_{l}\frac{(k.l)\ q(k,l)-\mu_k\mu_l}{\sigma_k\sigma_l}$

Features	Equations
Cluster Prominence	$\sum_k \sum_l (k + l - \mu_k - \mu_l)^4 \, q(k,l)$
Cluster Shade	$\sum_k \sum_l (k + l - \mu_k - \mu_l)^3 \, q(k,l)$
Dissimilarity	$\sum_k \sum_l \lvert k - l \rvert \, q(k,l)$
Energy	$\sum_k \sum_l q(k,l)^2$
Entropy	$-\sum_k \sum_l q\,(k,l)\,.\,\log((q(k,l))$
Homogeneity I	$\sum_k \sum_l \frac{q(k,l)}{1 + \lvert k - l \rvert}$
Homogeneity II	$\sum_k \sum_l \frac{q(k,l)}{1 + \lvert k - l \rvert^2}$
Maximum Probability	$max\ q(k,l)$
Sum of Square	$\sum_k \sum_l (k - \mu)^2 \, q(k,l)$
Sum of Average	$\sum_{k=2}^{2L} k.\, q_{k+l}(k)$
Sum of Entropy	$-\sum_{k=2}^{2L} q_{k+l}(k).\ \log(q_{k+l}\,(k))$
Sum of variance	$\sum_{k=2}^{2L} (k - sum\ of\ Entropy)^2 . q_{k+l}(k)$
Difference Variance	$\sum_{k=0}^{2L} k^2 \,.\, q_{k-l}(k)$
Difference of Entropy	$-\sum_{k=0}^{L-1} q_{k-l}(k).\ \log(q_{k-l}\,(k))$
Information Measure of correlation I	$\frac{H_{kl} - H'_{kl}}{\max(H_k, H_l)}$
Information Measure of correlation II	$1 - \exp[-2(H''_{kl} - (H_{kl})]^{1/2}$
Inverse Difference Normalized	$\sum_k \sum_l \frac{q(k,l)}{1 + \lvert k - l \rvert^2 / L}$
Inverse Difference Moment Normalized	$\sum_k \sum_l \frac{q(k,l)}{1 + (k - l)^2 / L}$

In Table 4.1, $q(k,l)$ are entries in the co-occurrence matrix, L is gray tone levels in the quantized image and μ is mean value of $q(k,l)$. q_k and q_l are the k^{th}, l^{th} entries in the marginal probability matrix obtained by summing the rows and columns of $q(k,l)$, where $q_k = \sum_{l=1}^{L} q(k,l)$, $q_l = \sum_{k=1}^{L} q(k,l)$. μ_k, μ_l, σ_k and σ_l are respectively the mean and standard deviations of q_k and q_l. H_k and H_l are entropies of q_k and q_l. H_{kl} is the joint probability at (k,l). The equations for some of these important terms used in GLCM features are given below:

$$\mu_k = \sum_k k.q_k \tag{4.12}$$

$$\mu_l = \sum_l l\,.\,q_l \tag{4.13}$$

$$\sigma_k^2 = \sum_k \sum_l (k-\mu_k)^2\, q(k,l) \tag{4.14}$$

$$\sigma_l^2 = \sum_k \sum_l (l-\mu_l)^2\, q(k,l) \tag{4.15}$$

$$H'_{kl} = -\sum_k \sum_l q(k,l)\,.\,log(q_k q_l) \tag{4.16}$$

$$H''_{kl} = -\sum_k \sum_l q_k q_l\,.\,log(q_k q_l) \tag{4.17}$$

4.5.2 Local Binary Pattern

The irregularity and heterogeneity of texture features form the primary characteristics of ultrasound images and therefore play an important role in the assessment of their quality. A powerful texture descriptor that has been successfully applied in the field of medical image analysis is called the Local Binary Pattern (LBP) (Jianguo Zhang, Marszalek, Lazebnik, & Schmid, 2007) (Sorensen, Shaker, & Bruijne, 2010). This feature is derived by comparing the intensity at each pixel with its eight neighbours and encoding the information in an 8-bit integer value. This encoding can be viewed as a transformation of the input image into an LBP image as shown in Figure 4.8.

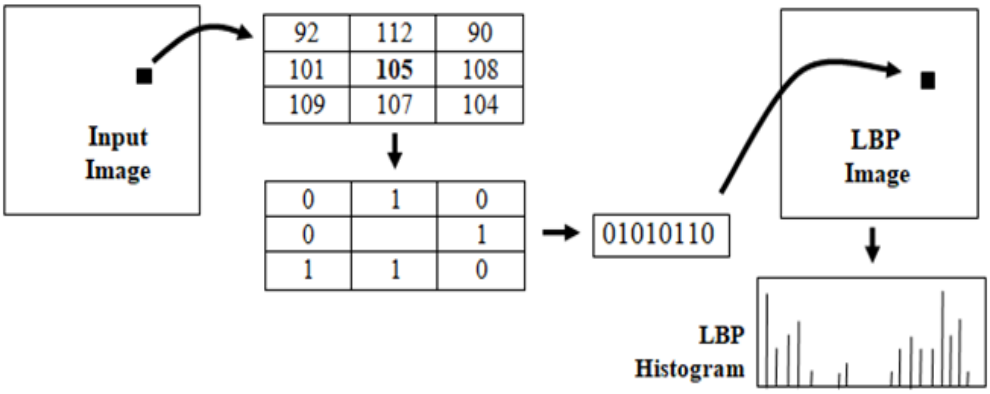

Figure 4.8: The intermediate steps in the computation of the LBP histogram of an image.

The histogram of the LBP image is generally used for texture classification (M. Zhang, Xie, Zhou, & Fujita, 2013). In the area of medical image analysis, LBP methods have been successfully used in characterizing disease patterns (Sorensen, Shaker, & Bruijne, 2010). There has also been a limited number of applications of local binary patterns in image quality assessment (Pietikäinen, Hadid, Zhao, & Ahonen, 2011). In this research, we also propose a novel approach for objective quality evaluation of synthetic ultrasound images using features derived from the LBP histogram.

4.6 Experimental Results and Discussion

The proposed framework allows several options and parametric variations in each stage of the pipeline. As seen in Section 4.1 and section 4.4, the three sampling methods and three interpolation schemes themselves give nine possible combinations. Each sampling scheme has its own set of parameters that can be varied over a wide range of values. The speckle artifact generation algorithm also has a set of statistical parameters governing the artifact distribution.

The experimental work presented in this chapter are based on images derived from three reference ultrasound images sourced from the online ultrasound image gallery (www.ultrasound-images.com, accessed 2017) (Chapter 3). These are ultrasound scans of the liver, and have very similar image features, intensity distribution and noise content. Three reference images were used because ultrasound images could present variations in texture, image quality and speckle artifact content.

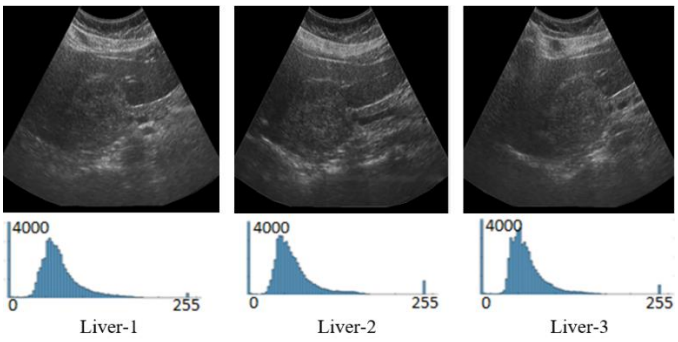

Figure 4.9: Reference ultrasound images and their histograms.

The three reference images in Figure 4.9 were used by an artist to sketch the image features which formed our base synthetic image (Figure 4.10). The histogram of the synthetic image bears similarity with those of the reference images.

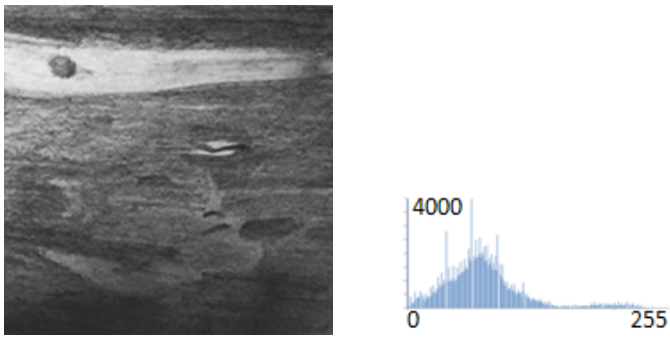

Figure 4.10: Artist rendered synthetic image and its histogram.

The main methods used in the speckle simulation modelling and evaluation pipeline are depicted in Figure 4.11. Within the simulation model, the synthetic image is first sampled based on an acquisition model, speckle noise is then generated at the sampled points, and an interpolation algorithm used to fill the sector scan region. The evaluation model uses image quality metrics computed for the output are then compared with those of the reference ultrasound images for a quantitative assessment of the quality of the final synthetic images. A subjective evaluation is also performed using expert sonographers (Chapter 3).

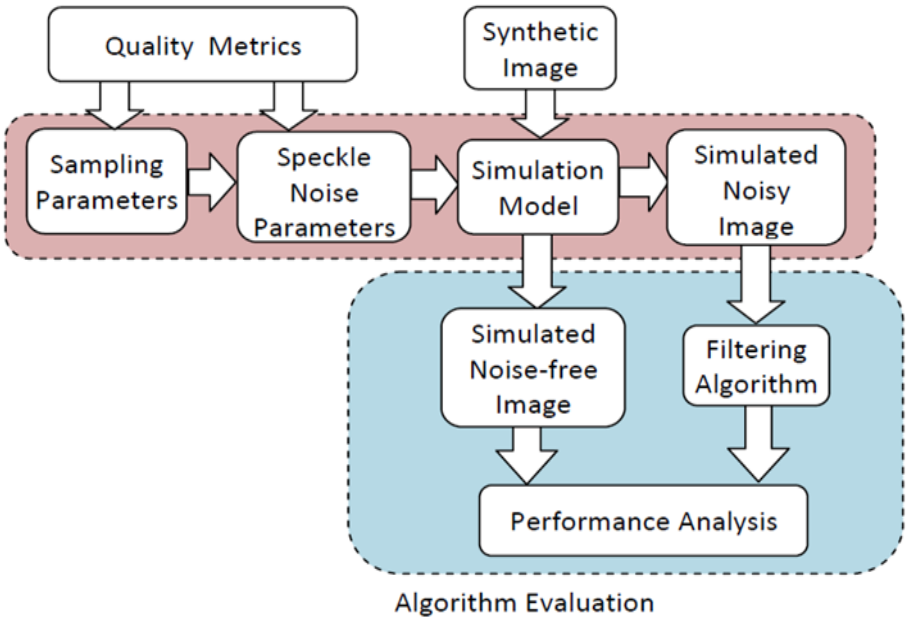

Figure 4.11: Application of the proposed system in the evaluation of filtering algorithms.

The values of the entropy, SFM, SAM computed for the three reference images (Liver-1, Liver-2, Liver-3 given in Figure 4.9) are shown below in Figure 4.12. From the SFM and SAM values, it can be seen that the reference images have higher predictability and less details, as is common in ultrasound images.

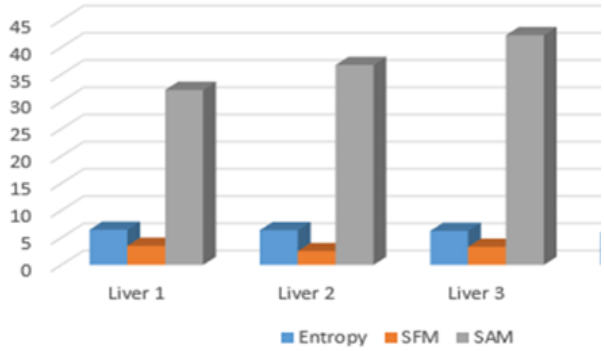

Figure 4.12: Entropy, SFM, SAM values of the reference images.

An assessment of quality of synthetic images using first order statistical features such as histogram and entropy will give only an overall measure of image quality based on global characteristics of the intensity distribution. Image quality assessment using metrics such as entropy, SFM, and SAM. As seen in Figure 4.8, texture forms a very important image attribute that should be considered in quality evaluation of ultrasound images. To analysis the texture feature two techniques are considered that are GLCM and LBP that computes and analyses these features of synthetic images in comparison with those of reference images. Table 4.2 gives the average values of the GLCM features listed in Table 4.1 computed for the reference images.

This work also presents a quality evaluation model using local binary patterns (LBP) and proposes a set of quality metrics (LBP feature values) that can provide consistent results on both synthetic and real ultrasound images.

Table 4.2: Texture Features Extracted using GLCM of three liver images.

Features	Average
Autocorrelation	25.7759
Contrast	0.4710
Correlation I	0.9668
Correlation II	0.9668
Cluster Prominence	1147.8
Cluster Shade	-82.5575
Dissimilarity	0.1642
Energy	0.2601
Entropy	1.7292
Homogeneity I	0.9382
Homogeneity II	0.9370
Max. Probability	0.3615
Sum of Square	25.8748

Features	Average
Sum of Average	8.6960
Sum of Entropy	1.6115
Sum of variance	78.1355
Difference Variance	0.4505
Difference Entropy	0.4093
Information Measure of correlation I	-0.7216
Information Measure of correlation II	0.9261
Inverse Difference Normalized	0.9840
Inverse Difference Moment Normalized	0.9950

4.6.1 Experimental Evaluation using Entropy, SAM, and SFM

As seen in Section 4.1-4.4, the three sampling methods and three interpolation schemes themselves give nine possible combinations. Each sampling scheme has its own set of parameters that can be varied over a wide range of values. The speckle artifact generation algorithm also has a set of statistical parameters governing the speckle distribution.

The first row of Figure 4.13 shows the variations when the axial resolution m is increased in radial-polar sampling, keeping the lateral resolution fixed at n = 40. The interpolation used was Lanczos-3.

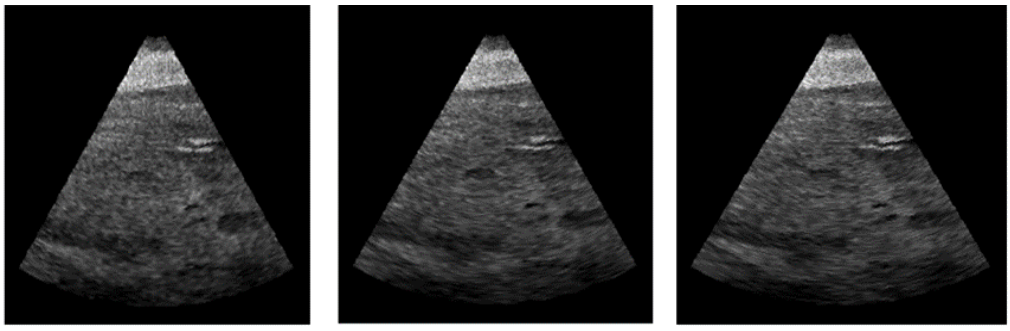

Figure 4.13: Effect of changing axial resolution in radial-polar sampling.

Similar results for radial uniform sampling are shown in Figure 4.14.

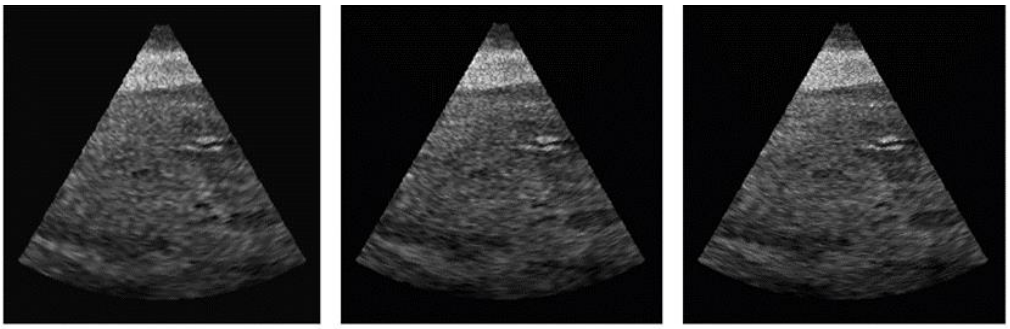

$m = 120$ $m = 160$ $m = 200$

Figure 4.14: Effect of changing axial resolution in radial-uniform sampling.

Some of the commonly found artifacts in simulated images when values of certain parameters become large are shown in Figure 4.15. In Figure 4.15(a), a large value for *m* results in a dense, overlapping set of points along beam directions resulting in smoothing/merging of pixels. A similar effect is seen when both *n* and *m* are large (Figure 4.15(b)). When the σ value is large in the speckle generation function, the image becomes too grainy with loss of fine details, as in Figure 4.15(c).

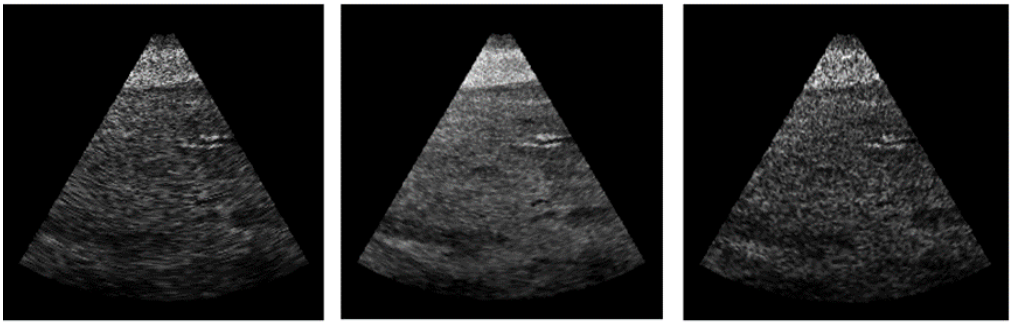

(a) n=40, m=240, σ=1.7 (b) n=60, m=160, σ=0.5 (c) n=80, m=120, σ=1.9

Figure 4.15: Image artifacts produced by large values of sampling and noise parameters.

Figure 4.16 gives a comparison of entropy, SFM and SAM values computed for the reference images and also the simulated images generated using various combinations of sampling and interpolation methods. The SAM values have been scaled by a factor of 10 to get a nearly uniform range of values for all three metrics. An important aspect to be considered while computing quality metrics is that the background pixels outside the sector region must be excluded from the computation.

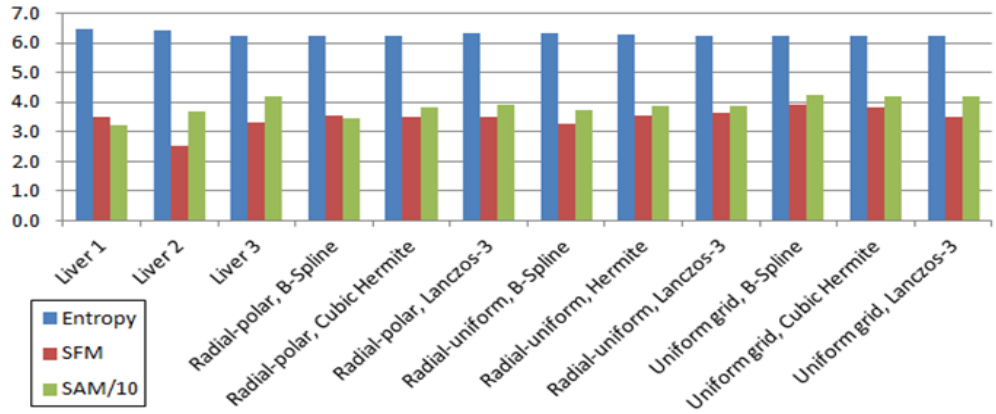

Figure 4.16: A comparison of entropy, SFM and SAM values computed for the reference and synthetic images (SAM values scaled by a factor of 10).

Figure 4.16 shows that the SFM and SAM values of the generated synthetic images are similar to that of the reference images on an average sense, which points to the fact that the synthetic image is visually similar to a real ultrasound image. The radial-polar sampling scheme with Lanczos-3 interpolation gave SFM values that are closest to the reference value. The SAM values showed larger range of variations. However, the values of all synthetic images were between the minimum and maximum of reference values. The uniform sampling method provided SAM values that are closest to that of the reference image. Four simulated synthetic ultrasound images which gave values closest to the reference values were shown to clinical experts for subjective evaluation. The images and their parameters are shown in Figure 4.17.

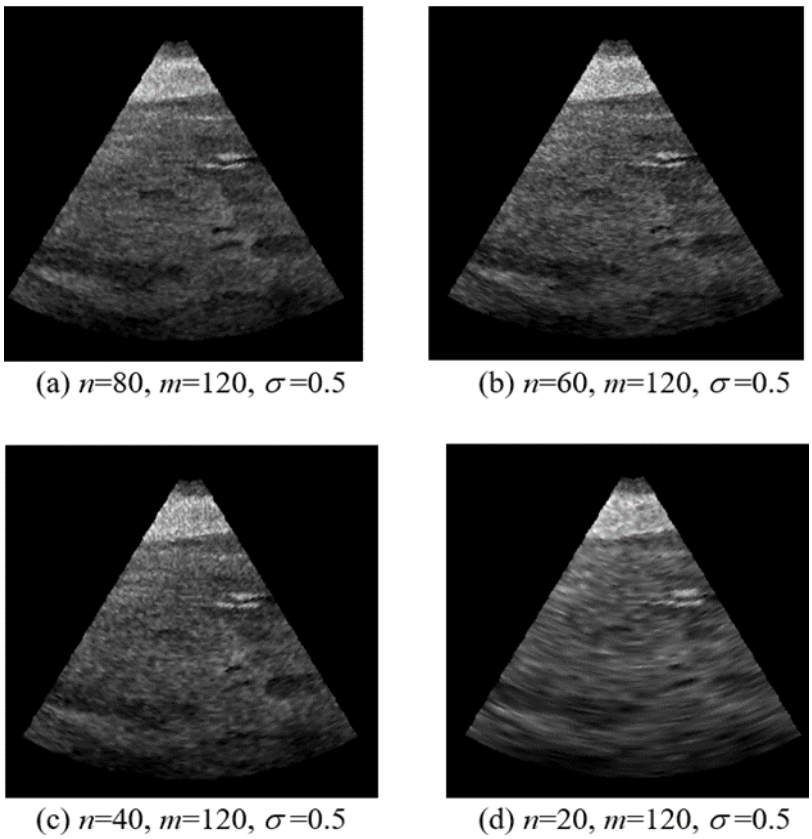

Figure 4.17: Synthetic images with speckle noise used for subjective evaluation.

The subjective evaluation was performed by three experts. They based their evaluation on key visual features such as contrast, grayscale variations, texture and graininess. The images were scored on a scale from 1 to 5. There was a general agreement among the assessors on image quality and how closely the simulated images resembled real ultrasound images. The mean subjective scores are given in Table 4.3.

Table 4.3: Mean subjective evaluation scores assigned by clinical experts.

Image	**4.17(a)**	**4.17(b)**	**4.17(c)**	**4.17(d)**
Scores	4	3	3	1

As the lateral resolution parameter n is varied from 20 to 80, the smoothing effect due to interpolation is significantly reduced, the graininess improved and image features became more clearly visible, which is important from a clinician's perspective. The assessors also observed that the images have gray-scale variation and graininess closely resembling real ultrasound images.

Overall, based on both quantitative and subjective evaluations, radial-polar sampling method with parameter values n = 80, m = 120 and speckle simulation with σ = 0.5 with linear and Lanczos-3 interpolation gave the most accurate simulation of real ultrasound images, where the image size used was 256x256 pixels. In general, for an

image of size *N*x*N* pixels, the optimal value *m* of axial resolution (the number of pixels per beam) depends on the value of *N*.

$$m = \text{floor}(0.56N - 23), \qquad 250 \leq N \leq 500. \tag{4.18}$$

The value of the lateral resolution *n* represents the number of ultrasound beams and it specifies the subdivisions of the sector angle. The optimal subdivision was found to be approximately 1 beam/degree, *i.e.,* if the sector angle is 60 degs, the optimal value of *n* is also around 60.

4.6.2 Texture Feature analysis using Co-occurrence Statistics

In this section, we analyse the image quality of the synthetic images in two steps. First, we analyse the variation of image quality with changes in the modelling parameters. Secondly, we compare the results with those of reference images to select the best set of modelling parameters and the sampling scheme that produces images with texture features closely resembling that of real ultrasound images.

To obtain the best technique out of nine combinations based on texture features using GLCM, we have calculated the normalized Euclidean distance (feature scaling is used to bring all values into the range [0,1]) between GLCM values obtained using nine modelling combination techniques and average values of reference images. Table 4.4 gives a comparison of nine speckle simulation techniques (three sampling: radial polar radial uniform and uniform grid, three interpolation: Lanczos-3, B-spline, and cubic Hermite). The sampling parameter for radial polar is n=80, m=120, for radial uniform m=120, Δ = 10 and for uniform grid δ = 2. All combinations are compared with average of reference liver images (Figure 4.8) based on normalized Euclidean distance. Radial polar sampling with Lanczos-3 interpolation gives the closest distance, followed by radial polar B-spline Interpolation, and it can be concluded that these images have texture features that are very similar to reference liver images. In Table 4.4 and Table 4.5 at the end of this section, provided the values of a few important GLCM parameters (contrast, entropy, homogeneity, energy) for radial-polar sampling with different values of the axial resolution *n*, where *m* fixed at 120 and for n=m.

Table 4.4: Normalized Euclidean Distance of nine simulation techniques.

Simulation Techniques	Normalized Euclidean Distance with average of reference images	Rank based on minimum distance
Radial polar , B-spline	0.0016	2
Radial polar ,Cubic Hermite	0.0050	7
Radial polar , Lanczos-3	0.0011	1
Radial Uniform ,B-spline	0.0019	3
Radial Uniform ,Cubic Hermite	0.0028	5
Radial Uniform,Lanczos-3	0.0056	9
Uniform Grid , B-spline	0.0036	6
Uniform Grid, Cubic Hermite	0.0052	8
Uniform Grid,Lanczos-3	0.0020	4

The quality of synthetic images generated using the modelling scheme given in Section 4 depends on several parameters used for sampling, interpolation and noise generation. In Table 4.4 we have given the values of GLCM features only for one candidate image for each of the three sampling methods and interpolation techniques.

Table 4.5: Four main GLCM texture feature assessment with *m*=120

Radial Polar , Lanczos-3	*n*=20	*n*=40	*n*=60	*n*=80	*n*=100
Contrast	0.4225	0.4027	0.4111	0.4329	0.5064
Entropy	1.5451	1.5865	1.6236	1.6991	1.6999
Homogeneity	0.9624	0.9521	0.9450	0.9355	0.9334
Energy	0.3657	0.3618	0.3570	0.3568	0.3498

Table 4.5 shows variation of contrast, entropy, homogeneity, energy with fixed sampling pixels m =120 and varying n from 20 to 120 in steps of 20. Variations in image contrast and entropy increase with increasing values of n (number of beams or lateral resolution) or with image quality. On the other hand, energy and homogeneity decrease with image quality or with increasing value n. In the analysis, the number of ultrasound beams used are n=80 and number of sampling pixels in each beam are m=120 with σ=0.5. In an average sense, contrast, correlation, homogeneity, sum of entropy values were found to be very close to the averages values of our reference real ultrasound images. It has been validated from GLCM texture feature analysis that subjective evaluation can be correlated with GLCM analysis.

Table 4.6: Four main GLCM texture feature assessment with *n*=*m*

Radial Polar , Lanczos-3	20	40	60	80	100
Contrast	0.2902	0.3338	0.3210	0.4005	0.4981
Entropy	1.5442	1.5174	1.5429	1.5256	1.6403
Homogeneity	0.9707	0.9713	0.9648	0.9658	0.9402
Energy	0.3661	0.3672	0.3689	0.3687	0.3566

Table 4.6 shows the variations of contrast, entropy, homogeneity, and energy with equal number of beams and sampling pixel per beam i.e., $n=m$=20, 40, 60, 80, 120. Contrast and energy increase with increasing values of n and m or with image quality. As observed previously, energy and homogeneity decrease with image quality or with increasing values n and m.

4.6.3 LBP Texture Feature Analysis

This section describes the methods used for analysing the texture characteristics of synthetic images based on LBP features by varying the sampling parameters for the radial polar, radial uniform and uniform grid methods.

The LBP histogram of ultrasound images contains predominant features that represent texture characteristics in the image. As an example, a synthetic ultrasound image of size 256x256 pixels, the corresponding LBP image and the LBP histogram are shown in Figure 4.18.

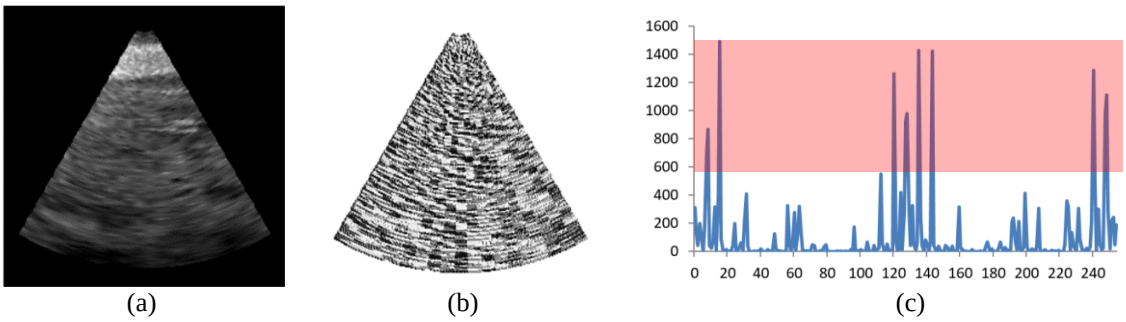

(a) (b) (c)

Figure 4.18: (a) A synthetic ultrasound image; (b) The LBP image; (c) the LBP histogram.

In Figure 4.18, we have highlighted the important LBP features based on their magnitudes. The LBP histogram contains 256 values L_i, $i = 0\ldots255$. The following feature vector consisting of eight LBP features for quality assessment:

$$V = \{L_8, L_{15}, L_{120}, L_{128}, L_{135}, L_{143}, L_{240}, L_{248}\}. \quad (4.19)$$

The above features show consistent variations with changes in axial and lateral resolutions at the modelling stage. The next section discusses the experimental results in

detail and also shows that the LBP features can also help select these modelling parameters so that the features closely match with those of real ultrasound images.

The feature vector given in the equation (4.19) was computed for the three reference images in Figure 4.9, and the average of the three sets were used as the reference feature vector. These values are given below:

$$V_{Ref} = \{447.3, 597.3, 508.7, 433.7, 691.7, 435.3, 459.3, 290\} \quad (4.20)$$

4.6.3.1 LBP Feature Vector for Radial Polar Sampling

Here, the images generated using the radial-polar sampling scheme. Quality analysis using global features such as entropy, SAM and SFM, and subjective evaluations revealed that an axial resolution value m = 120, and speckle noise level σ = 0.5 gave acceptable results. We therefore fixed these parameters and varied only the lateral resolution n from 10 to 120. A few sample images are shown in Figure 4.19.

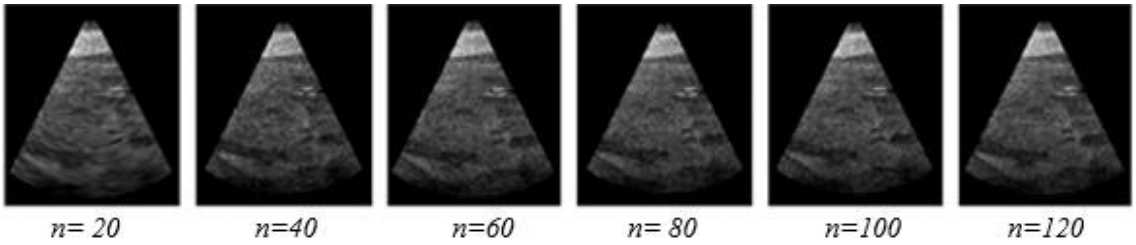

Figure 4.19: Synthetic images generated using radial polar sampling with a coarse to fine variation of lateral resolution parameter *n*.

The variations of each of the eight components of the feature vector (Equation 4.20) computed from the LBP histogram are shown in Figure 4.20.

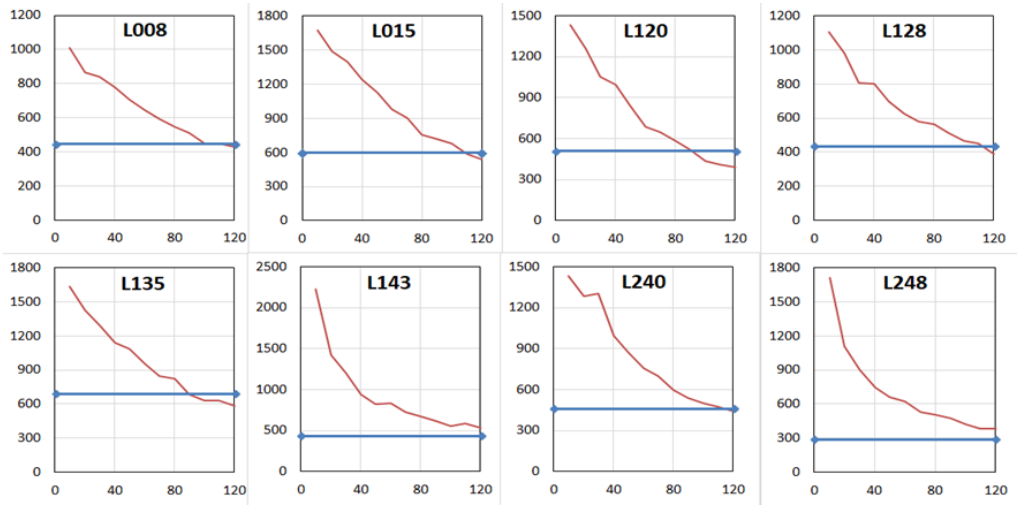

Figure 4.20: Variations of LBP feature vector components with lateral resolution in radial-polar sampling. The x-axis gives the values of *n*.

In Figure 4.20, the blue horizontal lines indicate the values of the reference feature vector as given in Equation (4.20). All components of the LBP feature vector show consistent variations towards the reference values as the value of the lateral resolution parameter *n* is increased.

4.6.3.2 LBP Feature Vector for Radial Uniform Sampling

The parameter affecting the lateral resolution in radial uniform sampling is *m* (axial resolution). The effect of variation of this parameter in the quality of the synthetic images is shown in Figure 4.21.

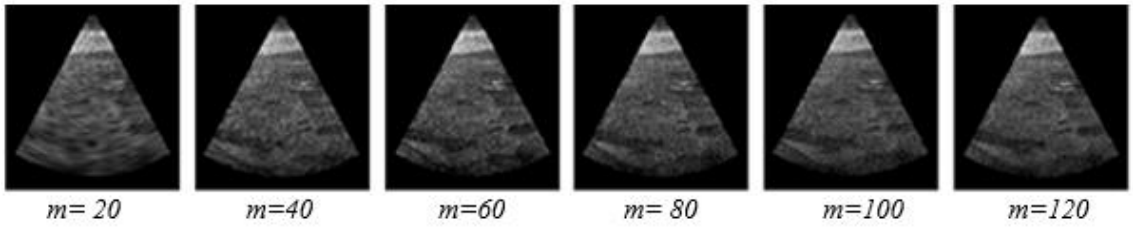

Figure 4.21: Synthetic images generated using radial uniform sampling with a coarse to fine variation of axial resolution parameter *m*.

The variations of the LBP feature vectors (Equation 4.20) with *m* are shown in the graphs in Figure 4.22.

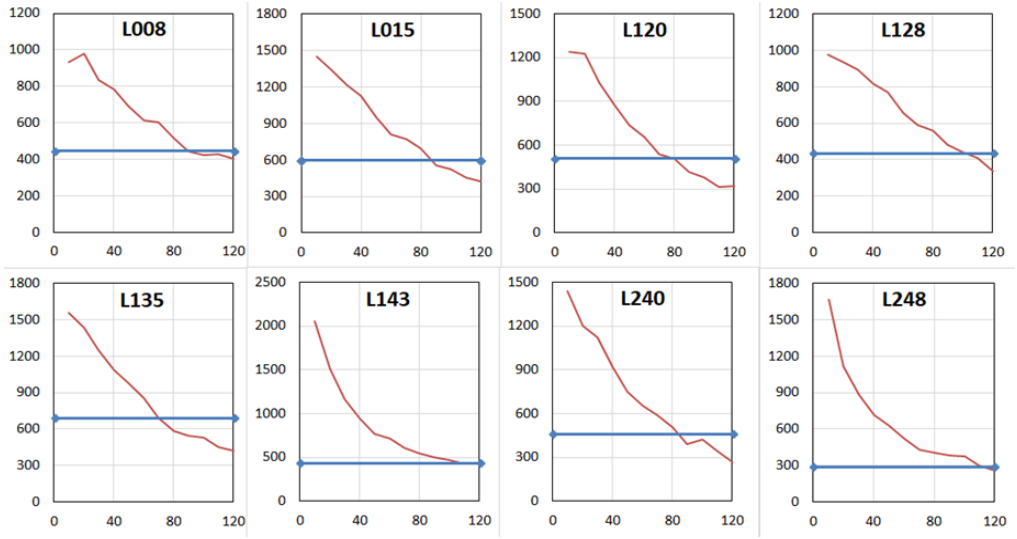

Figure 4.22: Variations of LBP feature vector components with axial resolution in radial-uniform sampling. The x-axis gives the values of *m*

In the case of radial uniform sampling also, we see a trend towards the reference values of the LBP features as the lateral resolution *m* of the images is increased from 10 to 120.

4.6.3.3 LBP Feature Vector for Uniform Grid Sampling

As previously mentioned in Section 3, the uniform-grid sampling method uses a constant spacing δ between sampling points along both x and y directions. Therefore, increasing δ reduces the resolution of the sampled image in both directions. Consequently, we will get a fine to coarse variation of quality in the image as δ is increased, as shown in Figure 4.23.

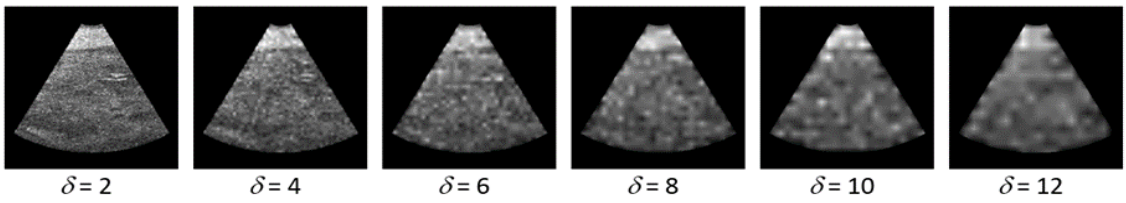

Figure 4.23: Synthetic images generated using uniform-grid sampling scheme with increasing values of the grid spacing parameter δ.

Since the image quality deteriorates as the value of δ is increased, the corresponding values of the LBP feature vector deviates further from the reference feature vector, as shown in Figure 4.23.

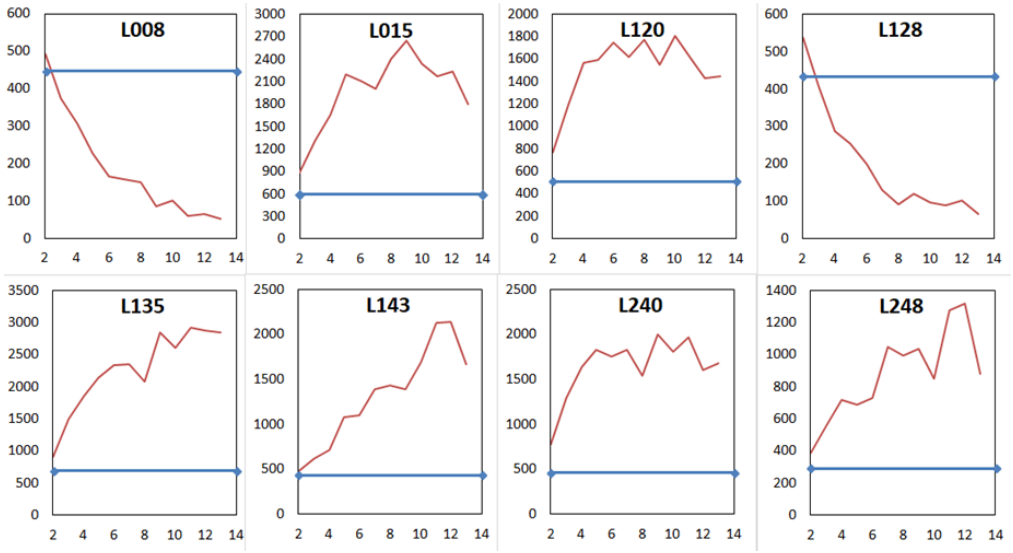

Figure 4.24: Variations of LBP feature vector components with grid spacing in uniform-grid sampling. The x-axis gives the values of δ.

4.6.3.4 Comparative Analysis of Sampling Techniques

The objective quality of the synthetic images produced by the three sampling methods is evaluated by computing the closest distance of the LBP feature vectors from the reference feature vector (indicated by the blue horizontal lines in Figures 4.20, 4.22, 4.24) using a Euclidean distance metric. The plots of the distance values for the three methods are given in Figure 4.25.

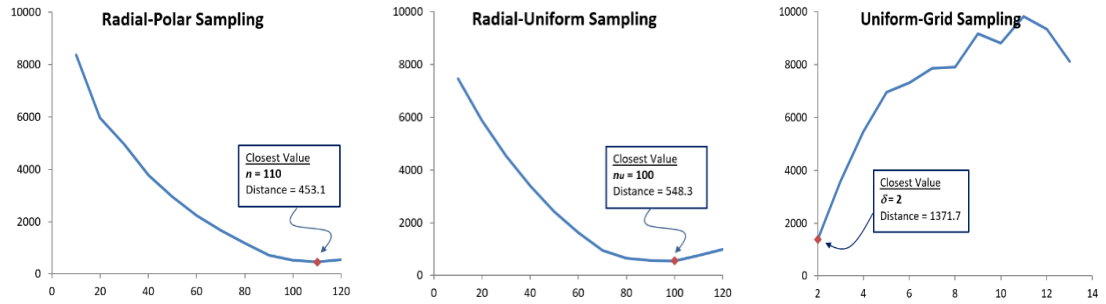

(a) (b) (c)

Figure 4.25: Plots showing the closest matching positions of the LBP feature vector with reference vector for images generated using (a) radial-polar sampling; (b) radial-uniform sampling; (c) uniform-grid sampling.

4.7 Chapter Summary

This chapter has presented the complete algorithmic framework for generating realistic and simulated ultrasound images incorporating image acquisition models, speckle noise formation processes and image interpolation schemes. The chapter has introduced three sampling schemes, viz., radial-polar, radial-uniform and uniform grid sampling methods. These methods together with the speckle simulation model and the interpolation scheme formed the simulation model of the processing pipeline. These processes within the simulation model allows users to vary a wide range of parameters that control the image and noise formation processes. The simulated images with speckle content could be used to evaluate filtering methods, as ground truth data (the corresponding synthetic images without noise) are readily available.

The chapter has also shown the detailed experimental study involving image quality assessment using entropy, SFM, an SAM. The quality of such synthetic images was further validated using subjective evaluations performed by clinical experts. Texture features analysis derived from GLCM and LBP. The overall experiment demonstrates that synthetic ultrasound images generated by the proposed system (based on same real ultrasound acquisition modality) are visually and theoretically very similar to real ultrasonography images. This research study finds useful applications in the performance evaluation of filtering algorithms.

This work has presented an extensive evaluation of noise and texture characteristics present in both real and synthetic ultrasound images using gray level co-occurrence matrices, with the aim of selecting synthetic images that closely match the features of real ultrasound images shown in Table 4.6. The analysis allows us to determine the modelling parameters that produce the most realistic images. The quality

scores of the synthetic images measured by GLCM features closely correspond to the subject evaluation scores assigned by clinicians. Thus, it is further verified that the generated images contain all texture features that correspond to real ultrasound images.

The comparative analysis showed that radial polar sampling with lateral resolution n = 110 gave the closest distance of the LBP feature vector from the reference feature vector. This result also matches very closely with the subjective evaluation scores reported in Table 4.3. The components of the LBP feature vector showed changes consistent with variations in the resolution of the synthetic images. More importantly, the values of the LBP features approached the values computed from real synthetic images, thus providing us an optimal set of modelling parameters that could be used for generating realistic synthetic images.

The next two chapters deal with speckle atrifact reduction algorithms by implementing two types of filtering algorithms and feature improvement using CLAHE, with the aim of developing a robust framework for feature enhanced speckle reduction in real ultrasound images.

5 DESPECKLING USING CLUSTERING METHODS

This chapter presents a framework using clustering algorithms for speckle artifact segmentation from the main signal component present in medical ultrasound images. The framework is first tested and validated using synthetically generated ultrasound images (Chapter 4), and then applied on real medical ultrasound images followed by extensive quality analysis of the generated outputs. The clustering operation is performed on wavelet sub-bands consisting of high frequency components. The proposed method also preserves the edge information effectively for better clinical analysis and problem identification. This chapter also presents experimental results and quantitative analysis using both real and synthetic ultrasound images.

The main motivation for our work comes from successful applications of clustering algorithms in speckle artifact suppression with edge preservation for synthetic aperture radar (SAR) images (Shanthi & Valarmathi, 2013). Such algorithms have not been previously used for speckle artifact reduction in clinical ultrasound images. This thesis presents an exhaustive comparative analysis of six clustering methods, namely, K-Means, Fuzzy C-Means (FCM), cascaded K-Means and FCM (KFCM) Possibilistic C-Means (PCM), Fuzzy Possibilistic C-means (FPCM), and Possibilistic Fuzzy C-Means (PFCM) to analyse the suitability of these methods for ultrasound image despeckling, and to identify the clustering algorithm that gives the best performance measure for noise reduction.

5.1 Proposed Clustering Framework

The main stages of the processing pipeline using the clustering algorithms are shown in Figure 5.1. The primary edge features in the input image are detected with the help of the Canny edge detector. The LOG transform is applied to the image to convert the multiplicative noise into additive noise. We then use a 1-level Discrete Wavelet Transform (DWT) (Elamvazuthi, Muhd Zain, & Begam, 2013) to decompose the image into LL, HH, HL, LH sub-bands (low and high frequency components). The clustering algorithms are individually (K-Means, FCM, PCM, FPCM, PFCM) and in cascaded (KFCM) form applied on the HH, HL, LH sub-bands separately to segment the speckle noise content from the signal cluster. The low frequency and high frequency sub-bands are then combined by performing the inverse DWT. Finally, the exponential transform is used to obtain inverse of log-transformed image, and the edges are added back to get the output speckle suppressed image.

5.1.1 Edge Tracking Algorithm

In ultrasound images, edges contain useful information that are vital for clinical interpretations. Due to the presence of high noise levels in ultrasound images, the edge detection algorithm may produce false edges and, also fail to detect true edges. The Canny edge detection operator is an optimal edge tracker as it has better detection capability under noisy conditions, good localization and unambiguous response (Zheng, Zhou, Zhou, & Gong, 2015). In the proposed system, the Canny algorithm used to detect edges, as it reduces false edge detection to a sufficient extent. For all images used in our analysis, the standard threshold value for Canny edge operator is set at T_o=0.289 obtained using the two-dimensional Otsu's method (Huang & Wang, 2009). In order to detect the original edges, the threshold value should be estimated in such a way that it can detect both strong edges as well as fragmented weak edges that have connectivity in the image.

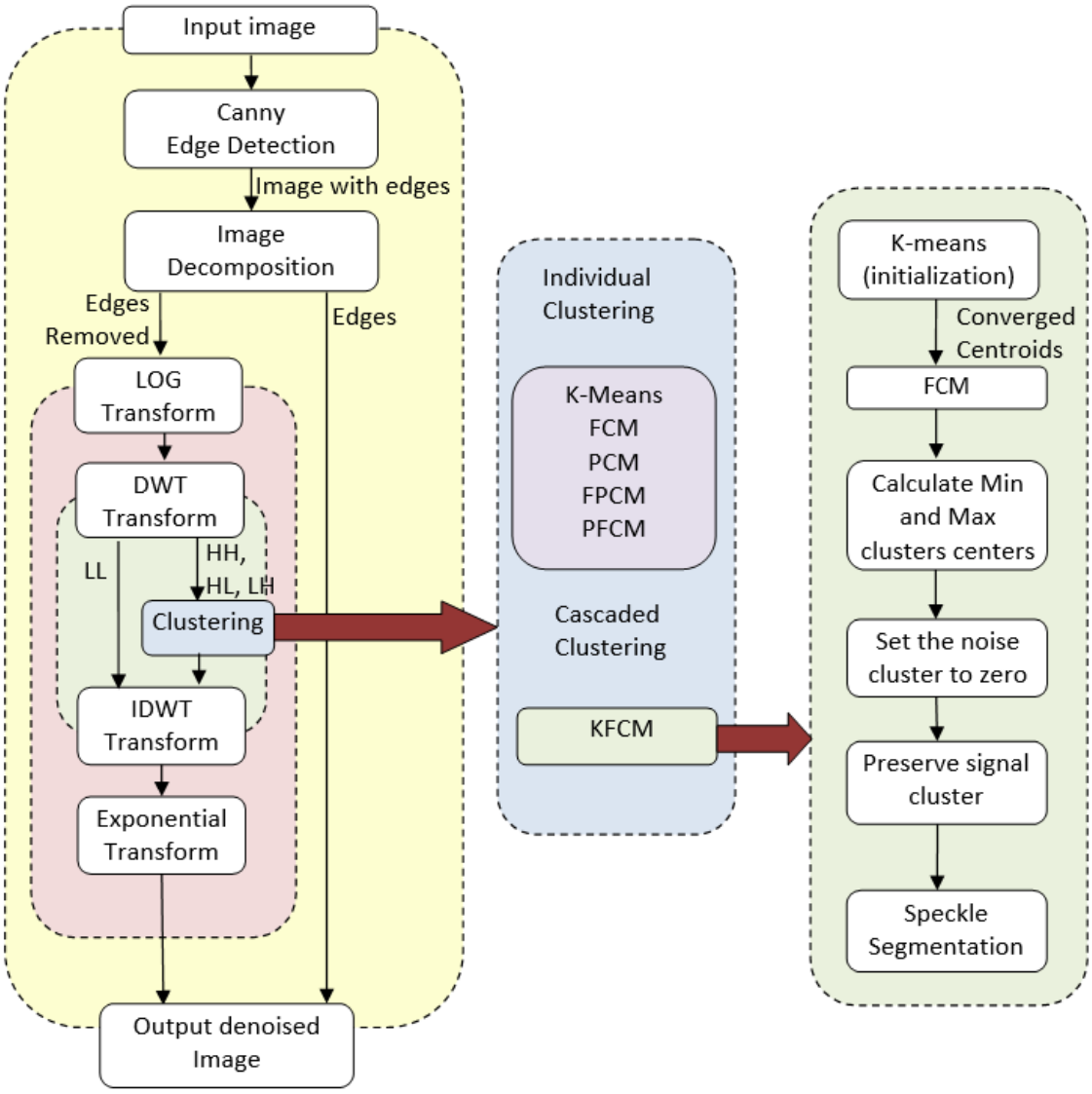

Figure 5.1: Speckle reduction pipeline using clustering algorithms.

5.2 Clustering Techniques

Clustering is a technique used for partitioning of data set into similar and non-similar regions. In this research study, clustering is used to separate the signal class from the noise class in the DWT sub-bands. A detailed discussion of individual clustering algorithms is provided below.

5.2.1 K-Means Clustering

The K-Means algorithm uses a pre-specified number K of clusters and the image (dataset) as inputs. The data set is a collection of features for each point. The algorithm starts with initial estimates for the K centroids of clusters, which can be either randomly generated or randomly selected from the dataset. Each point in the dataset is assigned to its nearest centroid based on squared Euclidean distance, and the centroid positions are

recomputed based on the points assigned to each cluster (Ma & Wang, 2014). The algorithm iterates until the convergence criteria for centroids is met. The objective function (Q) for K-Means algorithm is given by

$$Q = \sum_{m=1}^{\varphi} \sum_{n=1}^{\vartheta} ||K_n - C_m||^2 \quad (5.1)$$

where $||.||$ is squared separation measure between an information point K_n and the cluster center C_m. Also, φ is the number of clusters and ϑ is the number of the data points.

5.2.2 Fuzzy C-Means

The FCM algorithm allows each data point to belong to two or more clusters . FCM separates data automatically by using self-organization properties (Chi, Yan, & Pham, 1996). An iterative optimization procedure is used for assigning each cluster. It minimizes a cost function when high membership values are provided to pixels whose intensities are close to the centroid of their clusters and low membership values are given when the point is so far from the centroid. Cluster centers and membership degrees are updated sequentially for each and every iteration pixels close (Alamelumangai & Devishree, 2012). It is based on minimization of the following objective function:

$$Q(D, C, K) = \sum_{m=1}^{\varphi} \sum_{n=1}^{\vartheta} {D_{m,n}}^{\beta} ||K_n - C_m||^2 \quad (5.2)$$

$$0 \leq D_{m,n} \leq 1; \quad \sum_{m=1}^{\varphi} D_{m,n} = 1; \quad (5.3)$$

$$\sum_{m=1}^{\vartheta} D_{m,n} > 0; \quad 1 \leq m \leq \varphi, 1 \leq n \leq \vartheta \quad (5.4)$$

$$D_{m,n} = \frac{1}{\sum_{\alpha}^{\varphi} \left[\frac{||K_n - C_m||}{||K_n - C_\alpha}\right]^{\frac{2}{(\beta-1)}}}, 1 \leq m \leq \varphi, 1 \leq n \leq \vartheta \quad (5.5)$$

$$C_m = \frac{\sum_{n=1}^{\vartheta} (D_{m,n})^{\beta} K_n}{\sum_{n=1}^{\vartheta} (D_{m,n})^{\beta}}, \quad 1 \leq m \leq \varphi \quad (5.6)$$

where, $D_{m,n}$ is the fuzzy membership of K_n that belongs to m^{th} class, β is the quantity controlling factor for fuzziness $\beta \in (1, \infty)$. The objective function is minimized and optimal values of D and C returned when iterative process is terminated on meeting the convergence criterion.

5.3 Cascaded Clustering

The FCM clustering algorithm has been widely used in various applications, but it is more sensitive to membership accuracy of the outliers, and takes a long time. This case can be addressed by using K-Means clustering algorithm. The cluster centres obtained

using the K-Means algorithm are input into the FCM algorithm. By using this combined clustering algorithm, we can gain a better solution and speed up the rate of convergence. The iterative optimization procedure is used for assigning each cluster. It minimizes a cost function when pixels close to the centroid of their clusters are assigned high membership values.

5.3.1 Modified Versions of Fuzzy C-means Clustering Algorithms (PCM, FPCM, and PFCM)

In the FCM clustering technique, memberships to points allocated to each cluster are inversely related to the separation to the respective cluster centers. In the event that a point is nearly equally distant from two cluster centers, its membership in each cluster will be same. The primary issue related with FCM is membership accuracy. If the membership of data point in two clusters are equivalent then such data points will be assigned no membership in either cluster. In general, FCM is sensitive to noise and initialization of membership values, and takes a long computational time. The possibilistic C-means (PCM) algorithm (Krishnapuram & Keller, 1996) overcomes the above problems. More importantly, PCM is not sensitive to noise. PCM clustering minimizes the following objective function

$$Q(P, C; K, \gamma) = \sum_{m=1}^{\varphi} \sum_{n=1}^{\vartheta} {D_{m,n}}^{\beta} \left|\left|K_n - C_m\right|\right|^2 \tag{5.7}$$

$$+ \sum_{m=1}^{\varphi} \gamma_i \sum_{n=1}^{\vartheta} (1 - p_{mn})^{\beta} \tag{5.8}$$

$$p_{mn} = \frac{1}{\left(1 + \left(\frac{||K_n - C_m||^2}{\gamma_i}\right)^{\frac{1}{\beta - 1}}\right)} \tag{5.9}$$

The first term of Eq. (5.9) makes sure that the distance of the data points from the cluster centers be as low as possible. The second term requires p_{mn} (possibility) to be as large as possible to avoid membership inaccuracies. γ_i, i>0 is a user defined constant and considered $\gamma = 2.0$. PCM itself may face issues related to the generation of coincident clusters.

In order to use the benefits of fuzziness and possibilities the clustering algorithm has been modeled as fuzzy possibilistic C-means (FPCM) (Chaudhuri, 2015). FPCM is more robust algorithm than FCM and PCM. FPCM regularizes the possibility values, so that sum of possibilities of all data points in each cluster is 1.

PFCM clustering technique is derived from the combination of FCM and PCM, and it uses the benefits of both FCM and PCM clustering models (Pal, et al 2005). PFCM minimizes the following objective function.

$$Q = (D, F, K; C) = \sum_{m=1}^{\varphi} \sum_{n=1}^{\vartheta} (aD_{m,n}{}^{\beta} + bT_{m,n}{}^{\alpha}) ||K_n - C_m||^2 + \sum_{m=1}^{\varphi} \gamma_i \sum_{n=1}^{\vartheta} (1 - p_{mn})^{\alpha} \quad (5.10)$$

$$p_{mn} = \frac{1}{\left(1+\left(\frac{\beta. \ ||K_n - C_m||^2}{\gamma_i}\right)^{\frac{1}{\beta-1}}\right)} \quad (5.11)$$

where, a >0, b>0 , α>0, β>0 and $p_{mn} > 0$. The constants a and b define relative importance of fuzzy membership and possibility values in the objective function. (Pal, Pal, Keller, & Bezdek, 2005) the value of constants considered are $a = b = 1.0$, and β=2.0.

5.4 Experimental Results and Discussion

In order to evaluate the effectiveness of the clustering algorithms, two types of image databases are used in the experimental analysis: (i) synthetically modelled ultrasound images of resolution 256 × 256 pixels generated using a method proposed in chapter 4, (ii) clinical ultrasound images of resolution 472 × 425 pixels.. These two types of images form distinct classes due to differences in their content and the ways in which they are generated. To evaluate the performance of filtering algorithms, a data set is needed that consists of noiseless images representing the ground truth, to which noise can be added in a controlled manner. This enables an unbiased objective numerical comparison of algorithms using image quality metrics. In the recently proposed research work (Chapter 4) realistic synthetic ultrasound images were generated by using an acquisition model, speckle simulation and interpolation of the sample points. Synthetic images generated by this simulation model have texture properties very similar to real ultrasound images. To prove the effectiveness of the clustering algorithms we have performed a comparative analysis using these clustering methods individually and combination of K-Means and FCM. The performance of the proposed model is also compared with the recent state-of-the-art methods in speckle reduction.

To evaluate the performance of the clustering techniques, the quality of the output image is compared with reference input image using image quality metrics explained in chapter 3. In this chapter, peak signal to noise ratio (PSNR), structural similarity metric (SSIM), universal quality index (UQI), edge preservation index (EPI), and feature similarity index metric (FSIM) are considered for quality evaluation of the generated outputs. First, the proposed clustering framework is tested and validated on synthetically formulated images and then applied on real ultrasound images.

5.4.1 Synthetically Modelled Ultrasound Image Analysis

One of the challenges in the evaluation of noise removal algorithms for ultrasound images is the lack of ground truth information. Chapter 4, proposed a method to model highly realistic, yet synthetic ultrasound images. Figure 5.2(a) shows a noise-free synthetic image. The image is generated using radial polar sampling with n= 110 (number of ultrasound beams, or lateral resolution), m=120 (number of pixels per beam, or axial resolution), σ = 0.5 (standard deviation of speckle noise added to each sampling point of the sector image), and used as input to our algorithm. The noise-reduced output is shown in Figure 5.2(c)–(d). In this case, performance evaluation is done by comparing this image with the noise-free image in Figure 5.2(a).

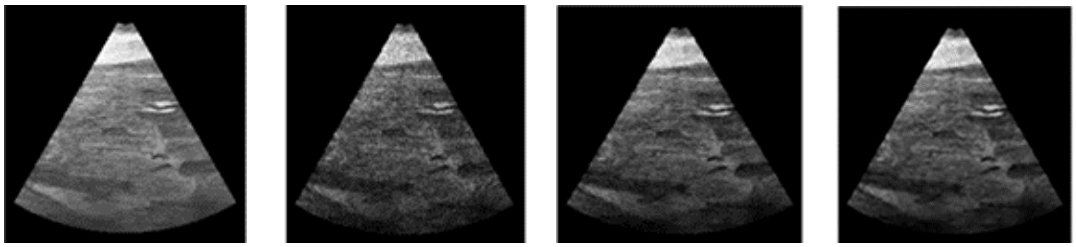

(a) (b) (c) (d)

Figure 5.2: Input images (a) Reference sector image, (b) Synthetic US image, (c)-(d) Resultant image of KFCM and PFCM clustering.

Table 5.1: Comparison of various clustering techniques on synthetic ultrasound image.

IQM	K-means	FCM	KFCM	PCM	FPCM	PFCM
PSNR	26.39	30.43	**34.47**	31.51	33.24	**37.51**
SSIM	0.93	0.99	**0.98**	0.98	0.99	**0.98**
UQI	0.92	0.99	**0.98**	0.97	0.96	**0.99**
FSIM	0.96	0.95	**0.99**	0.96	0.97	**0.97**

Experimental analysis presented in Table 5.1 shows that the PSNR values obtained using FCM, PCM, FPCM and PFCM are above 30dB giving good image quality. The performance of the PFCM followed by KFCM exceeds in terms of PSNR among all clustering techniques used in the analysis. Higher value of SSIM indicates that the output image has good image quality in terms of luminance, contrast, and structure similar to original image. Values of UQI and FSIM using PFCM is high and even close to unity, which shows reconstructed image using proposed pipeline, is less distorted and able to preserve similarity of input and despeckled images effectively.

5.4.2 Subjective Evaluation of Clinical Ultrasound Image Dataset

The proposed clustering system was applied on clinical thyroid ultrasonography images. Subjective analysis comprised of total 24 images in which 4 images are considered in each class of original and despeckled outputs of clinical ultrasound images of thyroid, gallbladder, liver, carotid arteries, breast and kidney were organized in pairs, and randomly presented to clinical experts. Four subject matter experts reviewed each pair of input and output images independently and scores are given on a 5-point scale based on their subjective preference as shown in Table 5.2. The mean score given by four experts was 3.75 for images generated by PFCM followed by KFCM attained score 3.5. The least score attained by K-Means that is 2.5 out of all six methods. The reviewers considered diverse image quality aspects amount of speckle suppression, resolvable details, contrast enhancement, improvement of diagnostic interpretation and reasoning. The subjective evaluation confirms that the outputs obtained by using PFCM clustering within the proposed pipeline provides speckle suppression and improved image quality as compared to the other clustering methods adopted in this despeckling approach. However, the clinicians were of the view that the overall visual quality of the outputs needs to be further improved.

Table 5.2: Mean subjective evaluation scores assigned by clinical experts for six clustering methods.

Methods	Subjective Scores
K-Means	2.5
FCM	2.5
KFCM	3.5
PCM	3
FPCM	3
PFCM	3.75

(a)

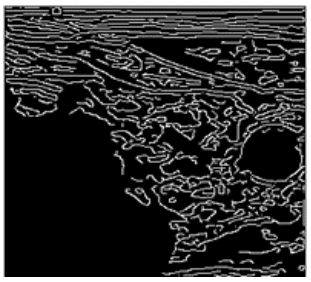

(b)

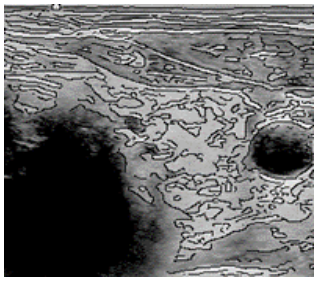

(c)

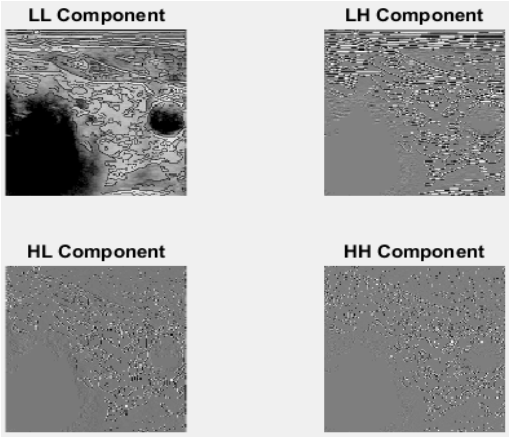

(d)

(e)

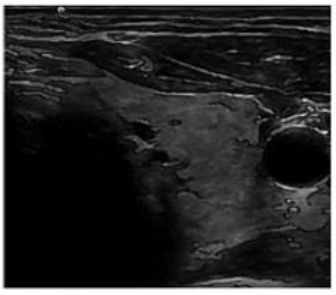

(f)

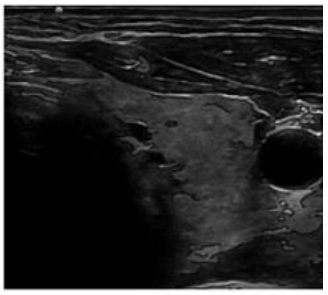

(g)

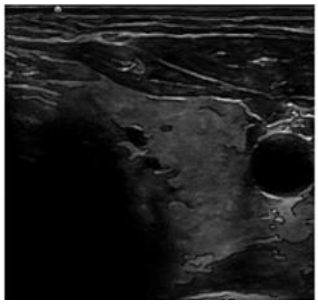

(h)

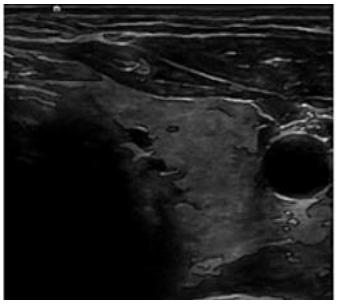

(i)

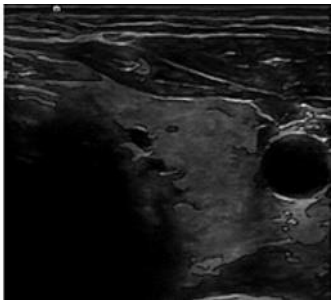

(j)

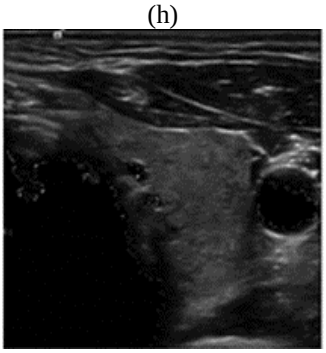

(k)

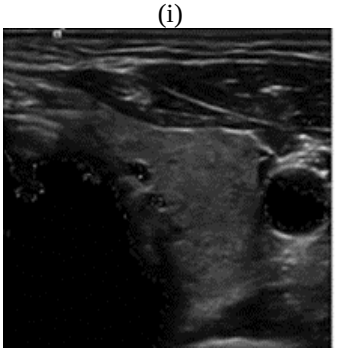

(l)

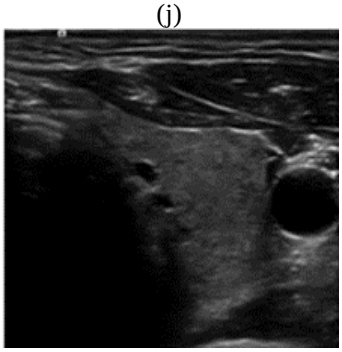

(m)

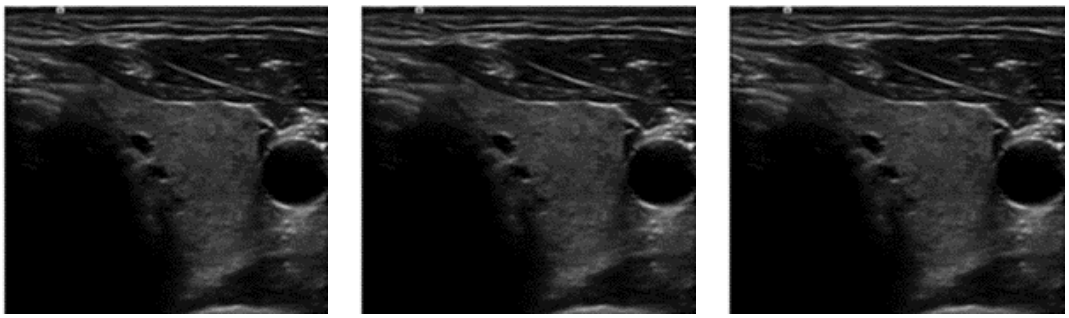

(n) (o) (p)

Figure 5.3:(a) Input thyroid image, (b) Edge detection, (c) LOG transform d) DWT-1-level, (e) Clustering of signal and speckle-,(f)-(j) Exponential transform, (k)-(p) Output images of K-means, FCM, KFCM, PCM, FPCM, and PFCM.

The ultrasonography image of thyroid as shown in Figure 5.3(a) is input to the processing pipeline. The intermediate results obtained in processing the image are shown in Figure 5.3 (b)-(j), and the final outputs of all clustering techniques in Figure 5.3 (k)-(p).

5.5 Comparative Analysis of Algorithms

This section presents a comparative analysis of best clustering method out of all clustering methods used in this study. The PFCM clustering based despeckling algorithm is compared with some of the recently proposed speckle suppression approaches using PSNR and SSIM image quality metrics as shown in Figure 5.4. These are adaptive fuzzy logic filters (AFLF) (Jai Jaganath Babu & Florence Sudha, 2016), curvelet domain using diffusion filter and MAP estimation (CD-MAP) (Bama & Selvathi, 2014), wavelet guided filter (WGF) (Ju Zhang, Lin, Wu, & Cheng, 2015), speckle reduction in neutrosophic domain (NSD) (Koundal, Gupta, & Singh, 2016), and Laplacian modified model with wavelet transform (LMMWT) (Gai, Zhang, Yang, & Yu, 2017).

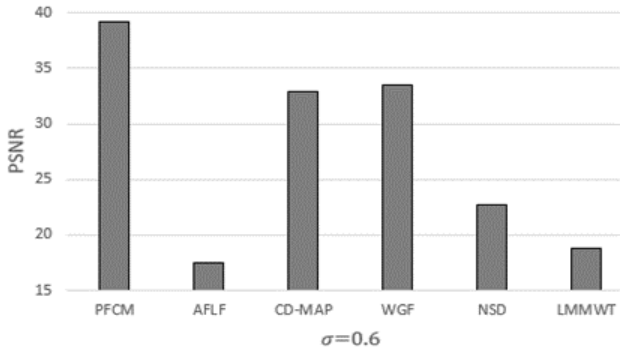

(a)

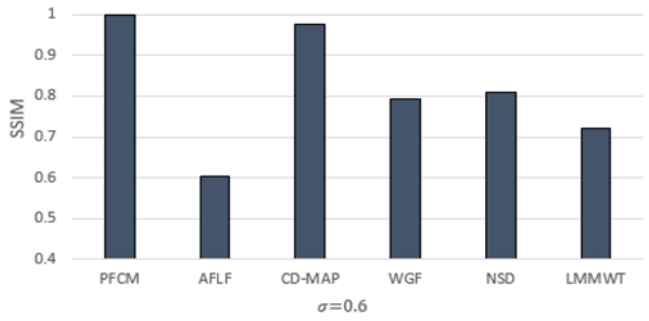

(b)

Figure 5.4: Comparison of PFCM clustering technique with other recently proposed algorithms using PSNR and SSIM.

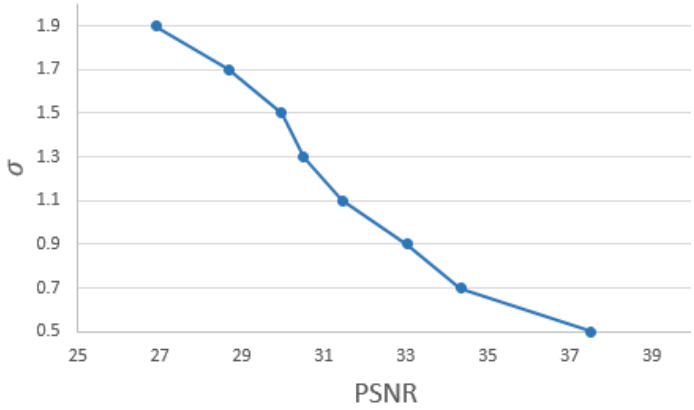

Figure 5.5: Proposed PFCM clustering algorithm on varying values of σ.

Figure 5.5 shows that the proposed PFCM clustering model can withstand even high speckle content. Here, we have considered 8 synthetically modelled ultrasound images generated using radial polar sampling as presented in chapter 4. All 8 images are individually passed through the proposed pipeline and PSNR quality metric was analysed, which clearly indicates that the speckle content of the processed images are sufficiently suppressed.

5.6 Chapter Summary

The chapter has presented a complete study of six clustering algorithms (K-Means, FCM, KFCM, PCM, FPCM, and PFCM), and analysed their feasibility and usability in speckle artifact separation in wavelet sub-bands using both synthetic and real ultrasound images. This framework placed emphasis on the preservation of edges and fine details to improve image quality by utilizing canny edge detection method. The experimental results were analysed using two types of images: medical ultrasound images and synthetically modelled ultrasound images. A comparative analysis using the five clustering algorithms K-Means, FCM, PCM, PFCM, and PFCM selected individually

and one clustering algorithm applied in sequence (KFCM) was used to show that the proposed PFCM followed by KFCM despeckling algorithm exceeds performance. Both objective and subjective experimental evaluation showed that the proposed framework with the PFCM clustering model performed well in speckle reduction, simultaneously preserving edge clarity as compared to the other clustering methods. The experimental study has also considered a few state-of-the-art techniques to compare the proposed PFCM clustering algorithm using PSNR and SSIM quality metrics. Despite obtaining improved performance in the objective evaluation of the proposed PFCM speckle reduction algorithm, the subjective analysis of the outputs pointed to need for further improvement of dominant feature clarity based on their diagnostic usefulness. Next chapter discusses another speckle suppression algorithm based on steerable pyramid transformation and coherent component extraction.

Chapter 5: Despeckling Using Clustering Methods

6 ENHANCED STEERABLE PYRAMID TRANSFORMATION FOR DESPECKLING

This chapter presents a novel approach for suppressing speckle artifacts in ultrasound images by using steerable pyramid transformation, at the same time improving visual features effectively for better clinical analysis and problem identification. The main aim of this work also considered contrast, edges, and fine texture details, which are higher frequency components, present in the images to which the human visual system is sensitive. The proposed algorithm addresses the need for further visual clarity improvement as indicated in the experimental analysis section of the previous chapter. The steerable pyramid transformation is found to be potential technique for denoising different kinds of noise in natural images (Bharath & Ng, 2005) and also image/video coding (Thakur & Chubach, 2015), but has not so far been utilized for despeckling and texture feature improvement of ultrasound images. The framework proposed in this chapter includes the modified adaptive Wiener filter (MAWF) along with the Canny edge detection method and enhanced steerable pyramid transformation (SPT) algorithm. The Canny algorithm is used to detect the true edges from the noisy ultrasound image, and the MAWF algorithm smoothens the speckle effect without affecting the edge information, which is preserved separately and added to the final output. The discrete

Fourier transform (DFT) is used to extract the low and high frequency coefficients. Unlike other multiresolution techniques used for speckle suppression, the proposed method uses the steerable pyramid transformation technique based on high frequency components extracted using DFT for image enhancement. The high frequency coefficients extracted using DFT, are input to the steerable pyramid transform. The coherence component extraction (CCE) method enhances the overall texture and edge features of the image even in the darker portions of the image. The output of this stage is finally combined with the stored edge information. This chapter also presents experimental results to show that the proposed technique outperforms other state-of-the-art techniques in terms of peak signal-to-noise ratio, structural similarity index, and universal quality index (Chapter 3). Finally, experimental verification has shown that the technique has been useful in enhancing the overall quality of the image when viewed by the human visual system (subjective evaluation).

6.1 Proposed SPT-CCE Framework

6.1.1 Despeckling and Feature Enhancement

In general, despeckling techniques in ultrasonography imaging implicate a trade-off between noise suppression and texture feature preservation because of the image's low resolution, high speckle artifact, and high texture content. Therefore, the main contribution of the proposed work is to develop a system, which not only suppresses speckle artifacts significantly, but also emphasizes the texture features and preserves the original image structure, contrast, and visual quality for clear clinical interpretation. The pipeline uses the following methods in the given order: Edge tracking algorithm, Adaptive Wiener filter, Discrete Fourier Transform, Enhanced Steerable Pyramid Transformation, and Coherence Component Extraction.

6.1.2 Processing Pipeline

Figure 6.1 shows the overall flow diagram for the proposed SPT-CCE method. An ultrasound image containing speckle artifacts is given as the input, and in the pre-processing phase, the Canny edge detection algorithm is used to extract the edges which are stored separately for later use. The image is then smoothened using the modified adaptive Wiener filter. The filtering coefficients are computed and used in the Wiener filter. Finally, high frequency coefficients, which are extracted using DFT, are fed into the enhanced SPT method. The proposed system uses three levels of steerable pyramid

transformation, which consists of three filters at each level of construction and reconstruction phases of SPT: oriented band pass filter (BPF), non-oriented band pass filter and high pass filter (HPF). By repeated smoothening and sub-sampling of high frequency coefficients of the previous stages, the image quality is enhanced. The coherence component extraction is implemented to enhance similar features between the input and output images, and finally the detected edges are added back to the speckle suppressed and feature enhanced output image.

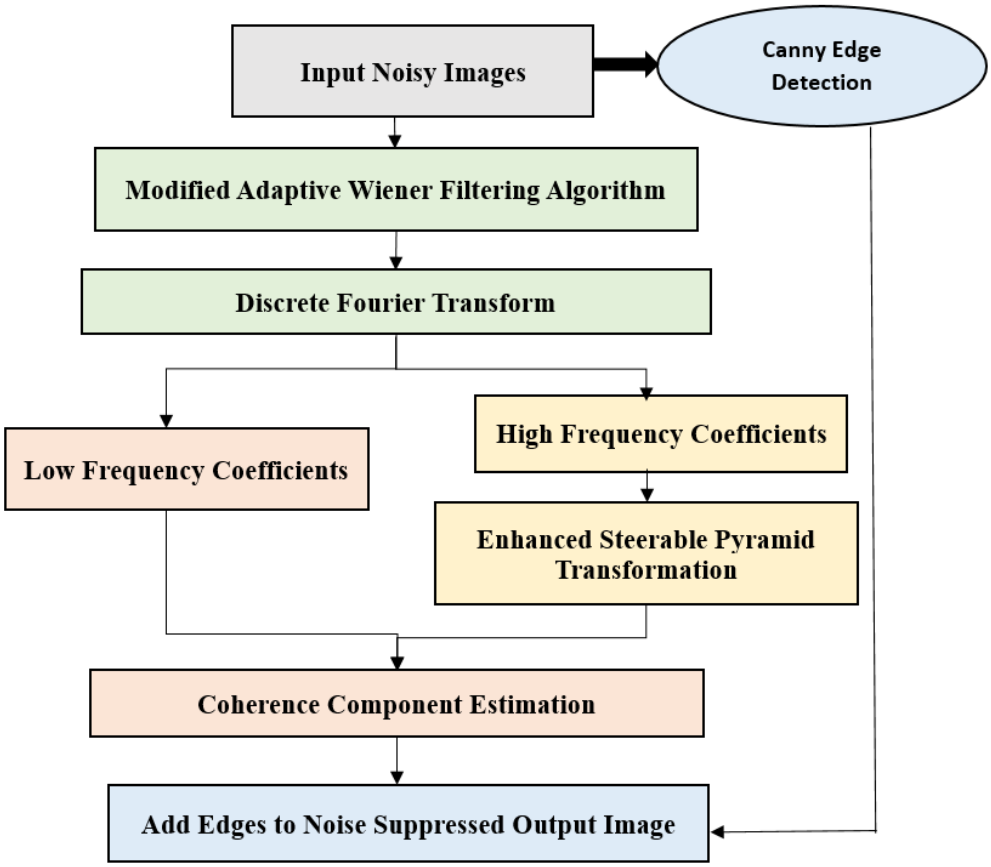

Figure 6.1: Workflow of the proposed SPT-CCE speckle reduction feature enhancement technique.

6.1.3 Edge Tracking Algorithm: Canny Edge Detection

Due to the presence of noise in ultrasound images, the edge detection algorithm may produce false edges and also fail to detect true edges. The Canny edge detection operator is an optimal edge tracker as it has better detection capability under noisy conditions, good localization and unambiguous response (Zheng, Zhou, Zhou, & Gong, 2015). In our proposed system, we have used the Canny operator to detect edges, as it reduces false edge detection to a sufficient extent. In ultrasound images, edges contain useful information that is vital for clinical interpretations. Preserving edges along with noise suppression therefore increases diagnostic accuracy. For all images used in our

analysis, the standard threshold value for the Canny edge operator is set at T_o= 0.289 obtained using the two-dimensional Otsu's method (Huang & Wang, 2009). In order to detect the original edges, the threshold value should be estimated in such a way that it can detect both strong edges as well as fragmented weak edges that have connectivity in the image.

6.1.4 Modified Adaptive Wiener Filter

The adaptive Wiener filter overcomes the drawback of inverse filtering, reduces the speckle artifact and additive noise as well as it inverts the blurring effect by applying inverse filtering to recover the image. (Udomhunsakul, 2015) used an adaptive Wiener filter for estimating the noise power from the local image mean and standard deviation.

In existing adaptive Wiener filter implementations, the local mean and variance of each pixel in the image are fully used in the filtering process. In order to improve the noise smoothening, the variance is considered instead of mean values in MAWF because the Wiener filter is designed to reduce additive noise. Based on the variance, the smoothening operation is performed; for example, larger the variance more smoothened the image becomes.

The optimal mean square error between the random process and the desired process is estimated using this filter. The equation of the modified adaptive Wiener filter is as follows:

$$y(i,j) = \sigma^2 + \frac{\sigma^2}{\sigma^2 - v^2}(x(i,j) - \mu) \quad (6.1)$$

Here, $y(i,j)$ is the filtered output of the input pixel $x(i,j)$. Also, μ and σ^2 are the local mean and variance around each pixel of the neighbourhood of the image, and v^2 represents noise variance estimated from the average of all locally estimated variances in the image.

The filtered image obtained from the above process is then inputted to the steerable pyramid transformation, which is described in the following section.

6.1.5 Enhanced Steerable Pyramid Transformation

The pyramid transformations are of three types: the Gaussian, the Laplacian, and the steerable pyramid. The Laplacian transform along with a discrete cosine transform decomposes the image in a pyramidal level (Kang, Young Lee, & Yoo, 2015). The proposed model uses three levels of steerable pyramid transform along with the discrete Fourier transform (Maycock et al., 2007) to enhance texture features of the image and

also to suppress the speckle content in the image effectively. Three levels of SPT are used because if too many scales are decomposed, high pass information (e.g., edges, boundaries) may be missed. The high frequency coefficients extracted using DFT, are inputted to the steerable pyramid transform. The coherence component extraction stage further finds the structural similarity between input and the SPT output images. Figure 6.2 as shown below this section, describes how the enhanced steerable pyramid transformation works at three levels, using the construction and reconstruction stages. The high frequency coefficients that are obtained from DFT are used as input for the enhanced SPT algorithm because detailed texture information is present in these coefficients to which HVS is very sensitive. The input is given to the first level of the filters which consists of a high pass filter, an oriented and a non-oriented band pass filter. Then the output of the first level of the HPF is down-sampled by 2. After this, the output is given to the next level of the SPT. This process continues up to three SPT levels. The output, obtained from the construction stage, is up-sampled by 2 and is given to the HPF, oriented and non-oriented band pass filter. The final output of the enhanced SPT gives better texture features compared to the existing SPT which uses only low frequency components as input (Guo & Hu, 2012).

The algorithm for steerable pyramid transformation is as follows.

Enhanced SPT Algorithm

Input: Filtered Image

Output: Edge Enhanced Image

Step 1: Aliasing effect elimination

Step 2: If $|\omega| > \pi/2$

$G_1(\omega) = 0$

Step 3: Recursive stability constraint

$$|G_1(\omega)|^2\left[|G_1(\omega)|^2 + \sum_{m=1}^{M} |B_{1,m}(\omega)|^2\right] = 1$$

Step 4: $B_{k,m}(\omega) = B_{k-1,m}(\omega/2)$

$G_k(\omega) = G_{k-1}(\omega/2)$

Step 5: Unity system response amplitude

$$|H_0(\omega)|^2 + |G_0(\omega)|^2\left[|G_1(\omega)|^2 + \sum_{m=1}^{M} |B_{1,m}(\omega)|^2\right] = 1$$

Step 6: To extract the high frequency component from input image

$$H_{0(\omega)} = \begin{cases} 0 & \omega < \omega_1 \\ \sqrt{1/2\left[1 - cos\left(\pi \dfrac{\omega - \omega_1}{\omega_{max} - \omega_1}\right)\right]} & \omega_1 \le \omega \le \omega_{max} \\ 1 & \omega > \omega_{max} \end{cases}$$

Step 7: To find the low bands in the input image

$$G_0(\omega) = \begin{cases} 1 & \omega < \omega_1 \\ \sqrt{1/2\left[1 + cos\left(\pi \frac{\omega - \omega_1}{\omega_{max} - \omega_1}\right)\right]} & \omega_1 \le \omega \le \omega_{max} \\ 0 & \omega > \omega_{max} \end{cases}$$

Step 8: Non oriented BPF

$$B(\omega) = \begin{cases} 1 & \omega < \omega_0 \\ \sqrt{1/2\left[1 - cos\left(\pi \left(\frac{\omega - \omega_0}{\omega_1 - \omega_0}\right)\right)\right]} & \omega_0 \le \omega \le \omega_1 \\ 0 & \omega_1 \le \omega \le \omega_{max} \end{cases}$$

Step 9: Oriented BPF

$$H(u, v) = \frac{1}{1 + 0.414\left(\sqrt{\left(u^*/D_h\right) + \left(v^*/D_v\right)}\right)^{2h}}$$

Step 10: Optimize the HPF and BPF

if (h<=1) //h=height of the pyramid

$$L_0^2(\omega) + H_0^2(\omega) + (H_1^2(\omega) + \sum_k B_k^2(\omega)) = 1$$

Else

$$H_0(w) = H_1(w/2)$$

Step 11: Split the 2^{nd} order HPF

$$G_1(\omega) = \begin{cases} 1 & \omega < \omega_0 \\ \sqrt{1/2\left[1 + cos\left(\pi \left(\frac{\omega - \omega_0}{\omega_1 - \omega_0}\right)\right)\right]} & \omega_0 \le \omega \le \omega_1 \\ 0 & \omega > \omega_1 \end{cases}$$

Step 12: Reconstruct the image

$$\hat{F}(\omega) = \left\{|H_0(\omega)|^2 + |G_0(\omega)|^2 + \left[|G_1(\omega)|^2 + \sum_{m=1}^{M} \left|B_{1,m}(\omega)\right|^2\right]\right\}$$

The first step of the steerable pyramid transformation is the elimination of the illumination component. When the frequency component $|\omega|$ of the image is greater than $\pi/2$, the illumination component will be eliminated. The next step is the recursive stability constraint in which $H_0(\omega) = H_1(\omega/2)$ retains the same initial high pass shape

as that used within the recursion. The next phase is the band pass filter in which $B_{k,m}(\omega)$ is the first level of the band pass filter and $B_{k-1,m}(\omega/2)$ is the next level of the band pass filter. $G_k(\omega)$ is the first level of the high pass filter and $G_{k-1}(\omega/2)$ is the next level of the high pass filter. The process is continued until the unity system response is equal to one. The high frequency component H_0 or the reflectance component is extracted from the image. ω_{max} is the maximum frequency. ω_1 is the frequency in which the $H_0(\omega)$ starts to attenuate. The next phase is the estimation of low bands of the input image where G_0 is the illumination component. The non-oriented band pass filter is estimated where B(ω) is the band pass filter and ω_0 is the minimum frequency. Unlike the non-oriented band pass filter the oriented band pass filter is estimated using $H(u,v)$. The cut-off frequency is D_h, D_v. The translated and the rotated frequency coordinates are u^*,v^*. The next phase after edge enhancement is the optimization of the high pass filter and band pass filter.

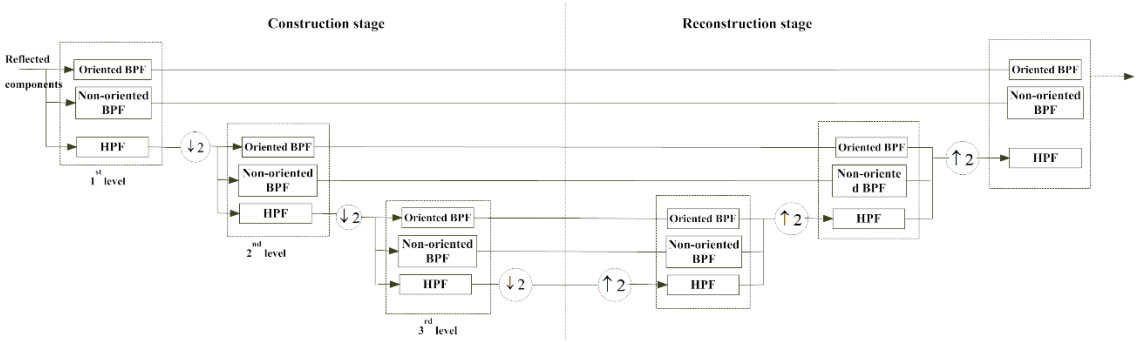

Figure 6.2: System diagram of enhanced steerable pyramid transform for proposed algorithm.

6.1.6 Coherence Component Extraction

The coherence component extraction method is used to examine the similarity between two signals or two datasets. The image consists of several low and high frequency components. These components are called locally narrowband or locally coherent. Although a locally coherent component may be wideband and highly non-stationary on a global scale, it is approximately sinusoidal over sufficiently small neighbourhoods (Kitlas Golińska, 2011) (Gardner, 1992). The system estimates structural similarity as follows:

$$C_{nm} = \frac{|G_{nm}|^2}{G_n G_m} \tag{6.2}$$

where, C_{nm} is evaluated on each pixel of the image, and G_n is the auto correlation of the input image. G_m is the autocorrelation of the SPT output image, and G_{nm} is the

cross correlation between input image and the SPT output image. Finally, the preserved edges are added back to the speckle suppressed output image.

(a) (b) (c) (d) (e)

Figure 6.3: Outputs of different stages of the proposed algorithm for a sample ultrasound image of the gallbladder. a) Input ultrasound image b) Canny edge detected image c) Output of MAWF, d) third level SPT image e) Feature enhanced output image after adding edges.

Figure 6.3 shows the output images of each phase of the proposed speckle artifact reduction pipeline using the ultrasonography image of the gallbladder as an example. The approach reduces the speckle content present in the image and enhances texture features, especially for regions with low intensity contrast. Additionally, as can be seen in Figure 6.3, edges of small regions are well retained, and some faint anatomical features of the input gallbladder ultrasound image have become more clearly visible.

6.2 Experimental Results and Discussion

The proposed SPT-CCE system is applied on a clinical dataset, synthetically modelled images (Chapter 4), standard test images (e.g. pepper image) and procedurally generated gray-level patterns. To validate the performance of the proposed system we first used synthetically modelled images for objective analysis. The subjective evaluation was then performed on real ultrasound images to determine their usefulness for clinical interpretation.

To evaluate the performance of the proposed SPT-CCE algorithm, the quality of the output images are compared with reference input images in terms of peak signal to noise ratio (PSNR), structural similarity index metric (SSIM), and universal quality index (UQI) as detailed in chapter 3.

6.2.1 Synthetically Modelled Ultrasound Image Analysis

To evaluate the performance of filtering algorithms, we need a data set consisting of noiseless images representing the ground truth, to which one can add noise in a controlled manner. This enables an unbiased numerical comparison of algorithms. In

chapter 4 realistic synthetic ultrasound images were generated by using an acquisition model, speckle simulation and interpolation of the sample points. The generated images were evaluated quantitatively, based on statistical analysis of texture features and qualitatively, based on subjective evaluation by clinical experts. Synthetic images generated by this simulation model have texture properties very similar to real ultrasound images. In this section, we discuss the performance of the proposed feature enhanced filtering algorithm (SPT-CCE) on synthetic ultrasound images.

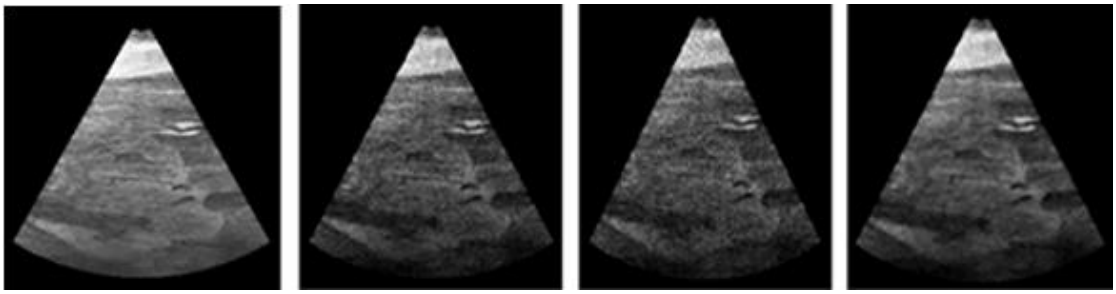

(a) (b) (c) (d)

Figure 6.4: Synthetic ultrasound images: (a) Reference noise free sector image, (b) Noisy image σ=0.3, (c) Noisy image σ=0.5, (d) Filtered output.

Figure 6.4 shows a set of four images each of resolution 256 × 256 pixels: (a) is a full sector image without the addition of speckle artifact. (b), (c) are synthetic ultrasound images that are generated using radial polar sampling technique with n=110, m=120 and $\sigma = 0.3, 0.5$ (chapter 4) and (d) is the filtered output image using the proposed technique. The above sampling and noise parameters were selected as they were found to generate images very similar in content and texture to real ultrasound images (Chapter 4). Here, n is the lateral resolution (number of simulated ultrasound beams), m the axial resolution (number of sampling points along each beam) and σ the standard deviation of speckle content added to each sampling point of the sector image.

Table 6.1: Performance analysis of synthetic ultrasound images for varying σ.

IQM	**0.3**	**0.5**	**0.7**	**0.9**
PSNR	41.71	40.54	39.24	35.73
SSIM	0.99	0.99	0.99	0.98
UQI	0.94	0.90	0.88	0.82

Table 6.1 shows the performance of the proposed SPT-CCE algorithm on synthetically modelled ultrasound images. This analysis clearly indicates that the proposed algorithm can withstand a high amount of speckle content from 0.3 to 0.9, since in all cases, we have obtained a PSNR value above 35. SSIM values were found to

be almost close to unity, which shows that the resultant image and reference image are structurally similar. Higher the value of UQI (its maximum value is 1), lesser is the distortion of output image relative to the input.

6.2.2 Subjective Evaluation of Clinical Ultrasound Image Datasets

The proposed system is applied on 30 real ultrasonography scans of resolution 472×425 pixels, with 5 images from each of the six dataset classes of thyroid, heart, gallbladder, liver, carotid arteries, ovary, and uterus fibroid. An outline of the analysis of results is presented below. In qualitative analysis, the original clinical ultrasound images (inputs) and despeckled images (outputs) of our algorithm for each dataset class were organized in pairs and randomly presented to four clinical experts for independent review. The evaluation scores were given on a 5-point scale based on their subjective preference as shown in Table 6.2. The reviewers considered various image quality aspects such as texture, heterogeneity, fine detailing, resolution improvement, easily distinguishable image features and structures. The subjective evaluation confirms that the outputs presented in Figure 6.5 obtained by our proposed despeckling pipeline provide better quality and features suitable for diagnostic interpretation and reasoning. The proposed SPT-CCE algorithm is able to perform sufficient speckle suppression with improved visual clarity. Clinicians suggested that the feature clarity in darker ultrasound images needs to be improved in a controlled manner. The subjective evaluators gave low scores to the thyroid and carotid artery output images, as both the images have dark structural content. The proposed system is able to enhance low intensity regions very well but not for images containing predominantly dark regions.

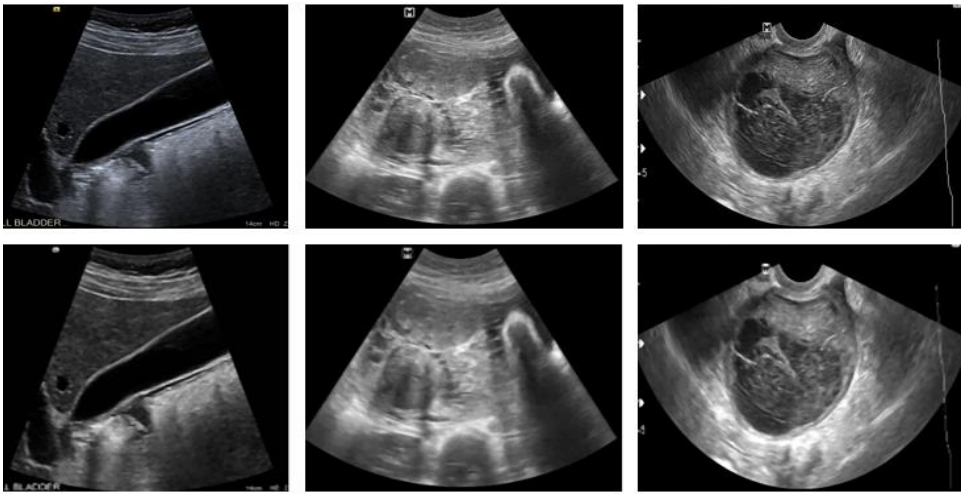

Figure 6.5: Clinical ultrasound images of the gallbladder, uterus, and ovary used as input (top-row) and feature enhanced speckle filtered output images (bottom row).

Table 6.2: Mean subjective evaluation scores assigned by clinical experts.

Experts	Thyroid	Ovary	Uterus	Carotid Artery	Gall bladder	Liver
Mean Score	3.5	4	4	3.75	4	4

6.3 Comparative Analysis of Algorithms

In this section, the proposed SPT-CCE algorithm is compared with recently proposed despeckling algorithms (Farouj, Freyermuth, Navarro, Clausel, & Delachartre, 2017) (J. Yang et al., 2016) (Uddin et al., 2016) (Gai, Zhang, Yang, & Yu, 2017) using PSNR, SSIM and UQI as quality metrics. All experiments presented in this section were performed on images of size 512× 512 pixels.

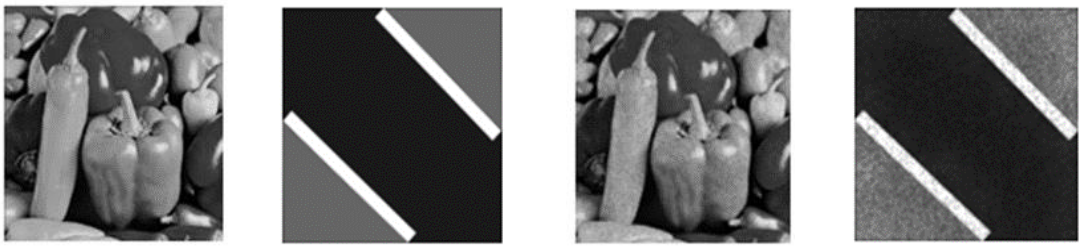

(a) (b) (c) (d)

Figure 6.6: (a) Input pepper image (b) Synthetic pattern image (c) and (d) Filtered output.

Table 6.3: Measure of PSNR for pepper image in Figure 6.6 (a) for varying σ.

Methods /σ	2	3	4
Noisy	20.21	16.65	14.16
HWF	29.25	27.65	26.44
DHWF	29.09	27.4	26.17
SPT-CCE	37.27	35.56	33.54

Table 6.4: Measure of SSIM for pepper image in Fig. 6.6(a) for varying σ.

Methods /σ	2	3	4
Noisy	0.35	0.23	0.16
HWF	0.78	0.75	0.73
DHWF	0.76	0.72	0.69
SPT-CCE	0.9753	0.9485	0.9176

Table 6.3 and Table 6.4 show the PSNR and SSIM values for different noise levels for the proposed and the existing systems, namely hyperbolic wavelet-Fisz

(HWF), and data-driven hyperbolic wavelet-Fisz (DHWF) (Farouj, Freyermuth, Navarro, Clausel, & Delachartre, 2017). The proposed system gives a better performance than the HWF and DHWF despeckling systems in terms of PSNR and SSIM values. The proposed SPT-CCE method has achieved a better PSNR even for the high σ values 5, 6 and 7. SSIM measures structural similarity between two images in the visual sense. When SSIM = 1 (its maximum value), it shows that two images are completely identical. The proposed SPT-CCE method attained a value close to unity.

Here, the proposed algorithm is compared with another well-established ultrasound speckle reduction algorithm i.e. non-local mean local statistics (NLMLS) (Yang, et al 2016) using SSIM for different noise levels ($\sigma = 0.2, 0.4, 0.6, 0.8$) for synthetic pattern images given in Figure 6.6(b).

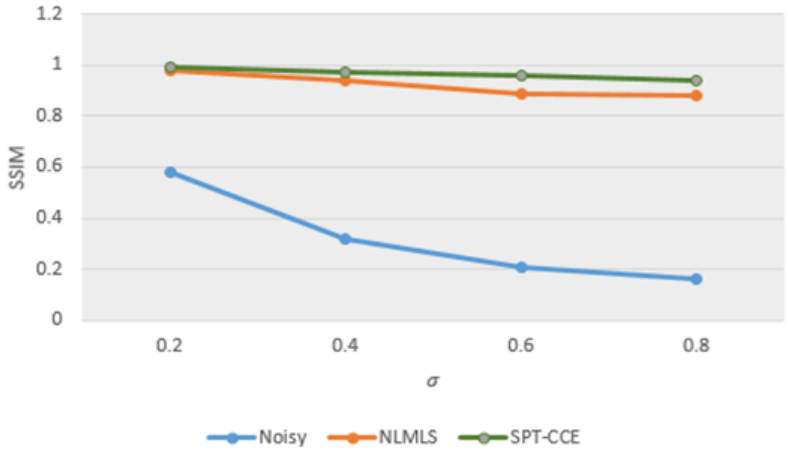

Figure 6.7: Comparison of NLMLS and SPT-CCE using SSIM with varying σ for synthetic image in Figure 6.6 (b).

Figure 6.7 shows that structural similarity between the input image and the processed image is nearly equal to unity even for higher values of σ content. The performance of the proposed method exceeds the NLMLS algorithm as shown above.

In Figure 6.8 (a)-(c), the proposed SPT-CCE system is compared with four methods: Detail Preserving Anisotropic Diffusion (DPAD) (Aja-Fernández & Alberola-López, 2006), Non-Linear Multi-scale Wavelet Diffusion (NMWD), Non-Linear Multi-Scale Complex Wavelet Diffusion Based Algorithm (NMCWDA) (Uddin et al., 2016) and Laplacian mixture model and wavelet transform (LMMWT) (Gai, Zhang, Yang, & Yu, 2017).

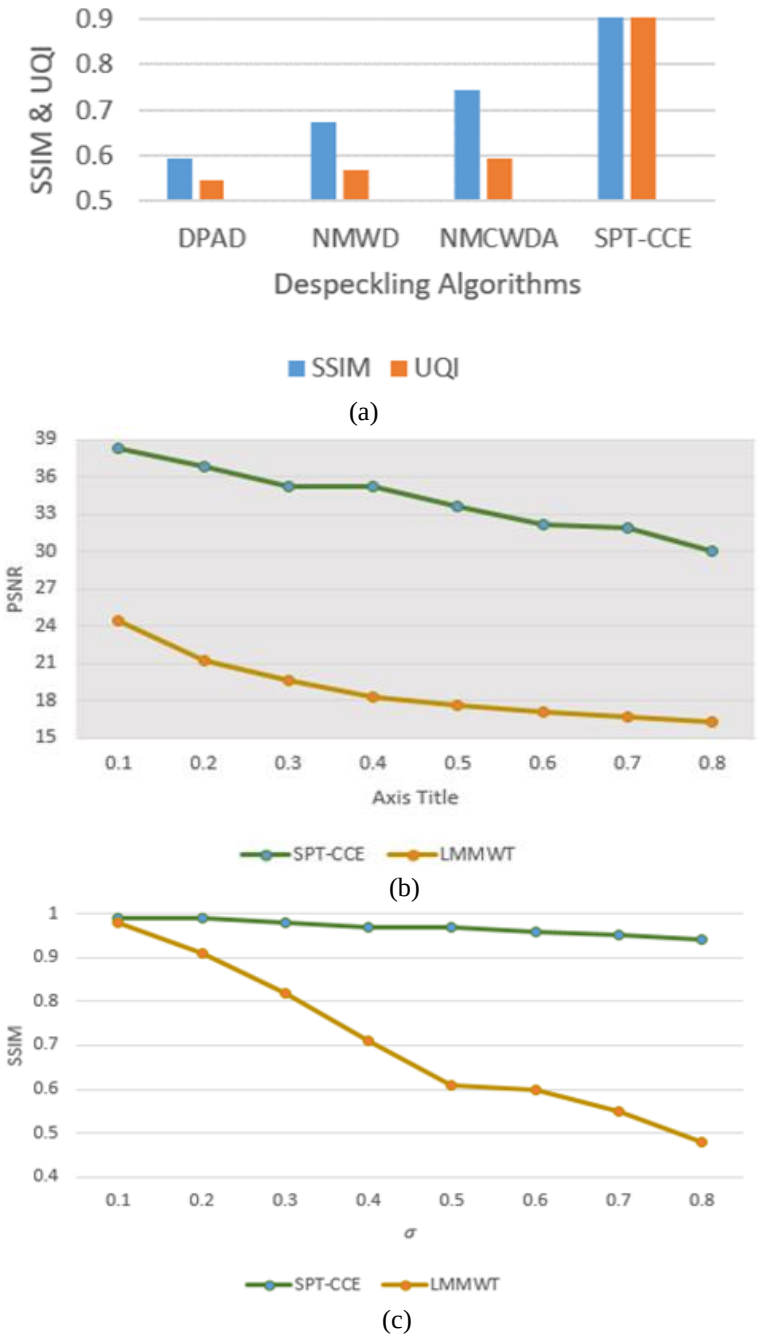

Figure 6.8: (a) SSIM and UQI values for synthetic image in Figure 6.6(b) σ=0.04,and (b) and (c) Comparison of SPT-CCE and LMMWT with varying σ.

Figure 6.8 (a) shows that the SSIM and UQI values computed from the outputs obtained using the proposed system were higher than those obtained using DPAD, NMWD, and NMCWDA speckle reduction techniques. Higher values of SSIM and UQI show high structural similarity and less distortion in the processed image. Figure 6.8 (b) and Figure 6.8 (c) show the results of a comparative study using PSNR and SSIM values of the proposed system and the LMMWT model with varying σ. The experimental analysis clearly indicates that the proposed system can withstand even higher noise content. As noise was varied from σ, 0.1 to 0.8, both PSNR and SSIM

started reducing significantly in the LMMWT model. It has been experimentally observed that images processed by the SPT-CCE pipeline were able to preserve both structural content and quality of the input image, while significantly suppressing the speckle artifact content.

Figure 6.9 presents a comparative analysis of the proposed method with various related state–of–the-art work in the area of ultrasound image analysis. Among most of the filters used for ultrasound image despeckling, the speckle anisotropic diffusion filtering (SRAD) is considered as suitable approach. Here, the despeckling method using SPT-CCE is compared with anisotropic diffusion filtering (ADF), speckle reducing anisotropic diffusion filtering (SRAD), Perona and Malik anisotropic diffusion method (PMAD), Frost filtering, wavelet method (WT), Wiener filter, and Gamma MAP (Loizou & Pattichis, 2015a) (Loizou & Pattichis, 2015b). We have considered two image quality metrics SSIM, and PSNR and the study was performed on synthetically modelled images.

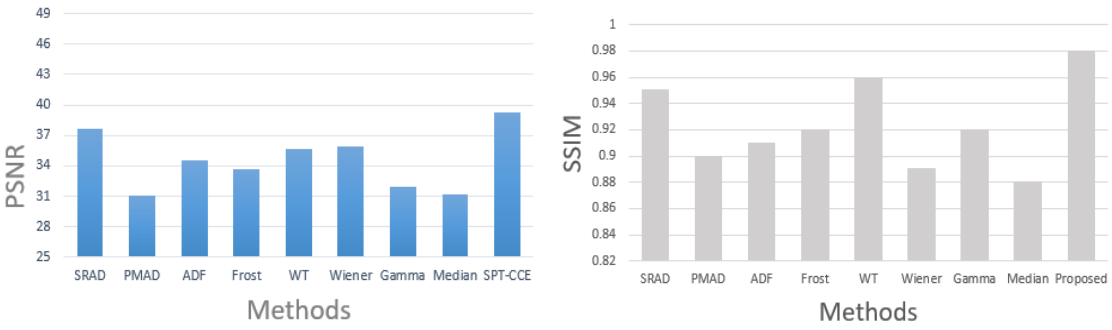

Figure 6.9: PSNR, and SSIM values for the synthetic outputs.

The main motivation of using well established filtering techniques for comparative analysis is that these methods are frequently used for ultrasound post-processing image analysis. Figure 6.9 indicates that the proposed system has yielded significantly higher values for image quality metrics as compared to other filtering techniques developed for speckle suppression and feature preservation. The proposed system has the capability to reduce speckle significantly as shown by a higher PSNR value and to preserve structural similarity as shown by a SSIM value near to unity. The SRAD filter also showed better results as compared to other filtering techniques used in this study. Wavelet filtering also demonstrated comparable results to the proposed system in terms of preserving structural content of the output frames as SSIM value is found to be sufficiently high.

6.4 Chapter Summary

The chapter has presented a novel SPT-CCE based speckle content reduction and feature enhancement algorithm for ultrasound images. The proposed SPT-CCE technique despeckled the ultrasound images without losing the edge information and significant feature details. The Canny algorithm with optimum threshold detected the edges effectively and the MAWF smoothened the speckle artifact content by modifying the filtering coefficients. The detected high frequency components using DFT were then enhanced using the SPT technique. The CCE technique enhanced the texture features of the ultrasound images and the preserved edges are added back to the despeckled image.

Subject matter experts considered a wide range of visual image features to score the usefulness of the output images through the proposed system. The experimental study has also considered a few state-of-the-art techniques to compare our proposed SPT-CCE using PSNR and SSIM, and experimental evaluation indicates the proposed clustering model performed very well in preserving the output image's visual quality and structure. In the overall analysis, it has been observed that the SPT-CCE technique provide improved results and found to be a better technique than clustering methods. The proposed algorithm gave the required results for even high levels of speckle content. The reconstructed ultrasound images had better contrast and achieved high speckle reduction levels that are useful for better diagnostic interpretation. However, it was also noticed that the proposed SPT-CCE method generates over contrast-enhanced images where large dark regions are present, which led to a low subjective evaluation score by clinical experts. We therefore need a system that can enhance medical ultrasound images in a controlled manner and handle contrast enhancement of darker image regions at the desired level. A contrast limited adaptive histogram equalization method is proposed in the next chapter to meet this objective.

7 FEATURE ENHANCEMENT USING CONTRAST LIMITED ADAPTIVE HISTOGRAM EQUALIZATION

We now focus our attention to improve contrast in clinical ultrasound scans. Ultrasound images generally have low contrast and may contain bright and dark regions. This chapter proposes an improved contrast limited adaptive histogram equalization (CLAHE) method for enhancing texture features, contrast, resolvable details, and image structures to which the human visual system is sensitive in ultrasound images (G. Yadav, Maheshwari, & Agarwal, 2014). The CLAHE method has been available over a decade and found to be an efficient technique to improve the overall visual quality of medical images, such as Computer Tomography, MR, and retinal images . However, sufficient importance has not been given to a detailed analysis of the CLAHE method for ultrasound image contrast enhancement, and a detailed study of parametric variations has not been performed. This chapter proposes a quantitative algorithm for automatically finding the tile size and clip limit used by CLAHE, based on the randomness (entropy) of the input frames and the quality of the output images. Three different types of distribution functions *viz*., uniform, Rayleigh, and exponential and also three different interpolation techniques *viz*., bilinear, cubic, and Lanczos-3 are used

in the experimental analysis to compare the quality of the generated contrast enhanced ultrasound frames. The main contributions of this chapter in feature enhancement using CLAHE can be summarised as follows:

1. The study shows that the performance of the CLAHE algorithm could be significantly improved by using a pre-processing phase for speckle noise removal.
2. The optimal clip-limit for the CLAHE algorithm is automatically determined using the quality metrics evaluated from output frames.
3. The size of the image tiles (contextual regions) is determined automatically using a global entropy function.
4. The work looks at three different types of distribution functions for the shapes of the target histograms in image tiles and performs a comparative analysis.
5. The study shows that the interpolation scheme used by the CLAHE algorithm also plays a vital role, and gives a comparative analysis of the experimental results using three types of interpolation algorithms.

7.1 Proposed CLAHE Framework

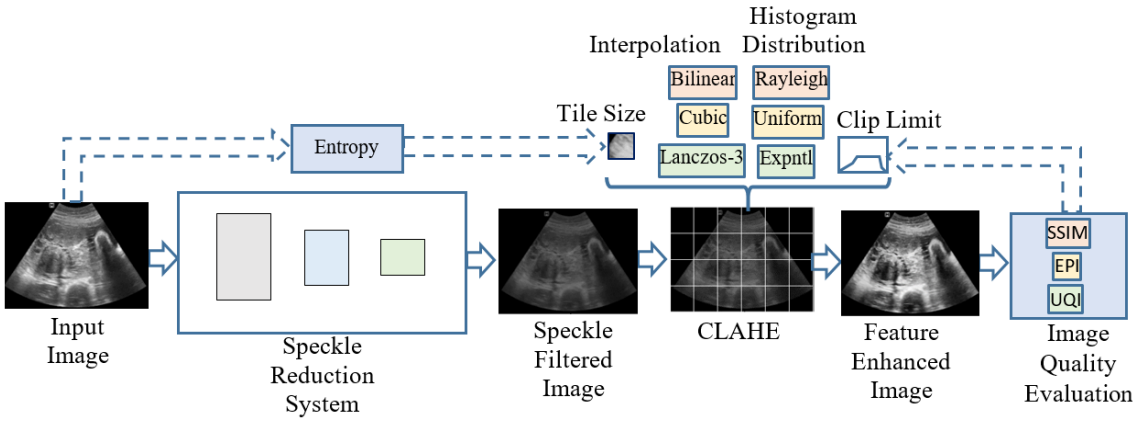

Figure 7.1: The processing stages of the proposed pipeline for speckle artifact reduction and followed by feature enhancement.

Figure 7.1 gives the complete framework presented in this chapter with the aim of producing speckle reduced feature enhanced ultrasound images. The proposed processing framework has two stages that are speckle reduction system and contrast limited adaptive histogram equalization to improve the overall visual quality of the images to which human visual system is sensitive. The speckle reduction system can be any filtering algorithm, as discussed in the previous chapters 5 and 6. In the following,

we outline a method to determine the best possible interpolation and distribution combination and optimum cliplimit in the CLAHE algorithm to improve the overall texture quality of the ultrasound images after despeckling.

7.2 Contrast Limited Adaptive Histogram Equalization

The CLAHE method subdivides the image into a number of tiles. We estimate the tile size *s* using the global entropy of the input frame. For a greyscale image with 256 levels, the entropy *E* is defined as

$$E = -\sum_{k=0}^{255} p_k \log_2(p_k) \quad (7.1)$$

where p_k is the probability associated with grey level *k*. We use an exponential decay function of the type

$$s = (M - E_{max})\, e^{-\lambda E} + E_{max} \quad (7.2)$$

to compute the tile size *s* based on the entropy value *E* for a given image of size *M*. The maximum entropy E_{max} for grey-level images is 8. The graph in Figure 7.2, generated for the input image size *M* = 256 pixels and λ=0.7 shows an example of the variation of tile sizes with entropy. When the entropy is maximum, the function gives a tile size of 8x8 pixels. For a very small entropy value 1 corresponding to a nearly uniform intensity distribution, we obtain a tile size that is half the size of the input image. Most ultrasound images have an entropy value within the shaded region of the graph in Figure 7.2, where the tile size ranges from 8x8 pixels to 16x16 pixels.

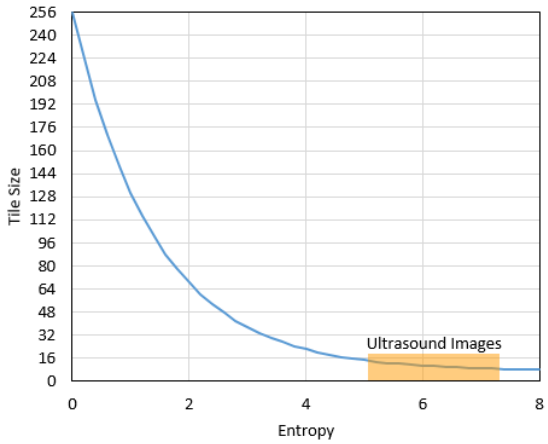

Figure 7.2: A sample graph showing the variation of tile size with the entropy of the input image.

This implementation used three different types of target histogram distribution functions and three types of interpolations of transformation functions to analyse the

performance of the CLAHE algorithm on ultrasound images. The distribution function specifies the shape of the target histogram of the contrast enhanced image within each tile. Finally, the transform functions of neighbouring small regions are combined using interpolation to eliminate any kind of induced artifacts. This work considers three different types of distribution functions that are uniform, Rayleigh, and exponential. The conventional method of CLAHE uses bilinear interpolation techniques for combining the transformation functions computed for neighbouring regions. This approach used three different interpolation systems, viz., bilinear, cubic, and Lanczos-3 individually to perform an extensive comparative analysis. The main aim of this evaluation is to find the best suitable combination for enhancing the contrast of ultrasound images. The computational steps in the CLAHE method are listed below.

Processing steps in the CLAHE algorithm

1. *Read the speckle filtered image.*
2. *Divide images into a number of contextual regions using tile size evaluated using Eq. (7.2).*
3. *For each sub-region calculate the uniform, Rayleigh, and exponential distribution function individually to get the desired histogram shape.*
4. *For each sub-frame compute the histogram and the highest peak value. Initialize the clip limit using quantitative measures of image quality.*
5. *For each grey level bin in the histogram, if histogram bin > clip limit level, then clip the histogram bin.*
6. *Compute the transformation functions for each tile, and use the selected interpolation method to combine the transform functions to get the new intensity value at each pixel position.*

The above steps result in the enhancement of fine details in ultrasound frames as shown in Figure 7.6 -Figure 7.8, and also in the subsequent sections.

It is important to choose the right value for the clip limit so that the enhancement of features across all frames are consistent and acceptable. If the clip limit is too high, it will cause contrast variation to oversaturate or if too low, will lead to an image with a flat histogram. An initial clip limit value of 0.01 has been experimentally determined and used for all nine combinations and all types of images for the ultrasound analysis. As seen in Figure 7.2, when the clip limit is increased from 0.01, the overall quality of

the images showed a reduction as measured by metrics such as the structural similarity index metric (SSIM), and universal quality index (UQI) presented in chapter 3.

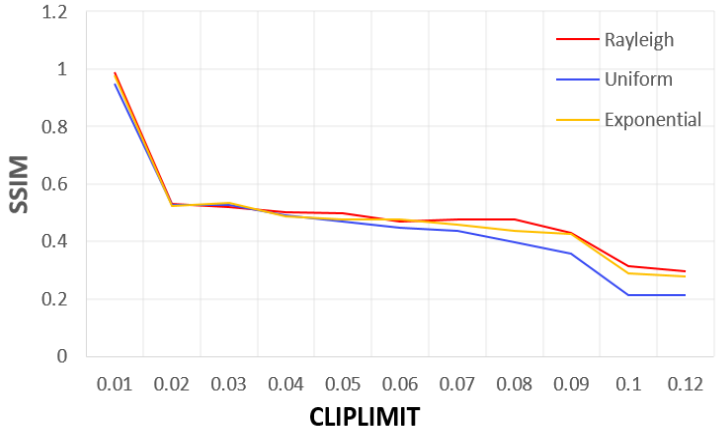

(a)

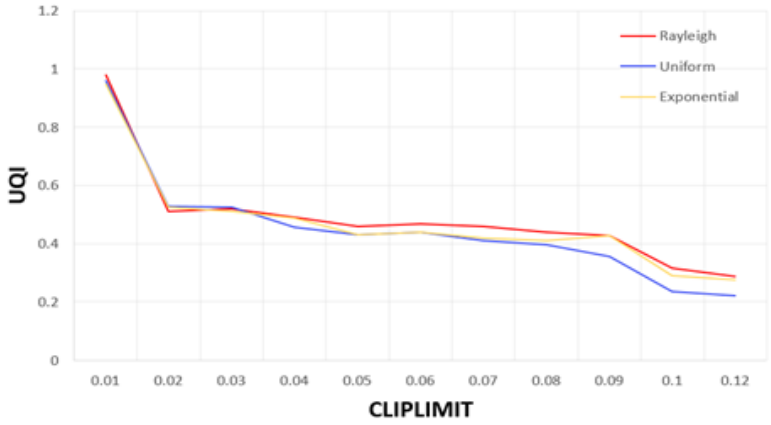

(b)

Figure 7.3: Variations of output image quality as measured by SSIM (a), UQI (b), with the clip limit used by the CLAHE algorithm for three different target distribution functions.

As seen in Figure 7.3, the initial clip limit provides nearly unity value for the SSIM metric for all three distribution functions. Similar results were obtained with other quality metrics (EPI, UQI) and interpolation functions used in our experimental analysis. In Figure 7.4, we provide the outputs generated using three different values of clip limits 0.02, 0.04, and 0.08, and see that all three images have larger than the desired levels of contrast enhancement, in comparison with the output for clip limit value 0.01. The SSIM, EPI, and UQI values indicated in Figure 7.4 also show that the overall quality of the images measured using their structure, edges, and visual information gradually reduce as the clip limit is increased.

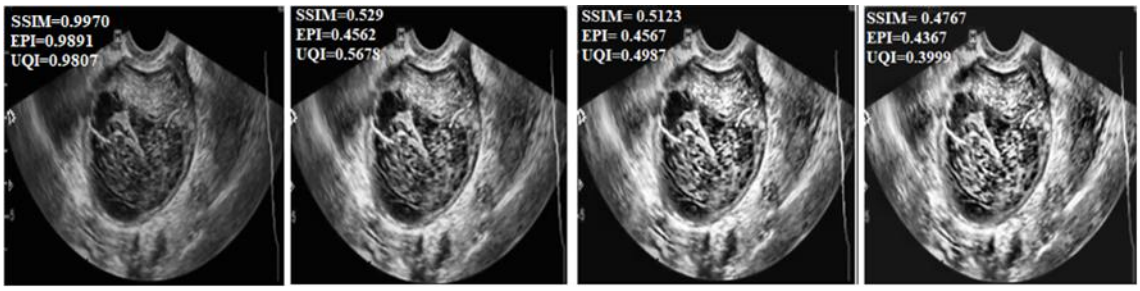

Figure 7.4: Sample outputs showing the effect of variation of clip limit. (a) 0.01, (b) 0.02, (c) 0.04, and (d) 0.08.

7.3 Integrated Filtering and Enhancement

This section implements an integrated system comprising of the filtering methods developed in chapters 5 and 6 and the modified contrast limited adaptive histogram equalization method presented earlier in this chapter. The main aim here is to improve the overall visual clarity of the images by passing them through a filtering stage followed by the contrast enhancement stage. We also aim to determine which of despeckling system out of two (PFCM and SPT) performed well and generated feature enhanced and speckle reduced medical ultrasound images when combined with CLAHE. For developing this system, we considered the clustering approach PFCM out of all clustering techniques as it yielded the highest subjective evaluation score (Chapter 5). The despeckled output generated using PFCM and SPT are input to the CLAHE system as shown in Figure 7.5. The performance evaluation model considers the time complexities of the two methods in the integrated system (PFCM+CLAHE and SPT+CLAHE). The objective and subjective evaluation of the output images generated by the above two combinations are also performed and presented in Table 7.1.

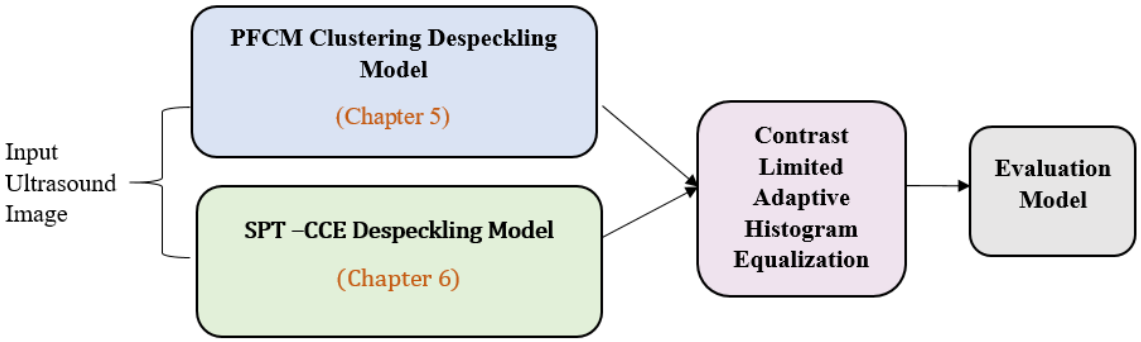

Figure 7.5: Integrated filtering system for despeckling and feature enhancement.

For both the combinations presented in Figure 7.5, we have carried out the objective evaluation of the outputs with three different types of distribution functions (uniform, Rayleigh, and exponential), three interpolation functions (bilinear, cubic and Lanczos-3), and three quality metrics (SSIM, EPI and UQI). The qualitative evaluation considered six types of human anatomical ultrasound scans e.g. breast cancer, uterine fibroids, transvaginal ovary, ovarian cyst, heart, and chest pleural effusion to show the effectiveness of enhancement after filtering. The analysis considered 30 images, 5 from each of the above types of ultrasound scans. Nine pairs of input and output images corresponding to 3 distribution functions and 3 interpolation techniques were generated by the system in Figure 7.5 for each of the above 30 images. 3 images from each of the generated sets was selected and reviewed independently by four subject matter experts and the mean scores are given on a 5 point scale based on their subjective preference as shown in Table 7.1. This subjective assessment shows Rayleigh distribution and Lanczos-3 interpolation as the most preferred combination for each of the filtering methods used. This combination is used in the following analysis.

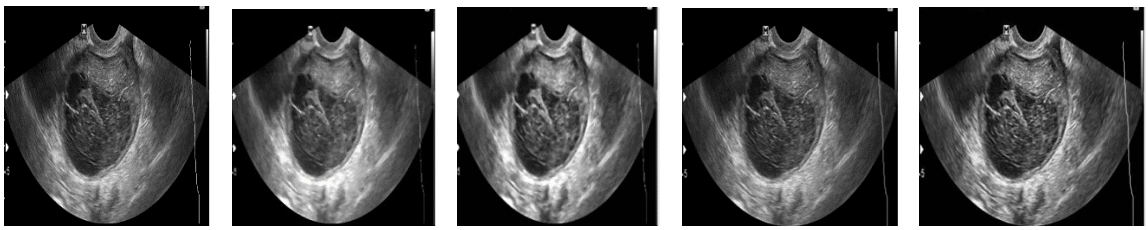

(a) (b) (c) (d) (e)

Figure 7.6: (a) Original ultrasound image, (b) SPT filtered output image, (c) SPT+CLAHE output image, (d) PFCM output image, and (e) PFCM+CLAHE output image.

Figure 7.6 shows the output images for the ovarian scan. Figures 7.6 (b) and (d) show outputs generated by independent despeckling system SPT and PFCM clustering. Figures 7.6 (c) and (e) show outputs obtained by the integrated system of SPT and CLAHE, and PFCM and CLAHE. The SPT and CLAHE combination as given in Figure 7.6 (c) clearly shows reduced speckle content along with feature improvement. The features of the output images of the PFCM+CLAHE system have also improved compared to the outputs attained using PFCM clustering model itself.

Table 7.1: Quality evaluation of integrated system.

Model	Time Complexity (sec)	SSIM	EPI	UQI	Mean Scores (Clinicians)
PFCM+CLAHE	3.17	0.9490	0.9789	0.8968	3.75
SPT+CLAHE	2.03	0.9970	0.9891	0.9807	4.75

Table 7.1 shows the final analyses of the two integrated models using time complexity and mean scores given by clinicians. Here, the study considered three quality metrics that are structural similarity index (SSIM), edge preservation index (EPI), and universal quality index (UQI). The time complexity of the SPT+CLAHE method is low as compared to PFCM +CLAHE model. The mean subjective score of the CLAHE based enhancement with SPT filtering algorithm is also improved as compared to the PFCM+CLAHE combination. The PFCM+CLAHE system attained low mean subjective score due to over amplification of certain granular patterns present within the image structure, which is not desirable for human visual analysis. The SPT+CLAHE based despeckling and feature enhancement is able to preserve the overall image quality in terms of contrast, resolvable fine details, and structural content with minimum loss. The subject matter experts also preferred the outputs generated by the SPT+CLAHE system. These outputs also gave improved SSIM, EPI, and UQI values in objective evaluation.

In the following figures, we present the outputs obtained using three different distribution and three interpolation techniques for six different anatomical structures. The outputs show varying levels of texture feature enhancement. Further, the speckle content has been suppressed significantly, and blurring is also reduced. The outputs clearly show that the processing pipeline has the capabilities to address speckle noise issues and perform acceptable levels of feature enhancement. As mentioned previously, out of the nine combinations presented in the figures, the Rayleigh distribution and Lanczos-3 interpolation provided outputs that were preferred by subject matter experts. Figure 7.7 shows that output images have improved contrast, resolvable details and visual image features for all different anatomical ultrasound scans used in this study.

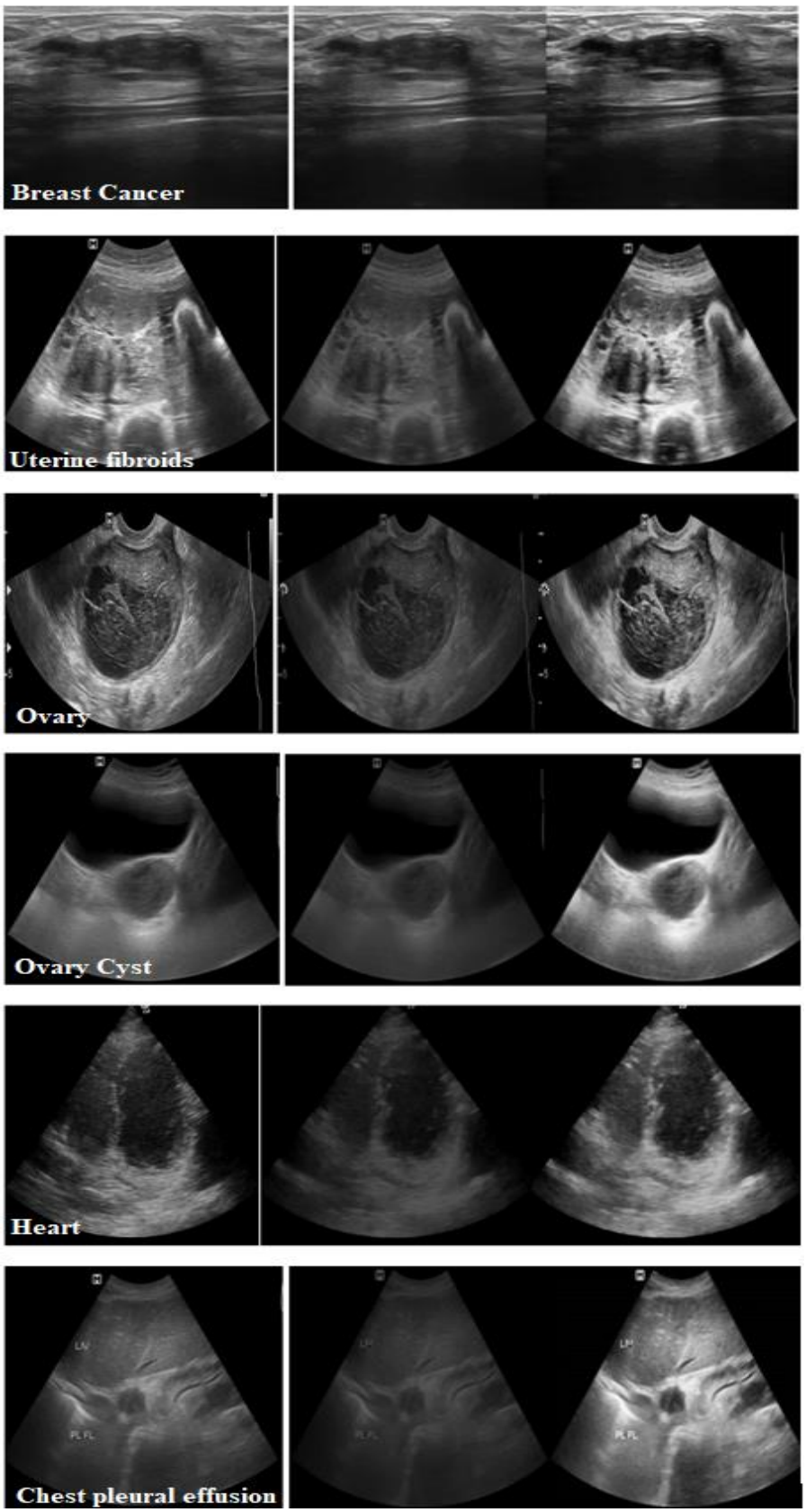

Figure 7.7: Original ultrasound input images (left side) before speckle filtering, speckle filtered images (centre), and feature enhanced images using SPT+CLAHE with a combination of Rayleigh distribution and Lanczos-3 interpolation (right side).

Figure 7.8 shows the results using the remaining two distributions in combination with Lanczos-3 interpolation. Even though these distributions gave comparatively lower scores than Rayleigh distribution, we present the images here for visual comparison.

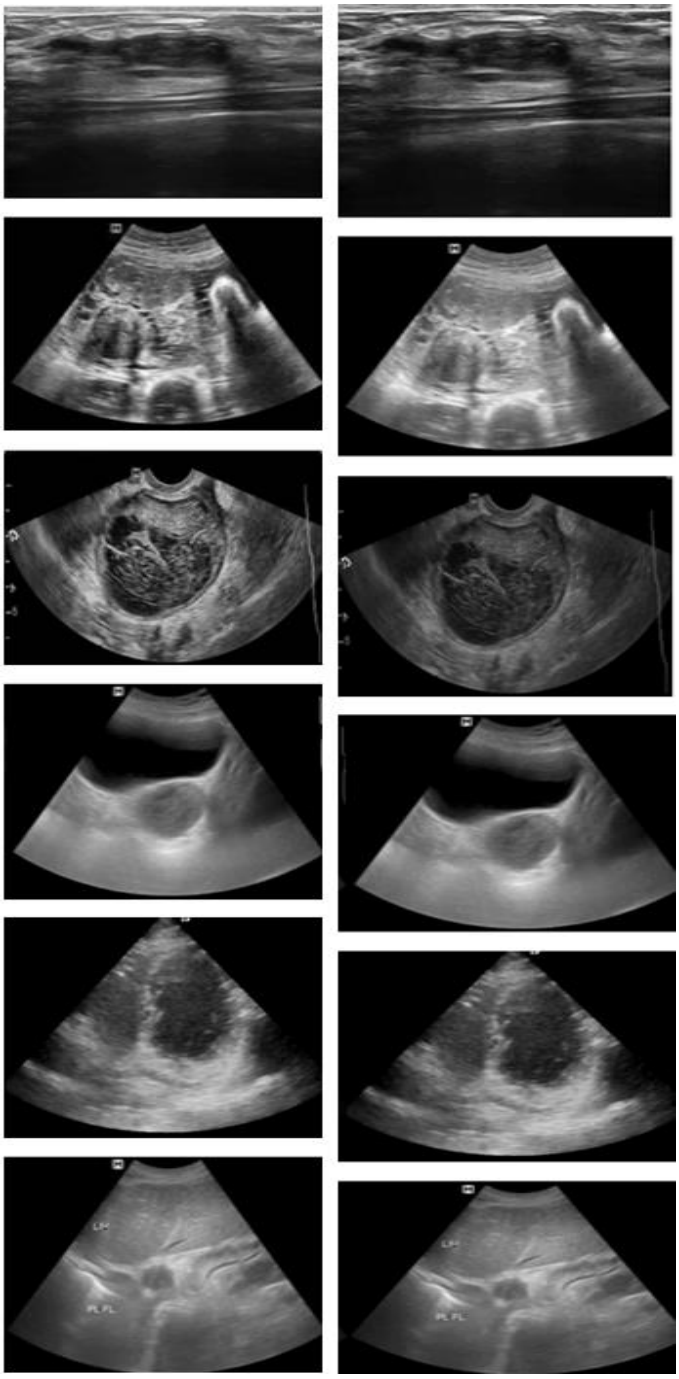

Figure 7.8: Feature enhanced ultrasound images using SPT+CLAHE with a combination of uniform distribution and Lanczos-3 interpolation (left column), and exponential distribution and Lanczos-3 interpolation (right column).

Figure 7.8 shows a comparison of outputs obtained from SPT +CLAHE method based on uniform and exponential distributions and Lanzcos-3 interpolation. The

outputs generated by using uniform distribution provides improved results except for the chest pleural effusion frames. This analysis demonstrates that we need the right combination of distribution function and interpolation technique for obtaining the desired levels of feature enhancement in images. Out of all three distribution functions used in this study (Figures 7.7 and 7.8), Rayleigh distribution in combination with Lanczos-3 interpolation gave better results as compared to the uniform and exponential distribution functions.

The subjective analysis and experimental demonstration using quality metrics clearly show that the modified SPT+ CLAHE using a combination of Rayleigh distribution and Lanczos-3 interpolation with clip limit 0.01and tile size obtained using the entropy measure provides impressive results by effectively reducing speckle noise, addressing the blurring issue and enhancing the required features of ultrasound images.

7.4 Chapter Summary

This study has presented a complete framework for speckle noise suppression and contrast enhancement of ultrasound images. The primary design requirements were to minimize blurring caused by speckle filtering algorithms, and to prevent over amplification of noise and contrast by feature enhancement algorithms. The two integrated system has designed by using the PFCM and SPT despeckling framework with CLAHE. This system implemented to derive a combine system, which provides feature enhanced speckle reduce ultrasound images. Out of the two-combined processing pipeline, output obtained using SPT+CLAHE found to preferred choice by clinicians over PFCM+CLAHE. The time complexity of SPT+CLAHE integrated system is also low.

The processing pipeline used a novel SPT based method for speckle noise removal and then the features were enhanced using an improved CLAHE algorithm. The processing pipeline used three different types of distribution functions that are uniform, Rayleigh, and exponential were considered in combination with three different types of the interpolation techniques that are bilinear, cubic, and Lanczos-3, for comparative evaluation. The CLAHE method also utilized the entropy of the image to determine the number of contextual regions used in the subdivision step. The optimum clip limit was found using a quantitative analysis of the output image quality.

The chapter also presented an extensive quantitative analysis of the proposed algorithm using image quality metrics, and also qualitative evaluation by subject matter

experts considering a wide range of image attributes to ascertain their usefulness in clinical applications. The experimental analysis conducted indicates SPT+CLAHE based on the Rayleigh distribution and Lanczos-3 interpolation technique improved features with the desired quality, for all types of ultrasound images used in this study.

The next chapter concludes the thesis with a summary of research findings, an outline of the contributions made by developing and validating algorithms for synthetic image modelling, speckle filtering and finally a feature enhanced speckle reduction framework. Further research possibilities are also discussed in the chapter.

8 CONCLUSIONS AND FUTURE WORK

8.1 Conclusions

This thesis has proposed novel algorithms in the field of ultrasound image analysis, specifically for speckle filtering and feature enhancement. It considered the primary requirement for synthetic ultrasound images for validating filtering methods, and developed a complete framework for modelling synthetic images that closely resemble real ultrasound images in terms of their image and texture characteristics. The thesis placed importance to edge preserving speckle filtering techniques and proposed two transform based methods, one using clustering algorithms and the other using steerable pyramid transformation. These algorithms were further analysed in combination with contrast limited adaptive histogram equalization for the development of an integrated framework for feature enhanced speckle reduction. All developed algorithms have been validated using extensive quantitative evaluation using several image quality metrics, and the corresponding outputs assessed for their usefulness and diagnostic value using subjective evaluation by clinical experts.

The main areas of contribution and a summary of research findings in each are area are outlined below:

Synthetic ultrasound image modelling (Chapter 4):

This thesis has developed a versatile framework for the generation of synthetic ultrasound images that allow several parameter variations such as lateral/axial

resolution, noise level, and interpolation schemes, specifically designed for validating filtering algorithms.

- The model supports three types of sampling and three interpolation methods.
- B-Scan images can be modelled using radial polar sampling.
- Linear scan images can be modelled using uniform grid sampling.
- Lanczos-3 is the preferred interpolation model.
- Entropy, SAM, SFM were used as image quality metrics, and rotation invariant LBP, GLCM as texture descriptors for comparing the quality of synthetic images with real ultrasound images.
- For B-scan simulation, the parametric values $n = 80$, $m = 120$, $\sigma = 0.5$ gave the best results with texture features closely matching real ultrasound images. An empirical formula $m = \text{floor}(0.56N\text{-}23)$ $250 \leq N \geq 500$ is derived to get the optimal value of m for a given resolution N.
- Currently, the input (noise-free) image to the sampling system is created by an artist including the primary features of an ultrasound image. In order to generate more realistic and a wide range of synthetic images, we require an automatic graphics based system.

Speckle atrifact reduction using clustering (Chapter 5):

This thesis has implemented a novel framework for despeckling of ultrasound images using clustering algorithms and identified the clustering algorithm that gives best performance.

- Demonstrated the feasibility of using clustering algorithms in the wavelet sub-band domain for speckle suppression.
- The PFCM algorithm performed better that other clustering algorithms
- The best PSNR value obtained using synthetic images is above 35dB. The SSIM obtained a value close to unit, i.e., 0.98.
- The best mean subjective score obtained is 3.75 out of 5.
- The clustering method is not very effective when noise is not uniformally distributed. The method performed well for synthetic images but was unable to attain the sufficient speckle reduction and desired quality in real images.

Speckle atrifact reduction using steerable pyramid transformation (Chapter 6):

This thesis developed an innovative framework for despeckling and visual feature preservation of ultrasound images by modifying steerable pyramid transformation. The study finds the potential for improved diagnostic evaluation.

- Implemented and validated a modified steerable pyramid transformation framework consisting of an adaptive Wiener filter, Canny edge detection, and coherence component extraction.
- The modified SPT performed better in terms of speckle suppression and visual image feature preservation compared to existing despeckling methods.
- The best PSNR value obtained using synthetic images is around 40dB. SSIM obtained a value very close to the unity i.e. 0.99.
- The best mean subjective score obtained is 4 out 5.
- Experimental results demonstrated that the modified SPT algorithm performs better than even the best clustering algorithm.
- The proposed framework was not found to be a very efficient approach for ultrasound images predominantly consisting of dark regions.

Feature Enhancement of ultrasound scans using Modified contrast limited adaptive histogram equalization (Chapter 7):

This thesis has formulated a versatile framework for feature quality improvement in ultrasound images that allow several parameter variations such as Entropy, cliplimit, distribution, and interpolation schemes. The study proposes novel algorithms for finding the optimal values of the above parameters.

- Demonstrated the usefulness of the modified CLAHE for overall image feature improvement after despeckling.
- The Rayleigh distribution and Lanczos-3 interpolation is found to be the preferred combination among possible nine combinations.
- The Entropy of the image is used for automatic tile size evaluation. An empirical formula to find the tile size is formulated as $s = (M - E_{max})\, e^{-\lambda E} + E_{max}$
- The optimal cliplimit is determined using quality metrics SSIM, EPI, and UQI. The optimum cliplimit found is 0.01 for ultrasound images.
- CLAHE highly depends on cliplimit and tile size. If proper values are not choosen it can generate conrtast amplified images or ring artifacts at strong edges.

Feature enhanced speckle reduction system (Chapter 7):

This thesis has implemented a complete processing pipeline to attain effective feature enhanced speckle content reduction in ultrasound scans. The study finds useful applications in improving the visual clarity of despeckled ultrasound images for better clinical interpretation.

- Two integrated systems PFCM+ CLAHE and SPT+CLAHE are designed, with the aim of deriving the most suitable combination.
- SPT+CLAHE is the preferred system.
- Time complexity of SPT+CLAHE is less than that of PFCM+CLAHE
- The values of SSIM, EPI, and UQI are close to unity.
- Mean subjective score obtained is 4.75 out of 5.
- The CLAHE algorithm can overamplify noise and contrast and therefore it is very important that the despeckling algorithm used in the system provides sufficent speckle reduction.

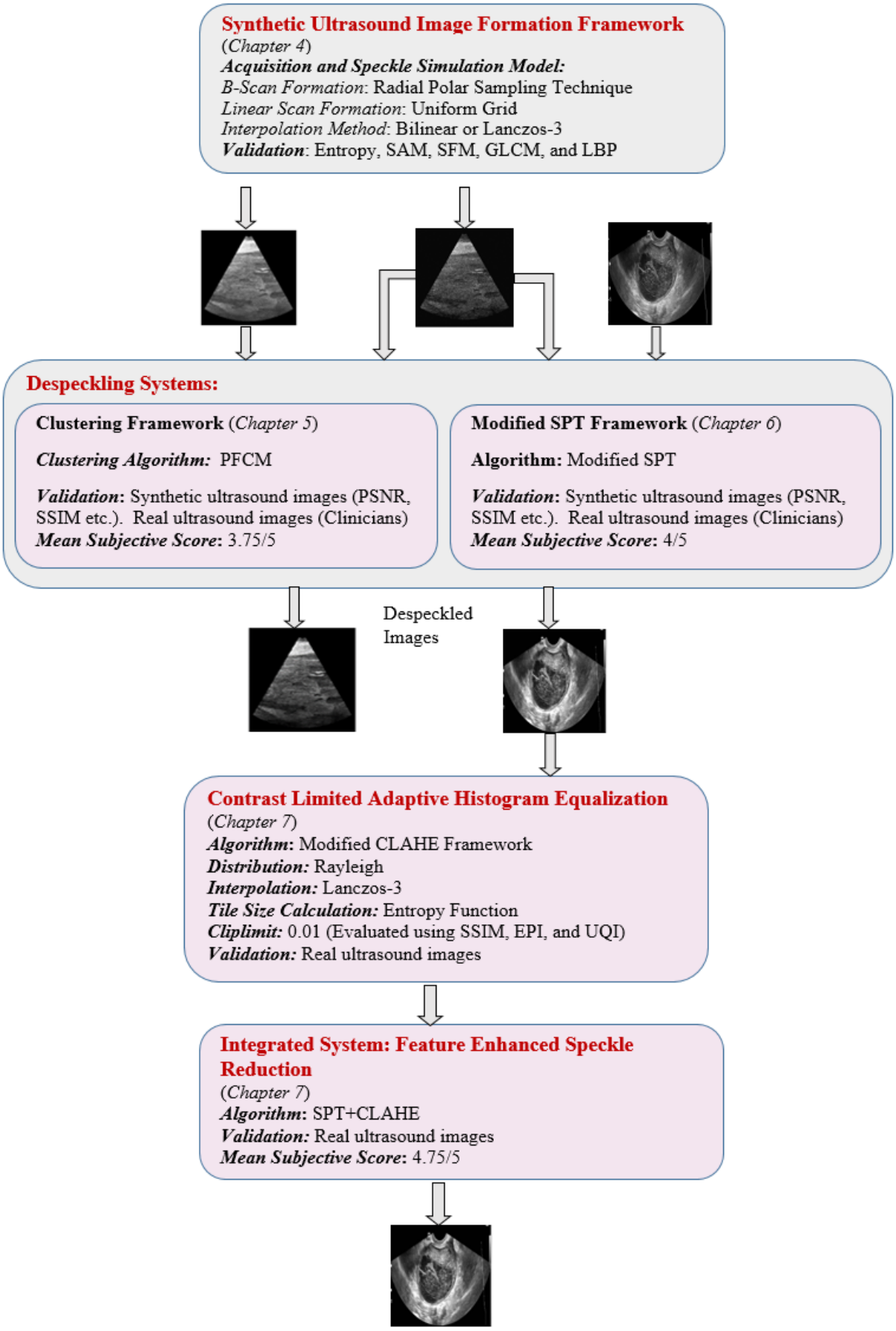

Figure 8.1: An overview of chapter-wise research contributions.

8.2 Ongoing Research and Future Work

The research work presented in this thesis is being further extended to the domain of advanced machine learning algorithms considering novel applications for image classification and segmentation. The speckle-filtering problem could be treated as a speckle segmentation problem for a neural network based implementation, where the network is trained using a large number of noise-free and noisy synthetic ultrasound images. With the availability of a framework for generating synthetic images, the training and cross-validation data for a convolutional neural network (CNN) could be constructed. This work is currently ongoing with a detailed study of CNN architectures and hyper-parameters for a despeckling application. Simultaneously, we are also endeavouring to generate a comprehensive database of synthetic ultrasound images with varying levels of speckle noise. Future research work is directed towards the development of the following systems and algorithms that could be considered as direct extensions of the work presented in the thesis:

- Agglomerative Clustering: Agglomerative Hierarchical Clustering methods can be used to mitigate some of the problems associated with clustering algorithms and to improve image quality in real ultrasound scans.
- Speckle filtering algorithms for realtime ultrasound video scans: The large number of consecutive frames in a video can provide a better characterization and a more comprehensive analysis of variations in speckle content and texture.
- Despeckling system for 3D ultrasound imaging: 3D ultroasund imaging provides more accuracy by revealing more information such as depth of images, more data collection, and image reconstructed from single sweep across the target organ.
- Feature based segmentation and classification systems for realtime ultrasound video scans: Segmentaion is the key stage in the conversion of ultrasound images into more meaningful clinical information, and it requires the extraction of important features of the region that needs to be segmented. Feature enhancement is therefore a vital preprocessing step in such applications.
- Development of speckle filtering methods on portable devices for emerging teleultrasound applications: Tele-ultrasound systems operate on resource constrained devices, and the resolution of generated images are generally much lower than standard clinical devices. Therefore, algorithms for speckle reduction and feature enhancement are essential for improving clinical accuracy.

- Machine learning algorithms for ultrasound despcekling: Hourglass networks are becoming increasingly popular for segmentation and density estimation problems in medical image analysis. Such models could be adopted for developing systems for speckle segmenation.

REFERENCES

Aja-Fernandez, S., & Alberola-Lopez, C. (2006). On the estimation of the coefficient of variation for anisotropic diffusion speckle filtering. *IEEE Transactions on Image Processing, 15*(9), 2694-2701. https://doi.org/10.1109/TIP.2006.877360

Alamelumangai, N., & Devishree, J. (2012). Automated clustering of cancer cells using fuzzy C means with repulsions in ultrasound images. *Journal of Artificial Intelligence, 5*, 14-25. https://doi.org/10.3929/jai.2012.14.25

Alelaiwi, A., Abdul, W., Dewan, M. S., Migdadi, M., & Muhammad, G. (2016). Steerable pyramid transform and local binary pattern based robust face recognition for e-health secured login. *Computers & Electrical Engineering, 53*, 435-443. https://doi.org/10.1016/j.compeleceng.2016.01.008

Alkhatib, M., Hafiane, A., Tahri, O., Vieyres, P., & Delbos, A. (2018). Adaptive median binary patterns for fully automatic nerves tracking in ultrasound images. *Computer Methods and Programs in Biomedicine, 160*, 129-140. https://doi.org/https://doi.org/10.1016/j.cmpb.2018.03.013

Andria, G., Attivissimo, F., Maria Lucia Lanzolla, A., & Savino, M. (2013). A suitable threshold for speckle reduction in ultrasound images. *IEEE Transactions on Instrumentation and Measurement, 62*, 2270-2279. https://doi.org/10.1109/TIM.2013.2255978

B. Burckhardt, C. (1978). Speckle in ultrasound B-mode scans. *IEEE Transactions on Sonics and Ultrasonics, 25*, 1-6. https://doi.org/10.1109/T-SU.1978.30978

Bama, S., & Selvathi, D. (2014). Despeckling of medical ultrasound kidney images in the curvelet domain using diffusion filtering and MAP estimation. *Signal Processing, 103*, 230-241. https://doi.org/10.1016/j.sigpro.2013.12.020

Bharath, A. A., & Ng, J. (2005). A steerable complex wavelet construction and its application to image denoising. *IEEE Transactions on Image Processing, 14*(7), 948-959. https://doi.org/10.1109/TIP.2005.849295

Burger, W., & Burge, M. (2008). *Digital Image Processing : an algorithmic introduction using Java*. New York: Springer.

C, V., rajan, E., Thangaraj, V., & Padma, S. (2018). Despeckling of ultrasound images using directionally decimated wavelet packets with adaptive clustering. *IET Image Processing, 13*. https://doi.org/10.1049/iet-ipr.2018.5011

Chaudhuri, A. (2015). Intuitionistic fuzzy possibilistic c-means clustering algorithms. *Advances in Fuzzy Systems, 2015*, 1-17. https://doi.org/10.1155/2015/238237

Chi, Z., Yan, H., & Pham, T. (1996). *Fuzzy Algorithms: With Applications to Image Processing and Pattern Recognition*. Toh Tuck Link, Singapore: World Scientific.

Chubach, O. (2015). *Texture analysis and synthesis using steerable pyramid decomposition for video coding*. presented at the 2015 International Conference on Systems, Signals and Image Processing (IWSSIP), https://doi.org/10.1109/IWSSIP.2015.7314212

Coupe, P., Hellier, P., Kervrann, C., & Barillot, C. (2009). Nonlocal means-based speckle filtering for ultrasound images. *IEEE Transactions on Image Processing, 18*(10), 2221-2229. https://doi.org/10.1109/TIP.2009.2024064

Dai, Y., Chen, L., Wang, Y., & Fu, X. (2015). Quantum-inspired hybrid medical ultrasound images despeckling method. *IEEE Electronics Letters, 51*. https://doi.org/10.1049/el.2014.3742

Durand, S., M. Fadili, J., & Nikolova, M. (2009). *Multiplicative noise cleaning via a variational method involving curvelet coefficients*. presented at the (eds) Scale Space and Variational Methods in Computer Vision. SSVM 2009. Lecture Notes in Computer Science, https://doi.org/10.1007/978-3-642-02256-2_24

Elamvazuthi, I., Muhd Zain, M. L., & Begam, M. (2013). Despeckling of ultrasound images of bone fracture using multiple filtering algorithms. *Mathematical and Computer Modelling, 57*. https://doi.org/10.1016/j.mcm.2011.07.021

Elyasi, I., & Pourmina, M. A. (2016). Reduction of speckle noise ultrasound images based on TV regularization and modified bayes shrink techniques. *Optik, 127*(24), 11732-11744. https://doi.org/https://doi.org/10.1016/j.ijleo.2016.09.054

Elyasi, I., Pourmina, M. A., & Moin, M.-S. (2016). Speckle reduction in breast cancer ultrasound images by using homogeneity modified bayes shrink. *Measurement, 91*, 55-65. https://doi.org/https://doi.org/10.1016/j.measurement.2016.05.025

Farouj, Y., Freyermuth, J., Navarro, L., Clausel, M., & Delachartre, P. (2017). Hyperbolic wavelet-fisz denoising for a model arising in ultrasound imaging. *IEEE Transactions on Computational Imaging, 3*(1), 1-10. https://doi.org/10.1109/TCI.2016.2625740

Finn, S., Glavin, M., & Jones, E. (2011). Echocardiographic speckle reduction comparison. *IEEE Transactions on Ultrasonics, Ferroelectrics, and Frequency Control, 58*(1), 82-101. https://doi.org/10.1109/TUFFC.2011.1776

Foucher, S., Beaulieu, M., Dahmane, M., & Cavayas, F. (2017). *Deep speckle noise filtering*. presented at the 2017 IEEE International Geoscience and Remote Sensing Symposium (IGARSS), https://doi.org/10.1109/IGARSS.2017.8128203

Gai, S., Zhang, B., Yang, C., & Yu, L. (2017). Speckle noise reduction in medical ultrasound image using monogenic wavelet and Laplace mixture distribution. *Digital Signal Processing, 72*, 192-207. https://doi.org/10.1016/j.dsp.2017.10.006

Gardner, W. A. (1992, 1992/11/01/). A unifying view of coherence in signal processing. *Signal Processing, 29*(2), 113-140. https://doi.org/https://doi.org/10.1016/0165-1684(92)90015-O

Gomez, W., Pereira, W. C. A., & Infantosi, A. F. C. (2012). Analysis of co-occurrence texture statistics as a function of gray-level quantization for classifying breast ultrasound. *IEEE Transactions on Medical Imaging, 31*(10), 1889-1899. https://doi.org/10.1109/TMI.2012.2206398

Grgic, S., Grgic, M., & Mrak, M. (2004). Reliability of objective picture quality measures. *Journal of Electrical Engineering, 55*, 3-10.

Guo, L. M., & Hu, J. L. (2012). Texture Image recognition algorithm based on steerable pyramid transform. *Advanced Materials Research, 562-564*, 2178-2182. https://doi.org/10.4028/www.scientific.net/AMR.562-564.2178

Gupta, N., Swamy, M. N. S., & Plotkin, E. (2005). Despeckling of medical ultrasound images using data and rate adaptive lossy compression. *IEEE Transactions on Medical Imaging, 24*(6), 743-754. https://doi.org/10.1109/TMI.2005.847401

Hiremath, P. S., Prema T. Akkasaligar, & Badiger, S. (2010). Speckle noise reduction in medical ultrasound images. https://doi.org/10.5772/56519

Huang, D.-Y., & Wang, C.-H. (2009). Optimal multi-level thresholding using a two-stage Otsu optimization approach. *Pattern Recogination Letters, 30(3)*, 275-284. https://doi.org/10.1016/j.patrec.2008.10.003

Islam, M., Mahbubur Rahman, S. M., Ahmad, M. O., & Swamy, M. N. s. (2018). Mixed Gaussian-impulse noise reduction from images using convolutional neural network. *68*. https://doi.org/10.1016/j.image.2018.06.016

J Gonzales, M., Sturgeon, G., Krishnamurthy, A., Hake, J., Jonas, R., Stark, P., D McCulloch, A. (2013). A three-dimensional finite element model of human atrial anatomy: New methods for cubic Hermite meshes with extraordinary vertices. *Medical image analysis, 17*(5), 525-537. https://doi.org/10.1016/j.media.2013.03.005

Jai Jaganath Babu, J., & Florence Sudha, G. (2016). Adaptive speckle reduction in ultrasound images using fuzzy logic on Coefficient of Variation. *Biomedical Signal Processing and Control, 23*, 93-103. https://doi.org/10.1016/j.bspc.2015.08.001

Jifara, W., Jiang, F., Rho, S., Cheng, M., & Liu, S. (2017). Medical image denoising using convolutional neural network: a residual learning approach. *Journal of Supercomputing, 75*, 1-15. https://doi.org/10.1007/s11227-017-2080-0

Joseph, S., Balakrishnan, K., Balachandran Nair, M. R., & Rajan Varghese, R. (2013). Ultrasound Image Despeckling using Local Binary Pattern Weighted Linear Filtering. *International Journal of Information Technology and Computer Science, 5*, 1-9. https://doi.org/10.5815/ijitcs.2013.06.01

Kang, J., Young Lee, J., & Yoo, Y. (2015). A New Feature-Enhanced Speckle Reduction Method Based on Multiscale Analysis for Ultrasound B-Mode Imaging. *IEEE Transactions on Biomedical Engineering 63*, 1-1. https://doi.org/10.1109/TBME.2015.2486042

Kitlas Golińska, A. (2011). Coherence function in biomedical signal processing: A short review of applications in neurology, cardiology and gynecology. *Studies in Logic, Grammar and Rhetoric 25*, 73-81.

Koundal, D., Gupta, S., & Singh, S. (2016). Speckle reduction method for thyroid ultrasound images in neutrosophic domain. *IET Image Processing, 10*(2), 167-175. https://doi.org/10.1049/iet-ipr.2015.0231

Krishnapuram, R., & Keller, J. M. (1996). The possibilistic c-means algorithm: insights and recommendations. *IEEE Transactions on Fuzzy Systems, 4*(3), 385-393. https://doi.org/10.1109/91.531779

Li, K. Y., Wang, W. D., Zheng, K. W., Liu, W. B., & Xu, G. L. (2015). *The application of B-spline based interpolation in real-time image enlarging processing*. presented at the 2014 2nd International Conference on Systems and Informatics, ICSAI 2014, https://doi.org/10.1109/ICSAI.2014.7009398

Liao, S., Law, M. W. K., & Chung, A. C. S. (2009, May). Dominant local binary patterns for texture classification. *IEEE Transactions on Image Processing, 18*(5), 1107-1118. https://doi.org/10.1109/Tip.2009.2015682

Loizou, C., & Pattichis, C. (2015a). *Despeckle Filtering for Ultrasound Imaging and Video, Volume I: Algorithms and Software, Second Edition* (Vol. 7). Morgan & Claypool Publishers.

Loizou, C., & Pattichis, C. (2015b). *Despeckle Filtering for Ultrasound Imaging and Video, Volume II: Selected Applications, Second Edition* (Vol. 7). Morgan & Claypool Publishers.

Ma, G. Q., & Wang, X. J. (2014). An efficient algorithm optimization of ct images segmentation based on K-Means clustering. *Applied Mechanics and Materials, 530-531*, 386-389. https://doi.org/10.4028/www.scientific.net/AMM.530-531.386

Maycock, J., Hennelly, B., B. McDonald, J., Frauel, Y., Castro, A., Javidi, B., & J. Naughton, T. (2007). *Speckle reduction using the discrete Fourier filtering technique*. presented at the International Machine Vision and Image Processing Conference (IMVIP 2007), https://doi.org/10.1109/IMVIP.2007.24

Mirza, S., Kumar, R., & Shakher, C. (2005). Study of various preprocessing schemes and wavelet filters for speckle noise reduction in digital speckle pattern interferometric fringes. *Optical Engineering - OPT ENG, 44*. https://doi.org/10.1117/1.1886749

Mishra, D., Chaudhury, S., Sarkar, M., Soin, A. S., & Sharma, V. (2018). Edge probability and pixel relativity-based speckle reducing anisotropic diffusion. *IEEE Transactions on Image Processing, 27*(2), 649-664. https://doi.org/10.1109/TIP.2017.2762590

Mitrea, D., Nedevschi, S., & Badea, R. (2012). *The role of the multiresolution textural features in improving the characterization and recognition of the liver tumors, based on ultrasound images*. 2012 14th International Symposium on Symbolic and Numeric Algorithms for Scientific Computing. https://doi.org/10.1109/SYNASC.2012.66

Moussa, O., & Khlifa, N. (2015). *Ultrasound image denoising using a combination of bilateral filtering and stationary wavelet transform*. presented at the International Image Processing, Applications and Systems Conference, IPAS 2014https://doi.org/10.1109/IPAS.2014.7043258

Pal, N. R., Pal, K., Keller, J. M., & Bezdek, J. C. (2005). A possibilistic fuzzy c-means clustering algorithm. *IEEE Transactions on Fuzzy Systems, 13*(4), 517-530. https://doi.org/10.1109/TFUZZ.2004.840099

Panayides A, Loizou C, Pattichis M, Kyriacou E, Shizas C, & Nicolaides A, e. a. (2013). *Ultrasound video despeckle filtering for high efficiency video coding in M-health systems*. presented at the 2013 Constantinides International Workshop on Signal Processing (CIWSP 2013), https://doi.org/10.1049/ic.2013.0020

Panigrahi, L., Verma, K., & Singh, B. K. (2019, 2019/01/01/). Ultrasound image segmentation using a novel multi-scale Gaussian kernel fuzzy clustering and multi-scale vector field convolution. *Expert Systems with Applications, 115*, 486-498. https://doi.org/https://doi.org/10.1016/j.eswa.2018.08.013

Peng, B., & Yang, X. (2010). *Ultrasound image enhancement using correlation techniques*. presented at the 2010 4th International Conference on Bioinformatics and Biomedical Engineering, iCBBE 2010 https://doi.org/10.1109/ICBBE.2010.5516938

Perperidis, A., Cusack, D., White, A., McDicken, N., MacGillivray, T., & Anderson, T. (2017, 2017/07/01/). Dynamic enhancement of b-mode cardiac ultrasound image sequences. *Ultrasound in Medicine & Biology, 43*(7), 1533-1548. https://doi.org/https://doi.org/10.1016/j.ultrasmedbio.2017.03.006

Perreault, C., & Auclair-Fortier, M. F. (2007). *Speckle simulation based on b-mode echographic image acquisition model*. Fourth Canadian Conference on Computer and Robot Vision, Proceedings. (CRV '07), https://doi.org/10.1109/CRV.2007.61

Pietikäinen, M., Hadid, A., Zhao, G., & Ahonen, T. (2011). *Computer Vision Using Local Binary Patterns*. London: Springer London.

Rafati, M., Arabfard, M., Zadeh, M. R. R., & Maghsoudloo, M. (2016). Assessment of noise reduction in ultrasound images of common carotid and brachial arteries. *IET Computer Vision, 10*(1), 1-8. https://doi.org/10.1049/iet-cvi.2014.0151

Sa-ing, V., Vorasayan, P., C. Suwanwela, N., Auethavekiat, S., & Chinrungrueng, C. (2017). multiscale adaptive regularization Savitzky-Golay method for speckle noise reduction in ultrasound images. *IET Image Processing, 12*. https://doi.org/10.1049/iet-ipr.2017.0391

Saadia, A., & Rashdi, A. (2016, 2016/12/01/). Fractional order integration and fuzzy logic based filter for denoising of echocardiographic image. *Computer Methods and Programs in Biomedicine, 137*, 65-75. https://doi.org/https://doi.org/10.1016/j.cmpb.2016.09.006

Sadda, P., & Qarni, T. (2018). Real-Time Medical Video Denoising with Deep Learning: Application to Angiography. *International Journal of Applied Information Systems 12*, 22-28. https://doi.org/10.5120/ijais2018451755

Sahu, A., Bhateja, V., Krishn, A., & Patel, H. (2014). *Medical image fusion with Laplacian pyramids*. presented at the 2014 International Conference on Medical Imaging, m-Health and Emerging Communication Systems, MedCom 2014, https://doi.org/10.1109/MedCom.2014.7006050

Santos, C. A. N., Martins, D. L. N., & Mascarenhas, N. D. A. (2017). Ultrasound image despeckling using stochastic distance-based BM3D. *IEEE Transactions on Image Processing, 26*(6), 2632-2643. https://doi.org/10.1109/TIP.2017.2685339

Shams, R., Hartley, R., & Navab, N. (2008). *Real-time simulation of medical ultrasound from ct images*. presented at the Medical Image Computing and Computer-Assisted Intervention – MICCAI 2008, Berlin, Heidelberg. https://doi.org/doi:10.1007/978-3-540-85990-1_88

Shanthi, I., & Valarmathi, M. L. (2013). SAR image despeckling using possibilistic fuzzy C-means clustering and edge detection in bandelet domain. *Neural Computing and Applications, 23*(1), 279-291. https://doi.org/10.1007/s00521-013-1394-y

Sivakumar, R., Gayathri, M. K., & Nedumaran, D. (2010, 5-7 Dec. 2010). *Speckle filtering of ultrasound B-Scan Images - a comparative study between spatial and diffusion filters*. presented at the 2010 IEEE Conference on Open Systems (ICOS 2010), https://doi.org/10.1109/ICOS.2010.5720068

Sonali, Sahu, S., Singh, A. K., Ghrera, S. P., & Elhoseny, M. (2019). An approach for de-noising and contrast enhancement of retinal fundus image using CLAHE. *Optics & Laser Technology, 110*, 87-98. https://doi.org/https://doi.org/10.1016/j.optlastec.2018.06.061

Song, L. P., Zhou, Z., Wang, X. Y., Zhao, X., & Elson, D. S. (2016). Simulation of speckle patterns with pre-defined correlation distributions. *Biomedical Optics Express, 7*(3), 798-809. https://doi.org/10.1364/Boe.7.000798

Sorensen, L., Shaker, S. B., & Bruijne, M. d. (2010). Quantitative analysis of pulmonary emphysema using local binary patterns. *IEEE Transactions on Medical Imaging, 29*(2), 559-569. https://doi.org/10.1109/TMI.2009.2038575

Sudeep, P., Ponnusamy, P., Rajan, J., Baradaran, H., Saba, L., Gupta, A., & Suri, J. (2016). Speckle reduction in medical ultrasound images using an unbiased non-local means method. *Biomedical Signal Processing and Control 28*, 1-8. https://doi.org/10.1016/j.bspc.2016.03.001

Szczepański, M., & Radlak, K. (2017). Digital path approach despeckle filter for ultrasound imaging and video. *Journal of Healthcare Engineering, 2017*, 9271251-9271251. https://doi.org/10.1155/2017/9271251

Uddin, M., Tahtali, M., J. Lambert, A., Pickering, M., Marchese, M., & Stuart, I. (2016). Speckle-reduction algorithm for ultrasound images in complex wavelet domain using genetic algorithm-based mixture model. *Applied Optics 55*, 4024. https://doi.org/10.1364/AO.55.004024

Udomhunsakul, S. (2015). *Adaptive noise reduction in ultrasonic images*. presented at the INFOCOMP 2015 : The 5th International Conference on Advanced Communications and Computation.

Vimalraj, C., Esakkirajan, S., & Sreevidya, P. (2017, 6-7 July 2017). *DTCWT with fuzzy based thresholding for despeckling of ultrasound images*. presented at the 2017 International Conference on Intelligent Computing, Instrumentation and Control Technologies (ICICICT), https://doi.org/10.1109/ICICICT1.2017.8342616

Wang, P., Zhang, H., & M. Patel, V. (2017). SAR Image despeckling using a convolutional neural network. *IEEE Signal Processing Letters, PP*, 1763-1767. https://doi.org/10.1109/LSP.2017.2758203

Xia, Z., Li, Q., & Wang, Q. (2012, 23-25 Aug. 2012). *Quality metrics of simulated intensity images of coherent ladar*. presented at the 2012 International Conference on Optoelectronics and Microelectronics, https://doi.org/10.1109/ICoOM.2012.6316255

Yadav, G., Maheshwari, S., & Agarwal, A. (2014, 24-27 Sept. 2014). *Contrast limited adaptive histogram equalization based enhancement for real time video system*. presented at the 2014 International Conference on Advances in Computing, Communications and Informatics (ICACCI), https://doi.org/10.1109/ICACCI.2014.6968381

Yang, J., Fan, J., Ai, D., Wang, X., Tang, S., & Wang, Y. (2016). Local statistics and non-local mean filter for speckle noise reduction in medical ultrasound image. *Neurocomputing, 195*. https://doi.org/10.1016/j.neucom.2015.05.140

Yang, M., Moon, W. K., Wang, Y. F., Bae, M. S., Huang, C., Chen, J., & Chang, R. (2013). Robust texture analysis using multi-resolution gray-scale invariant features for breast sonographic tumor diagnosis. *IEEE Transactions on Medical Imaging, 32*(12), 2262-2273. https://doi.org/10.1109/TMI.2013.2279938

Yang, X., Tridandapani, S., Beitler, J., Yu, D., J Yoshida, E., Curran, W., & Liu, T. (2012). Ultrasound GLCM texture analysis of radiation-induced parotid-gland injury in head-and-neck cancer radiotherapy: An in vivo study of late toxicity. *Medical physics, 39*, 5732-5739. https://doi.org/10.1118/1.4747526

Yousefi, S., Qin, J., Zhi, Z., & Wang, R. (2013). Uniform enhancement of optical micro-angiography images using Rayleigh contrast-limited adaptive histogram equalization. *Quantitative imaging in medicine and surgery 3*, 5-17. https://doi.org/10.3978/j.issn.2223-4292.2013.01.01

Zhang, J., Lin, G., Wu, L., & Cheng, Y. (2015). Speckle filtering of medical ultrasonic images using wavelet and guided filter. *Ultrasonics, 65*. https://doi.org/10.1016/j.ultras.2015.10.005

Zhang, J., Marszalek, M., Lazebnik, S., & Schmid, C. (2007). Local features and kernels for classification of texture and object categories: A comprehensive study. *International Journal of Computer Vision - IJCV 73*, 213-238. https://doi.org/10.1007/s11263-006-9794-4

Zhang, J., Wang, C., & Cheng, Y. (2015, 2015/01/01). Comparison of despeckle filters for breast ultrasound images. *Circuits, Systems, and Signal Processing, 34*(1), 185-208. https://doi.org/10.1007/s00034-014-9829-y

Zhang, K., Zuo, W., Chen, Y., Meng, D., & Zhang, L. (2016). Beyond a Gaussian denoiser: Residual Learning of Deep CNN for Image Denoising. *IEEE Transactions on Image Processing, 26*(7), 3142-3155. https://doi.org/10.1109/TIP.2017.2662206

Zhang, M., Xie, J., Zhou, X., & Fujita, H. (2013). *No reference image quality assessment based on local binary pattern statistics*. presented at 2013 IEEE International Conference on Visual Communications and Image Processing, https://doi.org/10.1109/VCIP.2013.6706418

Zheng, Y. F., Zhou, Y. L., Zhou, H., & Gong, X. H. (2015, Jul). Ultrasound image edge detection based on a novel multiplicative gradient and canny operator. *Ultrasonic Imaging, 37*(3), 238-250. https://doi.org/10.1177/0161734614554461

Zhu, L., Wang, W., Qin, J., Wong, K.-H., Choi, K.-S., & Heng, P.-A. (2017). Fast feature-preserving speckle reduction for ultrasound images via phase congruency. *Signal Processing, 134*, 275-284. https://doi.org/https://doi.org/10.1016/j.sigpro.2016.12.011